SISSA
Scuola Internazionale Superiore di Studi Avanzati

Neuroscience Area

Ph.D. course in Molecular Biology

Innovative approaches for the diagnosis of Parkinson's disease and multiple system atrophy based on the analysis of the olfactory mucosa

CANDIDATE

Chiara Maria Giulia De Luca

SUPERVISOR

Dott. Fabio Moda

Academic Year 2021-22

TABLE OF CONTENTS

ABSTRACT

Parkinson's disease (PD) and multiple system atrophy (MSA) are neurodegenerative diseases whose diagnosis is particularly complex, especially in the early stages, because the symptoms are similar to each other and to those of other diseases, including dementia with Lewy bodies (DLB), progressive supranuclear palsy (PSP) and corticobasal degeneration (CBD). All these disorders share a similar pathological process: the change in the structure of some proteins normally present in the brain which thus lose their function, begin to aggregate and deposit in specific brain areas, causing irreparable damage. In particular, PD, MSA and DLB are called α-synucleinopathies because they present aggregates of the α-synuclein protein (αSyn^{D}), which however are localized in different brain structures. PSP and CBD are instead called tauopathies because they are characterized by the presence of aggregates of the tau protein. These protein aggregates are considered disease-specific biomarkers because their detection and distribution (which can only be determined *post-mortem* on the patient's brain tissue) are used to formulate a definite diagnosis. As long as the patient is alive the diagnosis is only probable and does not have absolute accuracy. Consequently, some diagnoses made in life may change after the neuropathological assessments. Several evidence suggests that misfolded proteins can also appear in peripheral tissues such as the olfactory mucosa (OM, easily and periodically collectible with a nasal swab), but in such small quantities as not to be detectable with common diagnostic techniques.

The recent advances in molecular and structural biology have provided insights into the processes involved in the pathogenesis of neurodegenerative diseases and have made it possible to recapitulate the protein misfolding process *in vitro* in a limited period of time through the development of innovative techniques, called seed amplification assays (SAAs), among which the real-time quaking-induced conversion (RT-QuIC). This new methodology exploits the ability of misfolded proteins to transmit their abnormal conformation to normal monomers, which are used as substrate of the reaction. Abnormally folded proteins are able to interact with these substrates

and induce monomers to change conformation and subsequently aggregate. Therefore, the addition of misfolded proteins (considered "seeds") to the substrate is able to trigger an aggregation phenomenon, known as "seeding effect" that might be exploited for diagnostic and therapeutic purposes.

In my Ph.D. project I have firstly optimized the RT-QuIC assay, with the aim of analyzing OM samples collected from patients with PD, MSA, CBD and PSP, and evaluating the efficacy of the test in detecting traces of misfolded αSyn^D in α-synucleinopathy derived samples. The results of our study showed that most OM samples from patients with PD and MSA induced aggregation of the recombinant substrate protein, suggesting the presence of traces of αSyn^D. In contrast, the PSP and CBD samples had no effect on the substrate (since they do not contain abnormal αSyn). Interestingly, the RT-QuIC reaction products acquired biochemical and biophysical characteristics useful to discriminate, with a good degree of accuracy, patients with PD from patients with MSA. Moreover, by exposing neuronal-like differentiated SH-SY5Y cells to these products, we observed the induction of different inflammatory pathways. These findings suggested the existence of a link between the morphology of the aggregates and their inflammatory properties. To deepen this aspect, we have produced three different recombinant aggregates of αSyn, in order to generate, in a controlled environment, artificial αSyn seeds resembling to some extent the αSyn^D strains present in OM, and test their behavior by RT-QuIC without the presence of other tissue factors. Although capable to efficiently seed the aggregation of the substrate, αSv1, αSv2, and αSv3 did not transmit their seed-specific properties to the reaction products which showed comparable biochemical properties, instead. Probably, our experimental setting was too artificial to properly recapitulate the phenomenon of the seeding effect exerted by αSyn^D in RT-QuIC. However, when used to stimulate SH-SY5Y cells, αSv1, αSv2, and αSv3 acted on different activators of inflammatory pathways, thus strengthening the existence of a correlation between morphological and inflammatory properties of αSyn fibrils.

In the last part of my project, we decided to evaluate how much the RT-QuIC assay could be used for diagnostic purposes in the field of α-synucleinopathies, by studying its

reproducibility in other laboratories. Together with an American lab we have so analyzed a group of OM samples with the same experimental protocol and we obtained a 96% concordance of results. Furthermore, we observed that the OM of MSA behaved differently according to the pathological subtype. In fact, we know that this disease can manifest itself in a cerebellar form (MSA-C) or associated with parkinsonism (MSA-P). In our test, only MSA-P samples induced a seeding effect, allowing us to discriminate between the two pathological subtypes.

These preliminary studies provide evidence that RT-QuIC of OM samples represents a reliable assay for supporting the diagnosis of α-synucleinopathy and may limit the negative effects that misdiagnosis produces in terms of costs for the healthcare system and improve overall patient care, treatment, and possible enrollment in future clinical trials.

CHAPTER I

1. INTRODUCTION

1.1 α-synuclein

The α-synuclein (αSyn) is a protein belonging to the family of synucleins, small and soluble proteins expressed mainly in neural tissues and cancer cells. αSyn is mostly found in the brain, where it is located in the pre-synaptic terminals, and at this level, it can be associated with lipids and proteins. The gene that encodes for αSyn is the SNCA, on chromosome 4. In certain conditions, the protein acquires aggregating properties and is able to form amyloid aggregates, called Lewy bodies, which are the elements that characterize Parkinson's disease (PD) and other neurodegenerative diseases, defined as α-synucleinopathies [1].

1.1.1 αSyn structure

αSyn (Figure 1.1) is a small protein of 14 kDa (140 amino acids) that is characterized by three specific domains:

- The N-terminal region (1-60 aminoacids), is rich in lysine and is characterized by a preserved motif (KTKEGF) typical of the A2 class of apolipoproteins. This part of the protein is amphipathic and plays a crucial role in the modulation of αSyn interactions with membranes [1].
- The C-terminal region (95-140 aminoacids), is characterized by a disordered carboxyl tail and is involved in the regulation of the nucleic localization of αSyn and its interactions with metals, small molecules and proteins [2].
- The central region (61-94 aminoacids) contains a very hydrophobic structure and is known as the non-amyloid-β component (NAC) because it was first purified from amyloid plaques in patients with Alzheimer's disease (AD), in 1993 [3]. The NAC region is the portion of the protein that is essential for the aggregation of αSyn itself.

The protein is characterized by high flexibility that allows the protein to assume different conformations and interact at the same time with other compounds and other proteins. Various studies using different biophysical methods have shown how αSyn, in denatured conditions, exists mainly in the form of unfolded and stable monomers [1]; despite this, due to its particular structure, in some conditions the protein tends to aggregate in oligomers or fibrils. The accumulation of αSyn and the consequent formation of particular states of aggregation are harmful to the cell, while the normal presence of the protein is physiologically useful and protective [4]. αSyn is capable of adopting different structures under specific induced stress conditions or when interacting with other proteins, specific ligands, lipids and/or biological membranes [5]. When αSyn binds membranes, such as synaptic vesicles, it undergoes a conformational change that leads to the formation of amphipathic α-helices. It has been seen that the type of helix adopted varies according to the curvature of the membrane. In particular, vesicles with a large diameter (about 100 nm) and with a low curvature induce an elongated helix conformation, while vesicles with a small diameter and a membrane with a high degree of curvature, induce the formation of a shorter helix. αSyn binds principally to vesicles smaller than about 40 nm [6].

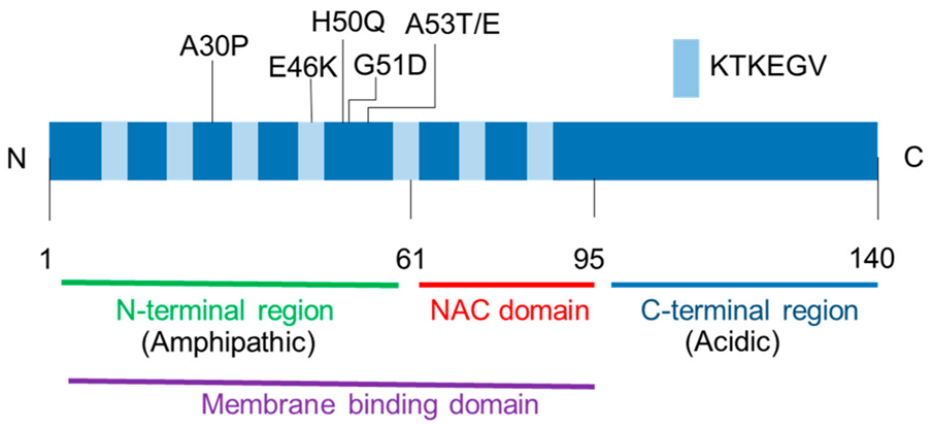

Figure 1.1 Schematic representation of human α-synuclein protein structure. The N-terminal region and the non-amyloid-component (NAC) domain have seven imperfect KTKEGV repeats that contribute to membrane binding. All mutations linked to the familial Parkinson's disease (A30P, E46K, H50Q, G51D, A53T, and A53E) are located in the N-terminal region (From *Mori et al., 2020*)

.

1.1.2 αSyn functions

The functions of the protein are not yet fully clarified. Recent studies showed that αSyn seems to have an important role in compartmentalization, storage and recycling of neurotransmitters [7]. In addition, the protein is associated with the physiological regulation of certain enzymes and is thought to increase the number of dopamine transporter molecules [8].

Regarding the role of αSyn in the trafficking of vescicles, it has been shown that yeast cells that over-express αSyn have a defect in the trafficking of vesicles from the endoplasmic reticulum (ER) to the Golgi apparatus. In particular, the protein interferes with the secretory pathway by inhibiting the activity of Rab GTPase YPT1 and, even if the vesicles have joined correctly at the ER level, they are unable to fuse with the Golgi membrane, resulting in their accumulation [9]. This observation has been extended to mammals, particularly hippocampal glutamatergic neurons and mesencephalic primary dopaminergic neurons, where a moderate increase in αSyn expression was found to inhibit the release of glutamate and dopamine, respectively, without generate toxicity or cellular inclusions of αSyn [10].

It is known that αSyn plays a role also in synaptic transmission as a chaperone in the formation of the protein complex attacking the soluble N-ethylmaleimide (NEM) sensitive factor, a system necessary for vesicle fusion and release of neurotransmitters at the synapse. The fusion of the vesicle is controlled by the interaction between the proteins of the SNARE complex, namely synaptobrevin, a membrane protein associated with the vesicle (VAMP2), and the proteins of the pre-synaptic plasma membrane (SNAP5). During the release of each neurotransmitter, the SNARE complex assembles and disassembles. This cyclical operation must be controlled: in this context, αSyn interacts directly with VAMP2 and promotes complex SNARE assembly [7]. The control action of αSyn is essential for neuronal homeostasis, as demonstrated in studies by Burre et al., 2010 and Greten Harrison et al., 2010 in which mice, lacking all three types of synucleins, developed neurological damage and died prematurely. The same group of researchers highlighted that the control function of αSyn on the SNARE protein complex is guaranteed only by the protein that assembles in multimeric form upon membrane binding [11,12].

Several cellular and animal models presenting mutant or over-expressed αSyn are characterized by mitochondrial alterations. Indeed, according to numerous studies, accumulations of αSyn lead to a dysfunction of the mitochondrial complex I [13–15] and defects in normal mitochondrial activity such as altered morphology, loss of membrane potential, increased ROS [13,14]. Numerous articles show that the protein interacts directly with mitochondria [16,17]. In particular, αSyn binds to highly curved and detergent-resistant membranes enriched in cholesterol, sphingolipids and acid phospholipids and cardiolipin, a lipid found almost exclusively in mitochondria [18–20]. The protein has an important role also in the modulation of the relationship between ER and mitochondria. Minimal over-expression of αSyn positively regulates mitochondrial calcium levels, favoring the binding of mitochondria to the ER. However, important over-expression of the protein determines its redistribution, reduces the ability of the mitochondria to accumulate calcium and, in addition, alters their morphology. Moreover, it also causes the reduction in the link between ER and mitochondria, a phenomenon that leads to an increase in autophagic flows, compromising cell survival [21].

1.1.3 Misfolding and aggregation of αSyn

αSyn, together with other proteins, such as prion protein, tau and Aβ, have been shown to contain intrinsically disordered regions (IDRs), as they lack stable tertiary and/or secondary structure under physiological conditions, presumably to interact with a broad range of binding partners. The flexibility of IDRs is thought to be important for the conformational rearrangements which drive the formation of amyloid structures [22].

As already mentioned, the NAC domain of αSyn is the region of the protein most prone to aggregation. Despite this, such region is protected from aggregation, albeit in part, by the positive and negative charges of the N- and C-terminal regions of the protein. αSyn seems to possess a dynamic conformation that is stabilized by long-range interactions that provide the protein with a substantial degree of compactness. More precisely, long-range interactions take place between the C-terminal region and the NAC region and between the N- and C-terminal

regions. These interactions are probably due to hydrophobic and electrostatic contacts, and it seems that they prevent aggregation [23]. Nevertheless, there may be situations, such as mutations or changes in external conditions, which can interfer with the compactness of the protein, subsequently causing misfolding and aggregation. Normally folded proteins are generally characterized by higher content of α-helix structures [24]. Misfolded proteins show a prevalence of β-sheet structures and are usually either degraded by the ubiquitin-proteasome system (UPS) or refolded correctly by chaperone proteins [25]. However, sometimes these systems fail and, as a consequence, misfolded proteins start to aggregate and form oligomers. Oligomers and protofibrils are then packaged into longer amyloid aggregates, ranging from 100 to 200 Ångström (Å) in diameter [26] (**Figure 1.2**). Once formed, these amyloids are deposited as intra- or extra-cellular aggregates into the CNS causing cell death and neurodegeneration. Protein misfolding can be due to mutations in protein-encoding genes (causing familial forms of neurodegenerative diseases) [27] or can be caused by several factors (e.g. proteotoxic stress, cellular aging) responsible of sporadic forms of α-synucleinopathy. At present, the exact molecular mechanism which leads to protein misfolding and aggregation remains still elusive [22]. It has been observed that αSyn can undergo phosphorylation phenomena at the level of serine 129 and would thus be more prone to change its conformation, passing from single monomers to insoluble oligomers and therefore to insoluble amyloid fibrils rich in β-sheet structures [28,29].

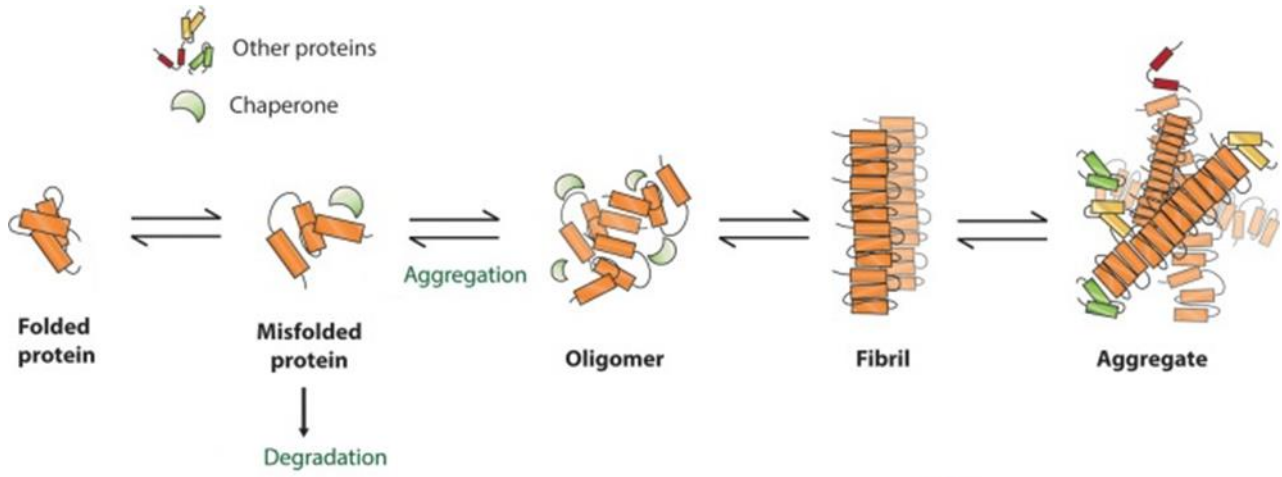

Figure 1.2 Proposed mechanism for amyloid formation. A misfolded protein can be refolded, degraded, or aggregated. The first step in the aggregation pathway involves oligomers, followed by fibril formation around the fibril axis until the initial aggregates (From *Rambaran et al., 2008)*.

One of the most puzzling aspects of misfolded proteins is their ability to interact with their physiological counterparts and force them to adopt similar structural alterations (**Figure 1.3**). This phenomenon was initially observed in prion diseases, where the misfolded prion protein, named prion (PrP^{Sc}), was found to propagate the disease by acting as seed for the conformational conversion of the normal protein (PrP^{C}) to the pathological isoform. By seeding misfolding of the PrP^{C} into PrP^{Sc}, prions spread in the CNS (and sometimes to the periphery) and can be transmitted (more or less efficiently) between individuals of the same or different species. Similarly, recent findings showed that misfolded αSyn can also transmit its abnormal conformation to its normally folded isoforms [30].

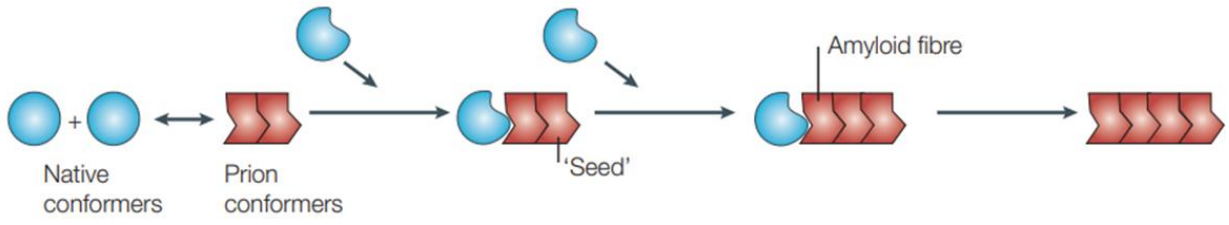

Figure 1.3 Replication of prion-like proteins. The prion conformation appears after a spontaneous conversion of native proteins. The prion seed converts further proteins by joining them to its two ends, thus the amyloid fiber starts to grow. As fibres fragment, new seeds are introduced, which further increase the speed of conversion (adapted from Shorter & Lindquist 2005).

The αSyn aggregation process can be divided into three phases:

- The lag phase, in which monomers come together to form aggregation nuclei (seeds);
- The elongation phase, in which the fibrils grow exponentially;
- The stationary phase, during which there is a depletion of monomers which leads to a decrease in the growth of fibrils [31].

The first phase of the αSyn aggregation process is very important because the speed of this phase can affect the speed of the next two phases. As demonstrated, an acceleration of the lag phase (which therefore becomes shorter) of the αSyn aggregation process can be obtained thanks to the addition of seeds, which behave as preformed nuclei for aggregation. This process seems to occur *in vivo* and drives disease progression along routes of neuronal connectivity on the basis of trans-cellular propagation of protein seeds [32]. The oligomers convert to protofibrils,

which combine to form a mature amyloid fibril. In all three phases there is a dynamic equilibrium in which different conformations and states of aggregation coexist simultaneously.

1.1.4 αSyn propagation

Since 2003 it has emerged that αSyn can have a behavior similar to the prion protein, in fact, the conversion of αSyn from α-helix to β-sheet is involved in the pathogenicity of the protein [31,33]. For this reason, αSyn is considered a prion-like protein. In his work, Braak defined the progression of lesions caused by αSyn: first in the brain stem and olfactory bulb, then proceeding caudo-rostrally to the midbrain and cortical areas [34]. Furthermore, as it was found that intra-gastric administration of rotenone in rats resulted in Lewy disease, first appearing in the enteric nervous system and then spreading in animal substantia nigra [35], it was assumed that αSyn can act as an exogenous pathogen at the onset of PD, through structural changes, formation of intracellular aggregates, propagation mechanisms [36,37].

According to studies by Kordower et al. [38] and Li et al. [39], it was found that human embryonic dopaminergic cells transplanted into the striatum of patients with PD developed Lewy bodies, highlighting the possible cell-to-cell transmission of αSyn occurred from the host to the grafted tissue. PD models of rodents were used to study the αSyn propagation process *in vivo*, indeed the intracerebral injection of brain extracts containing pathological αSyn into transgenic mice stimulated the formation of αSyn lesions. The progression of αSyn pathology along neuronal routes leads to progressive neurodegeneration and signs of motor dysfunction resembling those found in PD [40,41]. Moreover, also the inoculum of human αSyn fibrils leads to the appearance of αSyn depositions in brain areas distant from the injection site, thus suggesting that the injected αSyn is able to propagate [41–43]. Another important finding that emerged from these studies is that αSyn is able to cross the blood-brain barrier and accumulate in cortical neurons and spinal cord inducing diffuse microglial activation [44]. Furthermore, human αSyn derived from Lewy bodies of PD patients is able to induce α-synucleinopathy in monkeys following its administration at the substantia nigra level [45].

Different hypotheses for the spread of misfolded αSyn from cell to cell have been postulated so far. For instance, cellular endocytic mechanisms can be involved in the release and uptake of protein aggregates and in their trans-cellular spreading [46]. Aggregates might bind to heparan sulfate proteoglycans (HSPGs) on the cell surface and trigger the formation of large endocytic vesicles (macropinosomes) that bring aggregates into cells [47]. Receptor-mediated endocytosis may also occur through the binding of aggregates to specific proteins at the cell surface [48]. Moreover, a growing body of evidence proposes that exosomes play important roles in the cell-to-cell transmission of pathogenic protein aggregates, thereby contributing to the pathological and clinical progression of α-synucleinopathy [49]. Thus, traces of misfolded αSyn can localize in peripheral tissues (e.g. cerebrospinal fluid – CSF, urine, blood, olfactory mucosa, skin, saliva, tears) but, at this level, they are undetectable with the current diagnostic techniques, due to their limits of detection.

- OLIGOMERS OF α-SYN

Oligomers are a heterogeneous group of species ranging from dimers to larger protofibrillar structures, likely composed of hundreds of monomers [50]. Oligomeric species are characterized by marked instability, transient existence and variability and, for these reasons, the characterization of this protein species is rather difficult. The αSyn oligomers can be prepared thanks to different preparation and purification protocols, which allow to obtain oligomers composed of less than five to more than a hundred polypeptide chains, with different morphologies (spherical, elliptical, circular, tubular and shaped) [51–53]. Furthermore, as reported in the study by Ghosh et al. 2015, oligomers with different secondary structures were identified; in particular, from the initial phase to the end of the aggregation phase, the populations of oligomeric intermediates move from an α-helix towards a β-sheet structure [54]. Variants of αSyn prone to oligomerization, but not fibrillization, have been identified, leading to the hypothesis that oligomeric species could be the most toxic forms of αSyn [55]. This hypothesis is supported by studies that, using a well-defined species of recombinant αSyn, demonstrate how pre-fibrillar complexes can cause a wide range of harmful effects. Furthermore, multimers have also been

described, composed of more than 8 molecules of αSyn and enriched by α-helix structures. The latter are presumably formed from the monomer upon membrane binding and are related to the αSyn biological function in the SNARE complex assembly. Although further studies are needed, it seems that their formation can prevent the oligomerization of pathological αSyn [12]. It was originally thought that amyloids in the form of large fibrils and aggregates were neurotoxic, however now it is widely accepted that oligomers are the most neurotoxic species and fibrils formation may actually be a way for the cell to minimize their deleterious effects. Indeed, toxicity of oligomers may arise from the abnormal exposition of hydrophobic groups on their surface, resulting in inappropriate interactions with many functional cellular components like membranes and organelles [26,56,57].

- FIBRILS OF α-SYN

As already mentioned, αSyn is able to self-assemble into amyloid fibrils characterized by a predominantly β-sheet structure as shown by various studies [58,59]. NMR studies suggest that the nucleus of αSyn fibrils varies mainly from residues 30–38 to residues 95-110. These residues comprise the NAC region and part of the N-terminal domain, which are assembled into 5-6 β-strands separated by multiple loops. Part of the N-terminal region and the C-terminal region lie outside the nucleus. Thanks to electron microscopy and atomic microscopy it was possible to study and understand the morphology of the αSyn fibrils; more specifically, the width of the fibril, which varies from a minimum of 6 nm and a maximum of 18 nm, and the length, which varies from 0.1 μm to more than 5 μm, were measured. Furthermore, thanks to these microscopic techniques, twisted and untwisted, curved and straight, periodic and non-periodic fibrils have been described [60–62]. This variability is a consequence of the different experimental conditions of aggregation. In fact, many studies have focused on understanding how external factors can be determining factors in the fibrillar structure of αSyn, including the composition of the buffer, the conditions of aggregation or the effect of mutations. One theory speculates that the formation of aggregates could be protective; for example, the interference of oleuropein (polyphenol found in olive leaves and drupes) leads to the formation of αSyn aggregates that show altered biophysical

properties. The formation of this type of aggregates is accompanied by a decrease in cytotoxicity [63]. Moreover, experiments performed in a cellular model of αSyn aggregation demonstrate that αSyn inclusions can show a protective cellular aggresome (an aggregation of misfolded proteins within the cell) [64]. Recent studies performed with cryo electron microscopy (cryo-EM) were able to show that fibrils extracted from brains of patients with different forms of α-synucleinopathies possess distinct structures [65–67].

1.1.5 αSyn Mutations

As previously mentioned, the gene that encodes for αSyn is the SNCA gene. This gene can be subject to point mutations that are related to the inherited autosomal dominant form of PD. The best characterized point mutations are those that host the aminoacid substitutions A53T [68], A30P [69] and E46K [70]. The most frequent mutation is A53T. Carriers of this mutation develop Parkinson's symptoms around the age of 40-60 years and once the disease is overt, symptoms progress over the next decade [71]. Alongside this well-known point mutations, three new missense mutations, H50Q [72], G51D [73] and A53E [74], have been described thus expanding the family of PD-associated mutants. In particular, the H50Q mutation is related to a late onset of the disease with a cognitive deficiency [75]; the G51D mutation is associated with a form of disease that responds moderately to levodopa treatment and is characterized by rapid progression [76]; finally, the A53E mutation is also associated with atypical PD that begins early with numbness and hyper-reflexia and therefore results in parkinsonism associated with severe spasticity, myoclonic shots and psychiatric disorders [74]. In general, mutated forms of αSyn are less stable than the normal counterpart, and therefore possess a greater tendency to accumulate. The point mutations A53T, E46K, A30P and missense mutation H50Q have been observed to result in improved αSyn fibrillation; the missense mutations G51D and A53E cause instead a decrease in the fibrillation process parallel to an increase in the formation of amorphous aggregates [51,77–79]. It has been shown that the mutated G51D species forms αSyn oligomers more slowly and forms more toxic fibrils [76]. Furthermore, this mutated form, together with the

A30P mutant, show a defective interaction with membranes [77,80], as opposed to the mutated E46K form which is able to increase binding affinity of αSyn with membrane phospholipids [81].

1.2 α-synucleinopathies

α-synucleinopathies are a group of neurodegenerative diseases that include PD, multiple system atrophy (MSA), dementia with Lewy bodies (DLB) and pure autonomic failure (PAF). All these entities are characterized by the accumulation of disease-associated αSyn (αSyn^D) aggregates in different regions of the central nervous system, but protein aggregates have also been found in regions in the peripheral nervous system, such as autonomic nerve fibers but also skin somatic fibers [82–84]. In the context of α-synucleinopathies, the sites where the abnormal protein aggregates are found are different and allow to discriminate the diverse clinical entities: in PD and DLB the aggregates are found in neurons of the central nervous system (CNS) and are called Lewy bodies, if located in the soma, and Lewy neurites, if located in axonal extensions; in PAF they are found in the peripheral nerves of the autonomic nervous system; in MSA they are found in the cytoplasm of oligodendrocytes and are defined glial cytoplasmic inclusions (GCIs, glial cytoplasmic inclusions) or Papp-Lantos bodies, but are also found less frequently in the nucleus of oligodendrocytes and in the nucleus and cytoplasm of neurons [85] (**Figure 1.4**).

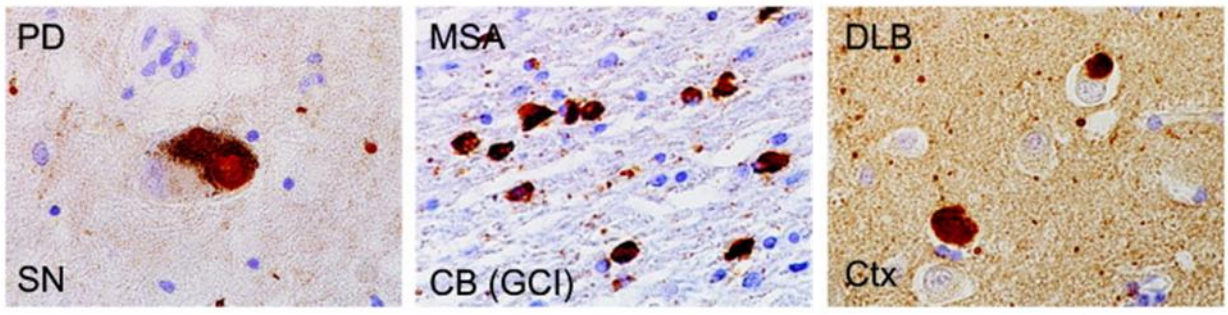

Figure 1.4 Neuropathology of α-synuclein deposits in different α-synucleinopathies. α-synuclein aggregates stained by anti-α-synuclein antibody showing different aggregates morphologies and distinct affected areas in PD (SN: substantia nigra), MSA (CB: cerebellum; GCI: glial cytoplasmic inclusion) and DLB (Ctx: cortex) (From: *Peng et al., 2018*).

Furthermore, recent studies have shown that the αSyn^D present in the aggregates does not have the same conformation in all α-synucleinopathies: for example, the αSyn aggregates that

form Lewy bodies in PD differ in conformation (in biotechnological terms, strain) from those forming the Papp-Lantos bodies in MSA [44,67,86,87]. This evidence was very recently confirmed with the aforementioned cryo-EM studies, which were able to identify the structure of αSyn aggregates extracted from PD, DLB and MSA brains [88,89].

α-synucleinopathies are pathologies that include both sporadic and genetic disorders. The etiology of these disorders is not yet fully understood, but it appears to include both genetic and environmental factors. To verify the impact of various environmental and lifestyle factors on the onset of α-synucleinopathies, prospective studies are required, as well as a detailed evaluation of genetic factors, followed by a systematic assessment of neuropathological changes. Regarding genetic factors, numerous genes of interest have been identified, which can cause autosomal dominant or recessive disorders [90] (See Paragraph 1.1.5). Among the environmental factors that have been studied the most interesting are pesticides, herbicides, insecticides, fungicides, metals, organic solvents, magnetic fields, smoking, alcohol, body mass index and dietary factors [91].

1.2.1 Parkinson's disease

PD is the second most frequent neurodegenerative disease after AD [92] and is the most frequent form of parkinsonism [93]. Parkinsonism is a clinical syndrome characterized by motor symptoms such as bradykinesia, muscle rigidity, tremor and postural instability, also common to other diseases, including MSA, DLB, progressive supranuclear palsy (PSP) and corticobasal degeneration (CBD). The name is related to James Parkinson, a 19th century pharmacist and surgeon, who first described most of the symptoms of the disease in "An essay on the shaking palsy" [94].

- EPIDEMIOLOGY AND ETHIOPATHOGENESIS

PD affects approximately 7 million people worldwide, most of whom are over 60 years old [95]. The incidence of PD steadily increases with age and men are more affected than women [96]. Mortality associated with PD does not increase compared to that of the general population over the first decade of the disease, but doubles from that moment on, however, making it possible

to live with the disease for over 20 years [92]. The etiology of most cases of PD is probably multifactorial, resulting from the combination of genetic and environmental factors. Some factors can increase the risk of developing PD, such as exposure to toxic chemicals; however, some lifestyle habits, such as proper nutrition and physical activity, can reduce the risk [97]. Most cases of PD are idiopathic, although genes whose mutations predispose to PD are known, these include the SNCA genes, encoding αSyn, LRRK2, encoding the leucinerich repeat kinase enzyme, PRKN, encoding the parkin protein and PINK1, encoding the PTEN-induced kinase 1 enzyme [98].

From the pathophysiological point of view, PD is characterized by the loss of dopaminergic neurons of the mesencephalic substantia nigra [93]. The substantia nigra is, together with the striatum, part of the nigrostriatal pathway, a dopaminergic pathway dedicated to the control of involuntary movement and part of the extrapyramidal system. The degeneration of dopaminergic neurons is the result of the neuronal accumulation of pathological Lewy bodies and Lewy neurites. Physiologically, the dopaminergic signaling starting from the substantia nigra and directed towards the striatum is important for the modulation of two pathways involved in the control of movement: the direct pathway, which from the nuclei of the base leads to a disinhibitory effect on the thalamus, with a final activation effect of the motor cortex; and the indirect pathway, which through the inhibition of the thalamus leads to the inhibition of the motor cortex [92]. The balance between these two parallel pathways is crucial for ensure that movements are correctly performed and controlled. Overall, the presence of dopamine shifts the balance between the two pathways in a facilitating sense and allows the access of thalamic neurons to the motor cortex. In PD, the loss of the dopaminergic signal at the level of the nigrostriatal pathway has the effect of increasing the inhibitory mechanisms that act on the thalamus, resulting in less cortical stimulation and reduced movement. This justifies the presence of the motor symptoms prevalent in PD, such as bradykinesia and difficulty in initiating movement, stiffness and tremor. However, non-motor symptoms are also found in PD, such as REM sleep disturbances and dysautonomic disorders. The reason for the presence of non-motor manifestations lies in the fact that in PD the neurons of the substantia nigra are not exclusively affected, but there are many other sites where αSyn

deposits are found. The sites of damage and the sequence with which they are involved are described in the so-called Braak hypothesis [36]. It argues that the diffusion of αSyn aggregates proceeds in a caudo-cranial direction, initially affecting the peripheral nervous system (PNS) and in particular the enteric nervous system (ENS), continuing then in the medulla oblongata, in the pontine tegmentum, in the midbrain and in the diencephalon, finally arriving at the cortex. This temporal difference in the involvement of various nerve structures reflects the clinical evolution of PD: non-motor symptoms, such as constipation, due to the involvement of the ENS, anosmia, due to the involvement of the olfactory bulbs, and REM sleep disturbances, due to the involvement of the pontine tegmentum, can be present up to 20 years before motor disturbances (prodromal period) [98]. These findings prompted the researchers to formulate the dual-hit hypothesis, according to which the formation of αSyn^{D} may occur in peripheral structures (e.g., gut and nose) and from those organs it could reach the brain [99]. Motor symptoms begin when more than 50% of dopaminergic neurons of the substantia nigra have degenerated.

- CLINICAL ASPECTS

  As already mentioned, PD presents clinically with both motor and non-motor symptoms.

  - Motor symptoms. The onset of motor symptoms is unilateral and the asymmetry usually persists during the course of the disease. The key symptom is bradykinesia, or slowness in the execution of movements. In addition to slowness, bradykinesia is also characterized by a decrease in the amplitude of repetitive movements: by repeating the same action over and over again, the range of movement will gradually decrease. Bradykinesia is an ever-present symptom in PD, unlike other motor symptoms (up to 20% of patients, for example, do not have tremor). Muscle stiffness is another important symptom in the context of parkinsonism. Another symptom present is tremor at rest, which typically involves the distal end of an upper limb at the beginning, and then extends to the ipsilateral lower limb. It is a rhythmic tremor, has a frequency of 4-6 Hz and typically ceases with action, unlike cerebellar tremor. Finally, postural instability manifests itself in deficit in maintaining balance during walking, standing and postural

passages. Postural instability can be associated with anteroflexion attitudes of the trunk (the so-called camptocormia) or laterodeviation of the trunk (named Pisa syndrome). A further sign of postural instability are alterations in walking: the steps are slow and of reduced amplitude, there is difficulty in changing direction and starting the march (freezing) and the pendular movements of the limbs (synkinesias) are reduced. Postural reflexes are also lost, which can be tested for objectivity by performing the pull test, consisting in unbalancing the patient by pushing him backwards, and the tendency to fall increases [92,93,98].

- Non-motor symptoms. The non-motor symptoms are various, as there are numerous other sites of damage in PD in addition to the nigrostriatal pathway and, as already stated, they may precede motor symptoms in onset. Non-motor symptoms include sleep disturbances such as insomnia, daytime sleepiness and REM sleep disturbances. Rapid eye movement (REM) phase-related behavioral sleep disorder (RBD) is a parasomnia manifesting in vivid, often terrifying dreams associated with behavior more or less complex motor skills during the REM phase. Patients seem to live and "act" their dreams. The presumed pathophysiological mechanism of RBD is represented by the damage to the centers of the brainstem (such as the reticular magno cell formation, the laterodorsal tegmental nucleus, the pontine peduncle nucleus) involved in the regulation of REM sleep, which leads to the loss of normal inhibition of motor neurons spinal cord during REM phase [100]. This disorder is often present in the period preceding the onset of motor symptoms (prodromal period) and, among the prodromal symptoms in the context of α-synucleinopathies, they are those that would have the greatest risk of phenoconversion to full-blown PD (their presence is associated with a high probability of developing the disease in the future). Dysautonomic disorders are common: constipation is the most frequent symptom in the prodromal period, but urinary disorders (urinary incontinence and urinary frequency), orthostatic hypotension, dysphagia and dysfunctions of the sexual sphere are also observed. Psychiatric disorders, such as

depression, anxiety and cognitive dysfunction up to dementia, are typical of the most advanced stages of the disease and justified by cortical involvement, which, according to Braak's theory, is the latest event in the pathogenesis of the disease. Psychosis and hallucinations may also be present. Another disorder frequently reported in the prodromal phase is hyposmia, or the reduction of olfactory sensitivity, justified by the deposition of αSyn^{D} aggregates at the level of the olfactory bulbs [36,92,93,98,101].

- DIAGNOSIS

Given the numerous overlaps between the clinical aspects of PD and those of other pathological pictures, first of all atypical parkinsonisms, the possibility of misdiagnosis must be considered. Indeed, according to a meta-analysis, the accuracy of the clinical diagnosis of PD does not exceed 80% [102]. The diagnosis of PD is a clinical diagnosis and remains a diagnosis of a presumptive nature, since it is possible to make a diagnosis of certainty only in two cases: with the search for disease genes in cases of genetically determined PD, or with the finding in autopsy of the neuropathological characteristics typical of the disease in sporadic PD [98]. In 2015, the Movement Disorder Society (MDS) drafted criteria for the clinical diagnosis of PD [103]. These criteria, although initially intended for use in research, are currently the most widely used for clinical diagnosis. According to the MDS, the clinical diagnosis of PD is based on the finding, on neurological physical examination, of a parkinsonism defined by the presence of bradykinesia and at least one other sign of muscle rigidity and resting tremor of 4-6 Hz frequency. This essential requirement is associated with support criteria (excellent response to levodopa therapy; presence of levodopa-induced dyskinesia; resting tremor of a limb; presence of hyposmia or cardiac sympathetic denervation on ^{123}I-MIBG scintigraphy), exclusion criteria (unambiguous cerebellar signs; vertical gaze paralysis; diagnosis of frontotemporal dementia; arkinsonism limited to the lower limbs for more than 3 years; use of drugs with anti-dopaminergic effects; absence of response to levodopa; cortical sensory deficit, apraxia of the limbs, progressive aphasia; normal pre-synaptic dopaminergic signaling on imaging) and the so-called red flags (rapid progression of walking deficit; no progression at 5 years; severe dysphonia, dysarthria or dysphagia within 5

years; inspiratory stridor; severe autonomic dysfunction within 5 years; recurrent falls within 3 years; severe anterocollous or limb contractures within 10 years; absence of non-motor symptoms typical of PD at 5 years; persistent symmetry of motor symptoms), in the presence of which an alternative diagnosis is suspected.

Starting from the essential finding of parkinsonism, based on the presence or absence of support, exclusion and red flags criteria, two different diagnostic categories can be outlined: clinically established PD and clinically probable PD. The clinically established diagnosis of PD includes: finding of parkinsonism, or bradykinesia plus at least one other sign between tremor at rest and rigidity; at least 2 supporting criteria; absence of exclusion criteria; absence of red flags. The diagnosis of clinically probable PD, on the other hand, includes: finding of parkinsonism, or bradykinesia plus at least one other sign between tremor at rest and rigidity; absence of exclusion criteria; presence of a maximum of 2 red flags, counterbalanced by as many support criteria.

What emerges from the MDS criteria validation study is that the two diagnostic categories have different levels of accuracy: the diagnosis of clinically probable PD is associated with high sensitivity and specificity values, respectively 96% and 95%, while the diagnosis of clinically established PD is even more specific (98%), thus minimizing the possibility of false negative diagnoses, but due to the more stringent criteria it has a lower sensitivity (60%). In any case, a possible limitation of the MDS diagnostic criteria is their application in the diagnosis of the early stages of the disease, indeed, as it has been noted, the sensitivity and especially the specificity of the diagnosis of clinically probable PD in patients with a duration of illness shorter than 5 years were shorter than in patients with longer disease duration (92% and 87%, respectively). In cases where the findings of neurological objectivity are not of univocal interpretation, brain scintigraphy (SPECT) with DaTscan, a tracer that binds to the dopamine transporter (DaT) present in the pre-synaptic neurons of the synapse, can be used and therefore investigates the state of dopaminergic transmission [93]. If the tracer uptake is demonstrated, it means that the neuron is intact and therefore the signaling is functioning, on the contrary a hypocaptation is a sign of neuronal degeneration. The sensitivity of SPECT with DaTscan in

detecting neuronal loss at the level of the nigrostriatal pathway is high (98%) [104], however it is not possible to distinguish PD from atypical parkinsonisms (MSA, PSP), as also in this pathologies hypocaptation of the tracer is detected. Motor symptoms are instead assessed using the Movement Disorder Society-Unified Parkinson's Disease Rating Scale (MDS-UPDRS). The knowledge of the neuropathological characteristics of PD and of the wide overlaps it shows with DLB, Parkinson's disease with dementia and other neurodegenerative diseases is increasingly widespread, so much so that the term 'Lewy Body Disorders' (LBDs) is used, with reference to a spectrum of morbid conditions whose common pathological substrate is represented by Lewy bodies [105].

- PROGNOSIS

PD has a progressive course, characterized by a gradual worsening of the clinical condition. However, a relatively long coexistence with the disease is possible, as evidenced by a meta-analysis according to which the survival of patients after the diagnosis of PD ranges from 7 to 14 years [106]. The most frequent cause of death is aspiration pneumonia [107]. The stability over time of the clinical conditions, as well as their too rapid decay, are not typical characteristics of PD and must raise the suspicion of an alternative diagnosis; they are in fact included among the red flags of the MDS diagnostic criteria.

- THERAPY

For the treatment of motor symptoms, the pivotal therapy of PD consists in the administration of levodopa, a precursor of dopamine, which acts on the deficient dopaminergic signaling. It is currently considered the gold standard therapy for PD and is administered in the form of tablets associated with inhibitors of the peripheral dopadecarboxylase enzyme such as carbidopa or benserazide [93]. This enzyme converts levodopa into dopamine; if its action were not inhibited, the administered levodopa would be completely metabolized at the peripheral level and could not reach the CNS. Prolonged use of levodopa is however linked to the development of motor complications, which are estimated to affect up to 50% of patients after 5 years of disease [92]. These complications are dyskinesias, or involuntary movements with a choreic or

dystonic aspect related to the peak of plasma concentration of the drug, and motor fluctuations, or the alternation of moments in which motor performance is clearly better (ON periods) and moments in which they are worse (OFF periods). Motor complications are largely due to the short plasma half-life of levodopa and the possible variability in the gastrointestinal absorption of the drug; for this reason, during the disease there is a tendency to progressively increase the administration of levodopa and to administer other drugs in addition to levodopa, such as the inhibitors of the catechol-Ometyltransferase (COMT) enzyme. Drugs of this class (entacapone, tolcapone, opicapone) inhibit the enzyme that degrades levodopa, thus increasing its half-life, and are especially indicated in patients who develop motor complications [108]. Dopamine agonist drugs (ropyrinol, pramipexole, rotigotine), which act by mimicking the effect of dopamine at the level of dopaminergic receptors are indicated both in the early stages of the disease, even in place of levodopa, and in the later stages in association with it, to avoid motor complications [92]. The rationale for their use in late stages lies in the longer half-life compared to levodopa and in the synergistic effect on dopaminergic receptors obtainable with the combined use of dopamine agonists and levodopa. A further class of drugs are monoamine oxidase B (MAO-B) enzyme inhibitors (selegiline, rasagiline and safinamide). MAO-B represents another dopamine degradation mechanism, so these drugs essentially act by increasing the neurotransmitter's half-life [109]. In most cases, the motor complications associated with the use of levodopa tend to become increasingly severe; therefore, in the advanced stages of the disease in which the available therapeutic combinations are exhausted, second level therapies are evaluated. These are the continuous infusion of levodopa, after placing a percutaneous endoscopic gastrostomy (PEG), directly in the intestine, which guarantees stable levels of the active principle in the blood, and deep brain stimulation (DBS), consisting in the implantation of leads at the level of the basal ganglia [92]. The functioning of DBS is based on the electrical stimulation of the basal ganglia, regulating their signaling and considerably alleviating the motor symptoms of parkinsonism [110]. For the treatment of non-motor symptoms, it must be considered that they often do not respond to dopaminergic therapies [92], it is therefore necessary to use drugs that act on specific

conditions. As for dysautonomic disorders, orthostatic hypotension can be treated by acting on the volume expansion with fludrocortisone, which increases salt and water retention, or on the arterial tone, with the α1-adrenergic agonist midodrine. Drugs with antimuscarinic action such as oxybutynin or tolterodine are indicated for urinary incontinence, since they increase the relaxation of the detrusor muscle of the bladder, while constipation can be treated with osmotic laxatives such as macrogol and lubiprostone [111]. Antipsychotics such as quetiapine and clozapine are indicated to manage possible behavioral disorders. Finally, the use of cholinesterase enzyme inhibitors such as donepezil and rivastigmine can be considered to treat cognitive disorders in advanced stages of the disease, motivated by the fact that, at the basis of the cognitive deficits in PD, there is thought to be a decrease in cholinergic signaling [112].

1.2.2 Multiple system atrophy

As already mentioned, MSA is characterized by deposition of αSyn^D in the cytoplasm of oligodendrocytes in different regions of the CNS. From a clinical point of view, MSA is part, together with PSP and CBD, of the so-called atypical parkinsonisms, that are pathologies that have some characteristics in common with PD, but which differ from the latter in other substantial traits, including specific clinical/pathological aspects, response to therapies and temporal evolution.

- EPIDEMIOLOGY AND ETHIOPATHOGENESIS

MSA is a rare neurodegenerative disease, with an incidence of about 0.6 cases per 100000 inhabitants per year and a prevalence of 3.4 to 4.9 cases per 100000 inhabitants, which increases to almost 7.8 per 100000 if we consider the population over 40 years of age. The parkinsonian variant (MSA-P) is 2 to 4 times more frequent in Western countries, while the cerebellar variant (MSA-C) is prevalent in Asian countries. There is no clear epidemiological difference between the two sexes, who are equally affected by MSA, and the average age of onset of the disease is between 50 and 60 years. Median survival is 6-9 years from onset of symptoms. MSA is considered to be a sporadic disease, although a possible concomitant role of

environmental, genetic or epigenetic factors has been hypothesized. A higher prevalence of the disease has been observed in some regions of the world (North America, Europe, Japan) and in some ethnic groups, where rare familial forms of MSA have also been identified linked to specific mutations (loss of function mutation of the COQ2 gene, coding for the enzyme that synthesizes coenzyme Q10, in Asian patients) or to genetic polymorphisms (α-synuclein locus, in European patients). The pathogenetic process of MSA has not yet been fully understood and is still being researched. Hypotheses have been formulated regarding the sequence of pathogenetic events that would be at the basis of the disease: the formation of cytoplasmic αSyn^D deposits in oligodendrocytes would be preceded by the displacement of phosphoprotein 25α (p25α), a stabilizer of the myelin sheath, in the soma of oligodendrocytes. This would lead to a greater uptake and/or increased expression of αSyn in oligodendrocytes and it would then be precisely the interaction between p25α and αSyn to cause phosphorylation at the level of serine 129 and the aggregation of αSyn in insoluble cytoplasmic inclusions. The presence of these protein aggregates not only interferes with the neuronal support function performed by oligodendrocytes, but also causes abnormally shaped αSyn^D to be released into the extracellular space and picked up by neighboring neurons, causing the formation of protein inclusions also in the neuronal area. Loss of trophic and supportive function of oligodendrocytes, associated with neuronal dysfunction secondary to αSyn^D inclusions and activation of microglia due to reactive neuroinflammation processes lead to neuronal loss and degeneration of specific brain areas, resulting in astrogliosis. Finally, αSyn^D would be able to propagate to other brain areas, causing them to degenerate [113–115].

The localization and deposition patterns of αSyn^D have allowed the identification of two distinct clinical-pathological variants of MSA:

- the parkinsonian variant (MSA-P), characterized by glial cytoplasmic inclusions (GCIs) of αSyn^D observed mainly at the level of the nigrostriatal pathway;
- the cerebellar variant (MSA-C), with prevalent localization of the protein in the olive-ponto-cerebellar bundles.

So, the areas that most undergo degeneration in MSA are the nigrostriatal pathway, the olive-pontic-cerebellar bundles but also some regions of the autonomic nervous system, which include the hypothalamus, the noradrenergic and serotonergic nuclei of the brain stem and the dorsal vagus nucleus. These areas reflect the predominant clinical findings in MSA: parkinsonism in the MSA-P variant, cerebellar ataxia in MSA-C and, in both variants, dysautonomic symptoms.

- CLINICAL ASPECTS

From a clinical point of view, MSA is characterized by disorders of the autonomic sphere (present in all patients); signs and symptoms of extrapyramidal involvement that configure a picture of parkinsonism (prevalent in MSA-P); signs and symptoms suggestive of cerebellar involvement (prevalent in MSA-C). In reality, the absolute correspondence between the two parkinsonian and cerebellar variants and the possible clinical presentations should not be considered definite, given that, as has been found, with the temporal evolution of the disease the prevalent motor disorder can change, and it is possible that, for example, a patient with a diagnosis of MSA-P also develops cerebellar symptoms at some point [116]. The two names of MSA-P and MSA-C refer to the type of motor disorder prevalent at the time of diagnosis, but it is not excluded that it may vary over time.

- Dysautonomy. Dysautonomic disorders involve multiple systems and apparatuses. For example, orthostatic hypotension is frequent. The definition of orthostatic hypotension provides a reduction in systolic blood pressure of at least 20 mmHg or diastolic blood pressure of at least 10 mmHg over the first 3 minutes from the transition from the supine to standing position. However, since the dysautonomic component is quite marked in MSA, it is not uncommon to find hypotension levels even more extreme than these values; for this reason, in the criteria of the Second consensus statement on the diagnosis of MSA it was decided to include more pronounced hypotension cutoffs than those of the standard definition, whose finding allows the diagnosis of probable MSA. Less marked degrees of hypotension are instead considered for the diagnosis of possible MSA. Genitourinary disorders are also often present, which include both problems with

urination (urinary incontinence, urgency, difficulty in completely emptying the bladder or urinary retention) and sexual disorders (erectile dysfunction in men, reduced genital sensitivity in women). Among the disorders of the gastrointestinal system, the most frequent is obstinate constipation, but dysphagia, diarrhea, feeling of fullness after early prandial, nausea and vomiting are also often reported. Vasomotor disorders are also present, with dyschromia of the extremities and thermoregulation disorders such as hypohidrosis or anhidrosis. Secretomotor disorders (sialorrhea, xerostomia, xerophthalmia), abnormalities of pupillomotor reflexes (excessive intolerance to daylight), and respiratory disorders such as stridor nocturnal laryngeal and sleep apnea are also sometimes present. Finally, frequent are the RBD, such as nocturnal agitation and restless dreams. Dysautonomic disorders usually precede the onset of motor symptoms by months or years: a study found that in 75 % of the patients analyzed the dysautonomic disorders had started 4 years before the onset of the motor symptoms. The dysautonomic disorders are therefore prodromal with respect to the other manifestations of MSA; it is important to take this aspect into account for the early diagnosis of the disease [113,115–118].

- Parkinsonism. Parkinsonism signs and symptoms include bradykinesia, stiffness and postural instability with a tendency to fall, which occurs earlier than in PD. Tremor is less common and is a positional or intentional tremor, in contrast to the resting tremor typical of PD. Parkinsonism of MSA shows, in line with other atypical parkinsonisms, an inconsistent and partial response to levodopa therapy, which is effective only in 30-40% of patients [113].
- Cerebellar involvement. Cerebellar signs and symptoms include ataxic walking with postural instability, difficulty in articulating speech (dysarthria), ataxia of the limbs and oculomotion disorders such as nystagmus and hypometric saccades. Finally, signs of dysfunction of the pyramidal pathways (as Babinski sign and hyperreflexia), frontal executive dysfunctions, pathological crises of crying or laughter of the pseudobulbar

type, myoclonus of the limbs and peri-buccal and dystons to orofacial can be found. In addition, axial deformities such as the anterocollo, or an exaggerated anteposition of the head, the Pisa syndrome and camptocormia can also be detected [115].

- DIAGNOSIS

From a clinical point of view, what has been observed in patients with MSA is in part comparable to the findings present in other neurodegenerative diseases, in particular PD. For this reason, misdiagnosis is frequent, especially at the onset and in the first years of the disease and in the context of α-synucleinopathies, with a diagnostic error rate of about 30% [119]. The first and most important diagnostic tool is the observation of clinical aspects. The diagnosis can then be supported by imaging and nuclear medicine examinations, but no examination is able to give diagnostic certainty, as there is in fact no absolutely pathognomonic trait of the disease. As for PD, at the moment the diagnosis of certainty is obtained only with the autopsy neuropathological assessment. The criteria of the Second consensus statement on the diagnosis of MSA identify three different categories of diagnostic classification, which divide the clinical diagnosis of MSA into probable and possible [116]. Diagnosis is probable if there is a sporadic, progressive disease with onset in adulthood, characterized by strictly defined dysfunctions of the autonomic nervous system, such as urinary incontinence, erectile dysfunction and orthostatic hypotension more severe than standard diagnostic criteria, in association with an unresponsive parkinsonism to levodopa (MSA-P) or a cerebellar syndrome (MSA-C). The diagnosis is finally possible in case of a sporadic, progressive disease, with onset in adulthood, characterized by parkinsonism or cerebellar syndrome, associated with at least one sign of dysautonomic alteration (urinary urgency, incomplete bladder emptying, erectile dysfunction, orthostatic hypotension which falls standard diagnostic criteria) and at least one sign of clinical alteration (Babinski's sign, hyperreflexia, stridor, choking episodes) or imaging (atrophy of the basal nuclei and cerebellum in magnetic resonance imaging, hypometabolism of the same sites on PET with 18-FDG fluorodeoxyglucose which allows the study of glucose metabolism in the brain, or signs of nigrostriatal denervation on SPECT).

- PROGNOSIS

The natural history of MSA foresees a progressive course which, following a gradual worsening of both motor and non-motor symptoms, leads to death within 9 years on average from onset [115]. Within 3 years from onset of motor symptoms, 50% of patients are no longer able to walk independently and there is a marked impairment of autonomy in the activities of daily living, up to bed rest within 6-8 years from onset. Exitus occurs mainly due to complications related to bed rest or acute dysregulation of the autonomic centers of the trunk that control the cardiovascular and respiratory systems. Negative prognostic factors are an advanced age at onset, the MSA-P phenotype and the early onset of severe autonomic dysfunction, while the factors that predict a more positive outcome include the MSA-C phenotype and the later onset of dysautonomia [113].

- THERAPY

With regard to therapy, there are currently no specific drugs for MSA, nor with disease-modifying potential, which are capable of significantly modifying the course of the disease. Treatment therefore aims to manage symptoms, both motor and non-motor. Parkinsonian symptoms are treated with levodopa, although the effectiveness of the therapy is much lower than in the case of PD. The response rate in MSA is estimated to be around 30-40%, and tends to decline over time. In order to test the effectiveness of the drug, the doses of levodopa can be gradually increased up to 1g/day, if tolerated [116]. For cerebellar symptoms there is no specific drug, although clinical trials have shown benefits in the administration of buspirone or gabapentin [120]. For incontinence or urinary urgency, linked to bladder over-activity, anti-muscarinic drugs can be used with the aim of inducing relaxation of the detrusor muscle. By the same principle, urinary retention can be relieved by cholinergic agents that cause the detrusor to contract, and as a last resort, self-catheterization can be used [113]. For monitoring orthostatic hypotension, it is recommended for patients to perform gradual postural transitions, avoid meals that are too rich and exposure to too high temperatures and excessively humid environments, avoid alcohol (in as vasodilators) or coffee (for the diuretic effect). From a pharmacological point of view, it is possible

to administer sympathomimetics such as midodrine, an α1-agonist that acts on arterial α-receptors with a vasoconstriction effect and therefore an increase in pressure, or droxidopa, a precursor of noradrenaline, which binds to the same vascular receptors [115]; desmopressin, a synthetic analogue of antidiuretic hormone (ADH), can also be administered, while fludrocortisone, a corticosteroid that acts by increasing salt and water retention in the kidney and therefore blood volume, is considered off-label, as its effectiveness has not yet been proven [113]. Positive pressure ventilation (C-PAP) is useful for resolving nocturnal stridor and sleep apnea [121]. Constipation is treated with non-pharmacological measures, such as increased physical exercise, increased intake of fibers and liquids and possibly laxatives as needed [122]. In the treatment of erectile dysfunction, phosphodiesterase-5 inhibitors, such as sildenafil, can be considered, taking into account however that the vasodilating effect of these drugs can exacerbate the symptoms of orthostatic hypotension [115]. Finally, RBD can be managed with drugs belonging to the benzodiazepine group, such as low-dose clonazepam, or with regulators of the sleep-wake rhythm such as melatonin [113].

1.2.3 Dementia with Lewy bodies

DLB is a neurodegenerative disease clinically characterized by progressive dementia, cognitive fluctuations, visual hallucinations and parkinsonism and, from a neuropathological point of view, by the presence of Lewy bodies at the level of cortical neurons, the limbic system and the nuclei of the brainstem. The first description of the disease dates back to 1961, when Okazaki et al. reported the clinical cases of two patients, aged 70 and 69, who had developed progressive dementia and severe extrapyramidal stiffness, whose autopsy revealed the presence of Lewy bodies in the cerebral cortex. In the following years, similar cases were reported in the literature. In 1990, Hansen et al. reported that 36% of patients who had received the clinical diagnosis of AD actually showed Lewy bodies on autopsy and decided to call them "Lewy Body Variant of Alzheimer's disease" [123]. It was only in 1995, within the CDLB (Consortium on DLB), culminating in the first drafting of the clinical criteria for the diagnosis of DLB, that the shared and

currently used term of "Lewy Body Dementia" was proposed. This "controversial" terminological history reflects the transversal dimension of DLB, which affects various morbid conditions, as well as the neuropathological heterogeneity of the DLB itself [124].

- EPIDEMIOLOGY AND ETHIOPATHOGENESIS

From its first appearance on the nosographic scene, DLB was considered a rare cause of dementia. Therefore, thanks to the advent of more specific and sensitive immunohistochemical techniques for the recognition of pathological lesions in autopsy (in particular, anti-αSyn antibodies), it has increasingly become a common cause of dementia, second only to AD [125]. In fact, it is currently estimated that DLB represents up to 20-25% of all cases of dementia observed in old age [126]. From an epidemiological point of view, most of the studies conducted so far have not revealed a particular predilection between the two sexes, who are equally affected. The age of onset is between 50 and 85 years, with an average of 68 years. The prevalence of DLB appears to be up to 5% in the general population and up to 30.5% in all cases of dementia, with an annual incidence rate of 0.1% in the general population and 3.2% referred to all new cases of dementia [127]. Despite numerous efforts to identify increasingly accurate and specific diagnostic criteria to make a correct diagnosis of DLB, the prevalence rates of DLB are found to be up to 50% lower than the post-mortem rates of DLB identified during autopsy. The etiology of the disease is still unknown, as there are potential risk factors. As in AD, it has been observed that in DLB there is a more frequent association with the ε4 allele of apolipoprotein E (apoE), the presence of which seems to be associated with a more rapid progression of cognitive deficits [127,128]. Only rare familial cases of DLB have been described, therefore also the genetic susceptibility still remains largely obscure [129]. Despite this, it is likely that genetic factors may also play a role in the development of DLB. For example, a potential candidate as a genetic susceptibility factor is represented by the GBA gene that encodes the enzyme glucocerebrosidase. Indeed, GBA mutations tend to be associated mainly with pathological pictures characterized by the presence of diffuse neocortical Lewy bodies, as observed in the brain tissue of patients with DLB [130]. Many of the patients with DLB have β-amyloid plaques and neurofibrillary tangles on

autopsy, often of such magnitude as to comply with the criteria for AD. The contextual presence of these neuropathological elements affects the clinical phenotype, which is closer to AD and with less typical characteristics of DLB. This pathological heterogeneity can also be present in AD, in fact, one to two thirds of patients diagnosed with AD have Lewy bodies in allo- and neo-cortical areas, defining the 'Lewy Body Variant of Alzheimer's disease (AD-LBv)' [123].

➢ CLINICAL ASPECTS

Similarly to the neuropathological aspects, the spectrum of clinical symptoms of DLB is also broad. The main categories of symptoms are represented by cognitive deficits (which include dementia, a "central" clinical characteristic and cognitive fluctuations, a "core" clinical characteristic for diagnosis), neuropsychiatric symptoms (in particular visual hallucinations, also considered a "core" clinical characteristics), extrapyramidal motor signs (third "core" characteristic), sleep disturbances and autonomic nervous system abnormalities (respectively "suggestive" and "supportive" clinical characteristics for the diagnosis of DLB) [131].

- Dementia. Dementia is the central and essential clinical feature for the clinical diagnosis of DLB. It is defined as a progressive cognitive decline of an entity sufficient to interfere with normal daily and occupational activities. Cognitive decline is the onset symptom of DLB in most cases and typically presents with recurrent episodes of confusion on a background of progressively worsening deterioration. Patients with DLB show both cortical and subcortical cognitive alterations with prevalent attention disorders, dysexecutive and visuospatial disorders. This cognitive profile differs from AD, as patients with DLB perform better in memory tests and worse in tests that explore visuospatial functions [127].
- Parkinsonism. Extrapyramidal motor signs are present in 25-50% of DLB patients at the time of diagnosis. However, the diagnosis of DLB can be made even in the absence of this characteristic motor profile, although it is of great help in the differential diagnosis compared to other forms of dementia (AD and vascular dementia) in which parkinsonism occurs more rarely [127,132]. Unlike PD, the pattern of extrapyramidal

signs in DLB shows an "axial tendency", with more pronounced postural instability and facial hypomimia and a propensity to show less tremor at rest [126]. The assessment of motor characteristics can be made more difficult by the simultaneous presence of cognitive impairment, thus the use of a simple UPDRS subscale that contains only those items that can be reliably assessed in DLB regardless of the severity of dementia (resting tremor, action tremor, bradykinesia, facial expression, rigidity) is recommended [126].

- Cognitive fluctuations. Cognitive fluctuations are spontaneous changes in cognitive functions, attention and alertness. The cognitive fluctuations that appear in DLB have the characteristics of a confusional state (delirium) that arises in the absence of identifiable precipitating factors. This phenomenon is characterized by a sort of "coming and going" of cognitive functions and vigilance and show extreme variability in duration (minutes or hours) and in alertness, up to a "pseudo-catatonic" state. [133].
- Visual hallucinations and other neuropsychiatric symptoms. Visual hallucinations are the most characteristic neuropsychiatric symptoms of DLB and it is their presence, especially in the early stages, which helps to distinguish them from the episodic perceptual disturbances that appear transiently and in the more advanced stages of dementias of other etiology [126,134]. Only a small portion of patients report also olfactory, auditory or tactile hallucinations. A frequency of visual hallucinations has been documented in a variable percentage from 59 to 85% of DLB cases confirmed at autopsy. Furthermore, the high prevalence of RBD in many of the patients with DLB raises the possibility that a potential mechanism is "dream intrusion" [135].
- Other neuropsychiatric symptoms. DLB is associated with a higher frequency of paranoid delusions and especially delusions of misidentification with prevalence values ranging from 13 to 75% [136]. Major depression appears in about 19% of patients at onset up to a prevalence of 50% during the natural course of the disease. The most common behavioral symptoms are represented by anxiety (67.4%), followed by depression (61.9%) and apathy (57.6%).

- Dysautonomia. The clinical manifestations of dysautonomia include orthostatic hypotension, bladder and intestinal motility disorders, changes in thermoregulation, anhidrosis and sexual dysfunctions [126]. Autonomic dysfunction typically appears after the development of cognitive and motor deficits, although it can sometimes precede its onset. Orthostatic hypotension has a 50% frequency in DLB [137,138]. Other dysautonomic manifestations include urinary and gastrointestinal dysfunction. Constipation is the main gastrointestinal manifestation. Although the mechanism of gastrointestinal dysfunction is multifactorial, Lewy body disease likely contributes to esophageal dysmotility, delayed gastric emptying and colic dysfunction, since Lewy bodies have even been found in nerve plexuses in DLB [139].
- REM sleep behavior disorder. This disorder was recently added as a supportive diagnostic criterion for DLB. Of particular interest is the observation that RBD can precede the onset of other clinical features of DLB even by years or decades, as is often observed in other α-synucleinopathies (PD, MSA). Sleep disorders can contribute to exacerbating some clinical manifestations of DLB, such as excessive daytime sleepiness and, above all, cognitive fluctuations; therefore, their treatment can also positively influence the cognitive aspects [127].

➢ DIAGNOSIS

All authors agree on the importance of an accurate clinical diagnosis, not only because DLB is characterized by a specific clinical picture that differs from that of other common types of dementia (such as AD, vascular dementia and frontotemporal dementia), but also for its peculiar therapeutic management. First, patients with DLB show extreme sensitivity to the adverse effects of neuroleptics, with a significant increase in morbidity and mortality associated with their use, which makes the treatment of psychotic symptoms problematic. On the other hand, patients with DLB show a good response to treatment with AChEI (cholinesterase inhibitors) which are tolerated and which substantially improve the cognitive picture and neuropsychiatric disorders [127].

The diagnosis of DLB is made according to clinical criteria revised in 2017 by the DLB Consortium. In the latter circumstance, the positivity of the DaT-Scan examination was introduced among the "suggestive" characteristics for the diagnosis and a greater diagnostic weight was given to some clinical characteristics suggestive of DLB such as the marked sensitivity to neuroleptics and the RBD. The presence of progressive dementia is a fundamental requirement for the diagnosis of DLB and therefore constitutes the "essential" clinical feature. The dementia must be of a magnitude that significantly interferes with normal social and/or work activities. Unlike AD, a marked memory deficit may not be present in the early stages, but generally appears with the progression of the disease. Conversely, impairments in attention, executive function, and visuospatial abilities are often prominent symptoms in the early stages. As previously described, in addition to the essential feature, the diagnostic criteria also identify "core", "supportive" and "indicative" characteristics for the clinical diagnosis of DLB. There are five "core" characteristics: fluctuating cognition with pronounced variations in attention and alertness; recurrent visual hallucinations (typically well formed and detailed); REM sleep behavior disorder (which may precede cognitive decline); one or more spontaneous cardinal features of parkinsonism (bradykinesia, rest tremor, or rigidity); Two of them, together with the "essential" characteristic, are sufficient for the diagnosis of probable DLB, while one is sufficient for the diagnosis of possible DLB. The "indicative" features are represented by: reduced dopamine transporter uptake in basal ganglia demonstrated by SPECT or PET; abnormal (low uptake) 123iodine-MIBG myocardial scintigraphy; polysomnographic confirmation of REM sleep without atonia. If the presence of one or more "indicative" characteristics is associated with one or more "core" characteristics, the diagnosis of probable DLB is justified, if instead it is not associated with any "core" characteristic then the diagnosis of DLB is made possible. Finally, the "supportive" features (often present, but not sufficiently specific for the diagnosis as they also emerge in the context of other pathologies) include: Severe sensitivity to antipsychotic agents; postural instability; repeated falls; syncope or other transient episodes of unresponsiveness; severe autonomic dysfunction; apathy; anxiety; depression; relative preservation of medial temporal lobe structures on CT/MRI scan; generalized

low uptake on SPECT/PET perfusion/metabolism scan with reduced occipital activity and the cingulate island sign on FDG-PET imaging; prominent posterior slow-wave activity on EEG with periodic fluctuations. The diagnosis of DLB, on the other hand, becomes unlikely: a) in the presence of any other physical illness or brain disorder including cerebrovascular disease, sufficient to account in part or in total for the clinical picture, although these do not exclude a DLB diagnosis and may serve to indicate mixed or multiple pathologies contributing to the clinical presentation; b) If parkinsonian features are the only core clinical feature and appear for the first time at a stage of severe dementia [140].

As far as instrumental investigations are concerned, both structural (MRI) and functional (SPECT and PET) neuroimaging exams can be useful in the diagnosis of dementia and, in particular, some techniques can be useful in the differential diagnosis of DLB. MRI of the brain shows in most patients with DLB, a condition of atrophy affecting the medial structures of the temporal lobe and hippocampus of a significantly lower degree than in AD patients. This observation could partly explain the lower impairment of memory function in DLB, at least in the initial stages, compared to AD. SPECT documents occipital and parietal hypoperfusion in the DLB. The use of PET with (18-FDG) fluorodeoxyglucose documents occipital hypometabolism in DLB [141]. A key finding in DLB is the marked loss of dopaminergic presynaptic terminals in the striatum.

- PROGNOSIS

Given the numerous and diverse clinical symptoms of DLB, it is not surprising that patients with this type of dementia have a functional deficit and improvement in quality of life that is superior to those with AD, even when the degree of dementia is similar. The survival time from the diagnosis of dementia appears to be around 7.3 years for DLB to 8.5 years for AD. In addition to an increased risk of mortality in DLB compared to AD, it has also been observed that DLB is associated with higher socio-health costs, earlier institutionalization of patients and a greater burden of stress for caregivers [142].

- THERAPY

DLB is a relatively common disorder for which, however, there are still no pharmacological therapies capable of modifying the course of the disease, while only symptomatic treatments are available. Furthermore, it is a morbid condition that poses particular difficulties in therapeutic management, since the treatment of a certain symptom is potentially capable of exacerbating another. For example, treatment of psychiatric symptoms with antipsychotics can not only lead to worsening of extrapyramidal motor symptoms, but can also trigger severe hypersensitivity reactions to neuroleptics (particularly with the use of antipsychotic drugs) in about half of exposed patients [127]. On the other hand, antiparkinsonian drugs, administered to improve the motor picture, can concomitantly exacerbate visual hallucinations and cognitive disorders. This underlines the need to follow a line of intervention based on the careful assessment of clinical priorities and to start pharmacological treatment only when deemed necessary. In DLB there are important deficits of the neocortical cholinergic function and this deficit is correlated to the presence of visual hallucinations and to the overall severity of the cognitive deficit. Thus, drugs that increase central cholinergic function represent a rational therapeutic approach. Indeed, the studies conducted so far on cholinesterase inhibitors in patients with DLB have shown improvements in both cognitive and psychotic symptoms with donepezil [143], rivastigmine [144] and galantamine [145] in the absence of a significant worsening of motor function. Therefore, the use of AChEIs as first-line drugs in the treatment of the cluster of cognitive and psychotic symptoms in DLB is recommended. Regarding the motor symptoms, the therapy of extrapyramidal signs is based on the administration of levodopa as monotherapy at the lowest possible dose [126]. The other classes of dopaminergic drugs, such as dopamine agonists, selegiline, anticholinergics and amantadine, can cause adverse effects (such as confusion, somnolence and hallucinations) that effectively preclude their use in DLB [134]. Treatment of RBD is needed when the disorder becomes particularly intense and frequent. The goals of RBD therapy are to minimize injuries to patients and their bed partners and to reduce sleep fragmentation. Low dose of clonazepam is generally effective. Melatonin may also be beneficial,

both in combination with clonazepam and as monotherapy, in patients who do not respond to clonazepam or in those who cannot tolerate therapeutic doses [100].

1.2.4 Other α-synucleinopathies

- Parkinson's disease with dementia (PDD). When a person with PD develops cognitive impairment during progression then it is defined as Parkinson's disease with dementia. Prevalence was reported as 0.3%; however, in cases of advanced PD, the prevalence of dementia has been suggested to be even higher [146].
- Incidental Lewy Bodies (iLB). Lewy bodies and glial cytoplasmic (oligodendrocytic) inclusions can be observed in the brains of subjects without clinical symptoms [147–149]. Filaments of αSyn^D have been observed in the peripheral organs of clinically unaffected subjects [150]. Furthermore, Lewy bodies and pathological αSyn^D can be observed as a concomitant alteration in other neurodegenerative diseases.
- Pair autonomic failure (PAF). PAF is characterized by predominantly peripheral αSyn^D deposition in ganglia and autonomic nerves and tends to manifest itself in adulthood. The clinical feature is orthostatic hypotension, however other symptoms such as genitourinary dysfunction may precede or accompany this feature. When symptoms become relevant, a dizzying effect is felt, which may be associated with dizziness, vision changes, symptoms, fatigue and cognitive symptoms. In severe forms, orthostatic hypotension can lead to syncope, and it can also be accompanied by supine hypertension in about half of all patients. To date this phenomenon being incompletely understood, it is probably thought to be involved in hypersensitivity to denervation, impaired baroreflex control and residual sympathetic activity. Minimal neurological motor manifestations may be observed, with bradykinesia, tremors, or abnormal gait [151].

1.2.5 Differential diagnosis of α-synucleinopathies

As already stated, it is not easy to distinguish PD from atypical parkinsonisms: in both cases the findings on the DaT-scan are suggestive of nigro-striatal degeneration and often the clinical presentations can be very similar, if we consider that, for example, some of the non-motor symptoms of PD, such as dysautonomic disorders, are also found in MSA. As previously reported, however, ^{123}I-MIBG cardiac scintigraphy is able to differentiate patients with PD and MSA, showing tracer hypocaptation in the first case and normal or minimally reduced uptake in the second [152]. The use of skin biopsy is also useful in differential diagnosis: in PD deposits of αSyn are found mainly at the level of the post-ganglionic autonomic fibers, while in the MSA-P the deposits are more localized in the somatic nerve fibers [153]. Numerous morphometric indices obtained from the images of MRI of the brain have been proposed as possible markers for the differential diagnosis between PSP and PD. Among these, the MRPI (magnetic resonance parkinsonism index), appears to be promising in differentiating patients with PSP (demonstrating significantly higher MRPI values) than patients with PD [154]. The differential diagnoses of PD also include conditions such as essential tremor and dystonic tremor; in these cases, however, beyond the clinical aspects, the scintigraphy with DaT-scan is decisive, detecting a normal uptake of the tracer [98].

From a clinical point of view, a possible fact that can allow to differentiate PD from MSA is the presence of hypo/anosmia, which is more frequent and marked in PD than in MSA, in which patients show preserved or only moderately reduced olfactory functions [155]. In MRI, characteristic signs of MSA were identified: the hot cross bun sign (a cruciform hyperintensity in T2 sequences at the level of the pons) and the putaminal slit (a hyperintensity in T2 at the margin of the putamen). In MSA, atrophy of putamen, middle cerebellar peduncles, pons and cerebellum with dilation of the fourth ventricle is also observed. Finally, diffusion weighted imaging (DWI) sequences make it possible to distinguish MSA-P from PD, as in MSA-P the putamen and the middle cerebellar peduncle show greater tissue diffusivity with respect to PD [156]. MRI findings are usually normal in PD [157]. Finally, in the event that the clinical presentation was

predominantly characterized by isolated autonomic dysfunction, another possible differential diagnosis of MSA is PAF [158]. An incorrect or late diagnosis has important consequences on prognosis, clinical evolution and therapeutic treatment, also increasing the risk of adverse effects and reducing the possibility of being recruited for clinical trials.

Regarding DLB, the most important differential diagnoses are with PDD and AD [136]. In particular, for the differential diagnosis with PDD, the distinction is based solely on the temporal sequence of the appearance of cognitive deficits and motor symptoms. Clinicians adhere to the arbitrary 'one year rule', that is, when the cognitive symptoms appear within a year of the onset of parkinsonism, the diagnosis of DLB is made, if instead the dementia occurs after more than a year with respect to the motor symptoms the diagnosis of PDD is made. The common clinical and neuropathological characteristics would seem to support the hypothesis of a continuum between PDD and DLB [159]. In any case, there are no clinical features that allow to completely differentiate DLB from PDD, since the cognitive and psychiatric symptoms of patients with DLB and PDD are substantially the same and with a similar rate of progression. Both patient groups have well-formed cognitive fluctuations and visual hallucinations. Other features in common include dysautonomia, RBD, and particular sensitivity to adverse effects of antipsychotic drugs. Neuropsychological profiles share numerous aspects including the prevalent attentional, executive, visuospatial, language and behavioral abnormalities. Finally, no significant differences were found even in instrumental examinations, with similarities in the distribution pattern of cerebral flow to SPECT and PET, in the frame of nigrostriatal degeneration at SPECT and in the frame of reduction of cardiac noradrenergic innervation at cardiac scintigraphy with ^{123}I-MIBG [105,160,161]. Maintaining a distinction between PDD and DLB can be clinically useful, since therapeutic approaches may differ for patients with prevalent motor dysfunction versus those in whom dementia symptoms are prevalent. The greatest difficulty during the diagnostic process remains, however, the discrimination from AD. Indeed, as already mentioned, patients with DLB often receive the diagnosis of AD *ante-mortem* and it is only at the autopsy level that the diagnostic error is revealed. However, despite some similarities, numerous studies have shown that DLB has

greater visuospatial and attention deficits compared to AD, while AD is associated with greater deficits in memory and naming [133,162]. Other clinical manifestations that differ in the two diseases are visual hallucinations, parkinsonism and dysautonomia. Depression also appears to be more common in DLB compared to AD. The extrapyramidal motor signs are strongly suggestive of DLB, as they are unusual in the early stages of AD and vascular dementia. Useful information, again in terms of differential diagnostics, can be obtained by ^{123}I-MIBG. Myocardial scintigraphy with ^{123}I-MIBG has shown in numerous studies a reduction in the uptake of the tracer at the cardiac level compared to mediastinal uptake in DLB, as in PD, evidence of post-ganglionic autonomic dysfunction. On the other hand, in AD the distribution of ^{123}I-MIBG is comparable to that observed in healthy control subjects [163]. Yoshita et al. reported that myocardial scintigraphy can discriminate between DLB and AD diagnosed clinically with high levels of sensitivity and specificity [164].

1.2.6 New diagnostic approaches for α-synucleinopathies

As previously said, a definite diagnosis of α-synucleinopathy is based on the evaluation of histological features (e.g. neuronal loss) and on the presence of αSyn^D accumulations, which are analyzed by immunohistochemistry complemented by biochemistry in *post-mortem* tissues [165]. Indeed, DLB and PD shows predominance of intraneuronal cytoplasmic and neuritic deposits (cortical and brainstem type Lewy bodies and Lewy neurites), whereas MSA is dominated by glial cytoplasmic inclusions (Papp-Lantos bodies) [126]. Despite studies suggesting that the biochemical pattern of αSyn^D may differ in distinct α-synucleinopathies [166], there are however no biochemical or morphological features that allow unequivocal distinction of potential molecular subtypes of abnormally folded αSyn [165].

Conversely, probable or possible diagnosis of α-synucleinopathy might be made on the basis of international consortium guidelines, which reviewed clinical records and compared the sensitivity and specificity of proposed diagnostic criteria with neuropathologically verified cases. According to the revised criteria, probable diagnosis is usually made in cases that match a

significant number of proposed clinically discriminating features, whereas possible diagnosis is made in cases presenting atypical clinical manifestations [167,168]. Naturally, these assessments are based on clinical biomarkers that are not perfectly specific for α-synucleinopathy and hence the clinical diagnosis has been shown some degree of inaccuracy (Table 1.1).

Even though the clinical diagnosis of parkinsonism might be relatively simple, the specific diagnosis of PD, especially at the early stages, can be difficult. It has been reported that in patients with possible PD only 26% had autopsy confirmation, while in probable PD the diagnostic accuracy was 82% [169]. In DLB, clinical diagnostic criteria for probable DLB identify αSyn pathology with a sensitivity of about 80%, however, early diagnosis is less accurate due to the overlapping symptoms with other types of dementia [170]. In addition, 15–20% of patients with confirmed AD at autopsy showed concomitant DLB pathology, with only a minority of patients exhibiting clear diagnostic features of DLB [171].

α-synucleinopathy	Diagnostic accuracy	References
Parkinson's disease (PD)	80%	Postuma R.B., et al. Mov Disor (2015) 30, 12:1591 – 601 [172]
Dementia with Lewy bodies (DLB)	80%	Rizzo G., et al. J Neurol Neurosurg Psychiatry. 2018 Apr;89(4):358-366 [173]
Multiple system atrophy (MSA)	62%	Gilman S., Neurology. 2008 Aug 26;71(9):670-6 [116]

Table 1.1 Diagnostic accuracy of the main α-synucleinopathies.

The identification of new biomarkers, in addition to their implication in the diagnostic accuracy, would also be useful in the development of different therapies, which could allow to differentiate the α-synucleinopathies even before the development of motor symptoms. Early detection would make it possible to take advantage of these therapies at the onset of the early stages, just when it is possible to delay or prevent the onset of the disease, making it more effective. For these reasons, it is extremely important to find new biomarkers. The principal requirements for a good biomarker is its preciseness and reliability, as it should be also able to distinguish between the healthy and the diseased patients and to differentiate between different diseases [169]. Molecular and biochemical markers are evaluated based upon their sensitivity,

specificity, positive predictive value and negative predictive value [174]. Sensitivity and specificity are statistical measures of the performance of a biomarker or a diagnostic method, based on the typical binary classification test that is widely used in medicine. In this field, true or false terminology indicates if the assigned classification is correct or incorrect, while positive or negative denotes the positive or negative output of the medical test. For a clinical usage, biomarkers should have good sensitivity and specificity (e.g. ≥90% each) and a positive predictive value of approximately 80% or more [175]. One of the major problems in the diagnosis of α-synucleinopathies is the lack of a widely accepted sensitive diagnostic test or easily accessible biomarkers able to support neuropsychological evaluation, monitor disease progression and identify affected individuals in the early stages of the disease. The only certain and valid biomarker corresponds to αSyn^D that accumulates within the brain, as previously described. Indeed, morphological and biochemical identification of disease-specific misfolded proteins in *post-mortem* brain collected at autopsy is still the only methodology enabling to formulate a definite diagnosis of α-synucleinopathy [176].

New biomarkers have been recently added in clinical diagnostic criteria for some neurodegenerative diseases, such as CSF protein concentrations and imaging biomarkers. In particular, the presence of the neurofilament light chain (NfL) in CSF reflects central axonal degeneration and appears to be a possible biomarker in several neurological disorders characterized by rapid disease progression and the presence of neuronal damage. Since an increase in NfL was found in both MSA-C and MSA-P, this evaluation makes it possible to differentiate early MSA cases from early PD and DLB with considerable sensitivity and specificity [177]. More recently, an ultrasensitive assay was developed with the aim to detect the traces of αSyn^D that circulate in peripheral tissues and that, as already mentioned, cannot be identified with common diagnostic techniques due to their very low amount. This assay is called real-time quaking-induced conversion (RT-QuIC) and was first developed in the field of prion diseases.

1.3 The RT-QuIC assay

The recent advances in molecular and structural biology have provided insights into the processes involved in the pathogenesis of neurodegenerative diseases and have made it possible to recapitulate the protein misfolding process *in vitro* in a limited period of time through the development of innovative techniques, called seed amplification assays (SAAs), among which the RT-QuIC. This new methodology exploits the ability of misfolded proteins to transmit their abnormal conformation to normal monomers, which are used as substrate of reaction. Abnormally folded proteins are able to interact with these substrates and induce monomers to change conformation and subsequently aggregate. Therefore, the addition of misfolded proteins (considered "seeds") to the substrate is able to trigger an aggregation phenomenon, known as "seeding effect" that might be exploited for a diagnostic and therapeutic point of view.

The RT-QuIC is based on this very principle of seeding-nucleation propagation of misfolded proteins. The assay is performed in a multi-well plate, in which the reaction substrate is usually a recombinant or synthetic protein and amyloid formation is monitored by Thioflavin T (ThT), an amyloid-specific fluorescent dye. Upon binding to amyloid fibrils, the central C–C bond connecting the benzothiazole and aniline rings of ThT molecule is immobilized and fluorescence signal strongly increases when excited at 450 nm, and detected at approximately 482 nm [178]. During the RT-QuIC reaction, we distinguish: an incubation phase, in which the sample containing minute amounts of misfolded protein is incubated with an excess of recombinant substrate to induce growing of amyloid polymers; an agitation phase, that allows to break down the polymers and to multiply the number of nuclei. After each cycle, the number of seeds increases in an exponential fashion, thus accelerating the seeding-induced conversion of the substrate into amyloid fibrils [179].

If we represent on a graph the aggregation process that occurs during RT-QuIC, in which we report the time on the abscissas and the fluorescence values on the ordinates, we obtain a curve with a sigmoidal shape in which we can identify 3 phases:

- Lag phase: initial phase of conformational change of the recombinant substrate and formation of the first aggregates, even if they are not a sufficient number to lead to an increase in fluorescence intensity.
- Exponential phase: phase in which we will observe the formation and growth of recombinant amyloid fibers with a very rapid speed, with consequent exponential increase of fluorescence.
- Plateau phase: equilibrium phase in which the fluorescence manages to maintain a constant value, given that the amyloid fibers have reached their maximum concentration (Figure 1.5).

The recombinant substrate, subjected to these cycles of incubation and shaking, is usually prone to aggregate, however, the fibrillization reaction is notably accelerated by the presence of pre-formed aggregates in a given sample. Therefore, in reactions containing seeds the lag phase is reduced and ThT fluorescence levels exponentially increase. RT-QuIC demonstrated high sensitivity and specificity in detecting traces of misfolded prion protein (PrP^{Sc}) in both animal and human biological samples (e.g, CSF, blood, OM) [180–187]. It has proved extremely reliable for the clinical diagnosis of prion diseases and has recently become part of the diagnostic criteria for the sporadic form of the Creutzfeldt-Jakob disease [188].

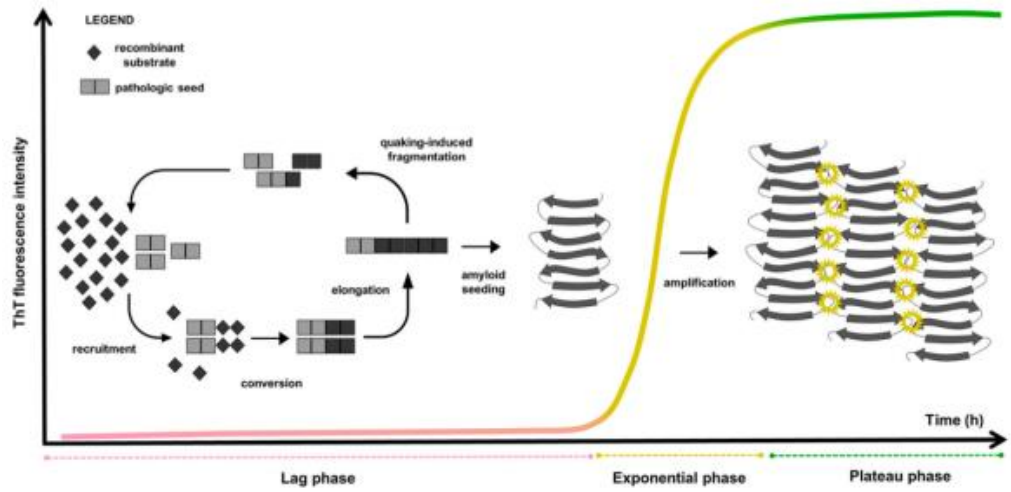

Figure 1.5 Representation of the three phases of the RT-QuIC reaction: the lag phase, the exponential phase and the plateau phase (From *Candelise 2020*).

Following the success achieved in the field of prion diseases, this technology has been extended to other pathologies caused by prion-like proteins, including α-synucleinopathies, with promising results.

1.3.1 The RT-QuIC in the field of α-synucleinopathies

Starting from late 2016, RT-QuIC assays have been applied to detect αSyn^D in the CSF of patients affected by α-synucleinopathies. Despite the differences in the analytical protocols, the assays produced similar results in terms of sensitivity and specificity in identifying α-synucleinopathy derived samples [189,190]. In the subsequent year, an independent research group developed another RT-QuIC protocol with a different experimental setting and by using a mutated form of recombinant αSyn (rec-αSyn), used as reaction substrate [191]. Subsequent studies confirmed the optimal performance of CSF RT-QuIC analysis in differentiating PD and DLB from controls. However, the same is not true for MSA. Whereas in some protocols αSyn seeds have been detected in the CSF of MSA patients with good sensitivity [192], in general, the tests showed a decreased ability in detecting MSA compared to PD and DLB [193,194], with diagnostic performances also depending on the MSA phenotype (MSA-C or MSA-P) [195].

The very encouraging results obtained from the analysis of CSF samples make RT-QuIC a promising tool to support the diagnosis of α-synucleinopathies. However, in order to apply this assay for monitoring disease progression and evaluating the efficacy of disease modifying treatments, there is the need of more accessible biomatrices in which repeated sampling is possible. Different easily accessible biological matrices have now gained attention. For instance, the multi-center Systemic Synuclein Sampling Study identified the skin biopsy, a minimally invasive procedure, as suitable biological matrix to investigate αSyn species, due to the richness in autonomic nerves [196,197]. Another interesting tissue is the olfactory mucosa (OM), that represents a window on the olfactory bulb [198], is one of the earliest sites of αSyn pathology in PD [199] and is easily collectable by a procedure known as nasal brushing [200]. These tissues were deepen analyzed in the field of prion diseases and, starting from this evidence, they are now

considered also for αSyn RT-QuIC. In skin biopsies, RT-QuIC showed performances comparable to CSF in differentiating PD and DLB patients from controls [201–204]. Promising results have also been obtained in biopsies from submandibular glands [205]; however, this approach is limited by its invasiveness. Finally, interest is recently paid to saliva. To date, only one study is available, reporting the diagnostic accuracy of RT-QuIC in saliva samples collected from patients with PD and MSA [206]. In this work, the assay produced good results in discriminating PD and MSA from controls (PD: sensitivity 76%, specifivity 94.4%; MSA: sensitivity 61.1%, specificity 94.4%).

Another relevant point is whether RT-QuIC is sensitive enough to detect α-synucleinopathy in prodromal disease phases. So far, only few studies focused on the potential of SAAs in the early detection of synucleinopathies. RBD can precede the overt clinical manifestation of PD, DLB and MSA [207], with more than 70% of people affected by idiopathic RBD (iRBD) developing a α-synucleinopathy in 10-12 years [208,209]. Three independent studies showed that the analysis of CSF enabled the identification of subjects with iRBD subjects at the prodromal stages of α-synucleinopathy with high sensitivity and specificity (90-100%) [190,193,210].

In CSF, RT-QuIC have shown a high accuracy in differentiating LBDs from other αSyn unrelated conditions (PSP, CBD, and vascular parkinsonisms) [193,211]. Indeed, several studies suggest that different αSyn^{D} strains may underlie the phenotypic heterogeneity of PD, MSA, DLB and other α-synucleinopathies. Remarkably, the biochemical, morphological and structural properties of the final RT-QuIC reaction products (fibrillary aggregates mostly made of rec-αSyn) could be influenced by αSyn strains. The identification of such structural differences can be pursued by means of atomic resolution technologies (electron microscopy, nuclear magnetic resonance spectroscopy) [212].

Recently, the atomic structure of the αSyn^{D} aggregates present in the brain of MSA patients has been characterized by cryo-electron tomography. Also, the filaments in MSA show structural differences from those observed in DLB brains [213]. In 2020, Van der Perren and colleagues applied RT-QuIC in brain specimens from PD, MSA and DLB [214]. The authors found

that each disease conferred specific structural fingerprints to the rec-αSyn substrate: the addition of PD or MSA brain samples favored the formation of flat and twisted rec-αSyn fibrils, while the addition of DLB brain samples induced the formation of cylindrical, non-twisted rec-αSyn fibrils. Although preliminary, these findings indicate that through specialized analyses of the final RT-QuIC aggregates it might be possible to distinguish between different α-synucleinopathies.

A significantly different seeding activity has been observed also in saliva from MSA and PD patients, able to differentiate the two disorders with 61% sensitivity and 94% specificity [206].

1.3.2 Contribution of RT-QuIC in therapeutics

RT-QuIC methodology has been also exploited to screen for molecules displaying anti-protein aggregation activities and can be used to evaluate the effects and the mechanisms of inhibitors of misfolding proteins formation and propagation *in vitro*.

Indeed, RT-QuIC assay has been used to analyze the impact of specific substances (e.g. doxycycline) on the conversion and aggregation of PrP^{Sc} *in vitro* [215]. Doxycycline was added in different concentrations and at different times to the RT-QuIC reaction mix seeded with brain tissue or CSF from sporadic CJD (sCJD) and control patients. They showed that the addition of doxycycline results in a dose- and time-dependent inhibition of the RT-QuIC seeding activity exerted by brain and CSF samples of patients with sCJD. In contrast, other tested molecules (e.g. ampicillin and sucrose) did not show any effect on RT-QuIC seeded reactions.

Also for αSyn, many studies were performed by incubating recombinant protein with several compounds at different concentrations. For instance, doxycycline, curcumin, Anle138b and Epigallocatechin-3-gallate (EGCG) were able to inhibit the self-assembly of rec-αSyn in a dose-dependent manner [216–218]. Another study demonstrated that pretreatment of αSyn preformed fibrils with different concentration of EGCG, reduced the ability of these aggregates to induce a seeding activity in RT-QuIC [219]. Finally, CLR01, defined as a "molecular tweezer", was found to not only inhibit the aggregation of rec-αSyn (by interfering with a combination of

hydrophobic and electrostatic interactions by binding to Lys residues) but also to disassemble aggregated αSyn [220].

CHAPTER II

2. AIM OF THE STUDY

1. The aim of the first part of my Ph.D. project was to find a sensitive and reproducible RT-QuIC protocol for the detection of abnormal α-synuclein in the OM samples of patients with PD and MSA and deepen if these samples may induce a different convertion of the substrate, somehow related to the strains present in the OM.
2. The aim of the second part of the project was to deepen if the RT-QuIC products obtained from the analysis of the OM of PD and MSA patients, other than acquiring specific biochemical and morphological features, were also able to induce different inflammatory responses when injected into cell cultures. For this reason, we have involved a group of the Neuroimmunology and Neuromuscular Diseases Unit of the Fondazione IRCCS Istituto Neurologico Carlo Besta, under the supervision of Dr. Fulvio Baggi, that helped us to carry on cellular model experiments.
3. The aim of the third part of the project was to optimize OM processing and RT-QuIC protocol, to develop a procedure that was reproducible in different laboratories. For this purpose, we have involved an american group from the Case Western Reserve University School of Medicine (here named USA-lab), under the supervision of Prof. Shu G. Chen, which introduced some important modifications to our RT-QuIC protocol. All the analyses were performed in both our lab (here named ITA-lab) and USA-lab, using the same reagents, samples and experimental procedures.

CHAPTER III

3 MATERIALS AND METHODS

3.1 Patients' recruitment and clinical evaluations

A consecutive series of patients affected by neurodegenerative parkinsonisms were selected. Patients were eligible for enrollment if they had a diagnosis of idiopathic PD according to the Hughes and Postuma criteria [172,221], MSA according to the Gilman criteria [116], PSP according to the Höglinger criteria [222] and CBD according to the Armstrong criteria [223]. Extensive clinical symptoms and signs, including treatment response, presence of REM sleep behavior disorder, and red flags helping the PD and MSA diagnosis were carefully assessed. The clinical diagnosis was confirmed by independent clinicians and supported by specific diagnostic tests including brain MRI, cardiovascular autonomic tests, nigrostriatal dopamine transporter imaging with 123I-ioflupane single-photon emission computed tomography, and cardiac uptake of I-123 MIBG single-photon emission computed tomography. Motor symptoms were assessed using part III of MDS-UPDRS. Patients suspected to have other neurodegenerative diseases (e.g. AD, DLB) or other relevantclinical conditions (including stroke, neuromuscular diseases, severe osteoarthrosis, or other musculoskeletal impairments affecting gait and standing) that could have affected the clinical scales (e.g. MDS-UPDRS III, H&Y) were excluded from the study. Similarly, patients unable to provide their informed consent were not included. We selected only patients whose diagnosis was characterized by the highest clinical level of certainty. All the procedures involving human participants were performed in accordance with the ethical standards of the institutional and/or national research committees and with the 1964 Helsinki declaration. The study and its ethical aspects were approved by the Fondazione IRCCS Istituto Neurologico Carlo Besta ethical committee. All the participants provided written informed consent before OM collection and analysis.

3.1.1 First study

Olfactory mucosa (OM) samples were collected from extensively characterized patients with a clinical diagnosis of probable PD (n=18), MSA (n=11), CBD (n=6) and PSP (n=12) (**Table 3.1**).

	PD	MSA	CBD	PSP
Clinical criteria (ref.)	[172]	[116]	[223]	[222]
Number of patients	18	11	6	12
Age at time of evaluation (years)	64.2 ± 7.8	62.3 ± 9.2	63.3 ± 10.6	68.3 ± 7.0
Age at disease onset (years)	52.4 ± 6.1	56.5 ± 9.5	60.2 ± 10.9	64.3 ± 8.2
Disease duration (years)	10.1 ± 5.1	5.8 ± 3.4	3.2 ± 1.6	4.0 ± 3.6
Gender (F/M)	8/10	5/6	4/2	5/7
Frequency of symptoms (%)				
• Rigid akinetic parkinsonism	100	90.1	83.3	91.7
• Tremor	88.9	81.8	50	8.3
• Ataxia	0	90.1	50	91.7
• Apraxia	0	0	100	33.3
• REM behavioral disorder	55.6	63.6	0	0
• Autonomic impairment	83.3	100	33.3	16.7

Table 3.1 Clinical data of all patients included in the *First study*.

3.1.2 Second study

OM samples were collected before the COVID-19 pandemic with non-invasive procedures from extensively characterized patients with a clinical diagnosis of probable PD (n = 2) or MSA-P (n = 2) or healthy control (HC, n = 1) (**Table 3.2**).

	PD	MSA-P	HC
Clinical criteria (ref.)	[172]	[116]	-
Number of subjects	2	2	1
Age at time of evaluation (years)	59 ± 5.6	58.5 ± 9.8	-
Age at disease onset (years)	66 ± 1.4	62 ± 8.7	-
Disease duration (years)	7 ± 1.4	3.5 ± 2.1	-
Gender (F/M)	1/1	1/2	-
Frequency of symptoms (%)			
• Rigid akinetic parkinsonism	100	100	-
• Tremor	100	100	-
• Ataxia	0	50	-
• REM behavioral disorder	50	0	-

Table 3.2 Clinical data of all patients included in the *Second study*.

3.1.3 Third study

OM samples were collected from extensively characterized patients with a clinical diagnosis of probable PD (n = 13), MSA-P (n = 20), MSA-C (n = 10), and a group of HS (n = 11). The age differences between patients and healthy subjects (61 ± 8 and 42 ± 10 years, respectively) as well as the disease duration between MSA and PD patients (4 ± 3.1 and 8 ± 4.3 years, respectively) were statistically significant (t-test $p < 0.01$) (**Table 3.3**).

	PD	MSA-P	MSA-C	HS
Clinical criteria (ref.)	[172]	[116]	[116]	-
Number of patients	13	20	10	11
Age at time of evaluation (years)	63.2 ± 7.36	60 ± 7.9	61 ± 8.6	41.7 ± 9.5
Age at disease onset (years)	55.2 ± 6.2	55.6 ± 9.4	57 ± 9.6	-
Disease duration (years)	8 ± 4.3	4.4 ± 3.4	4 ± 2.4	-
Gender (F/M)	5/8	9/11	4/6	6/5
Frequency of symptoms (%)				
• Rigid akinetic parkinsonism	76.9	90.1	83.3	-
• Tremor	46.1	81.8	50	-
• Ataxia	0	90.1	50	-
• REM behavioral disorder	23.1	50	60	-
• Autonomic impairment	38.4	100	80	-

Table 3.3 Clinical data of all patients included in the *Third study*.

3.2 Recombinant αSyn expression and purification

3.2.1 First study

Human recombinant α-synuclein (rec-αSyn) was produced in the Prion Lab of Prof. Giuseppe Legname (Scuola Internazionale Superiore di Studi Avanzati of Triste). In particular, it was cloned and expressed in pET-11a vector, using BL21 (DE3) *E. coli* strain. Cells were growth in Luria-Bertani broth medium with 100 mg/mL ampicillin at 37 °C, until an Optical density of about 0.6 measured at 600 nm. The induction of the construct was obtained with 0.6 mM isopropyl β-D-thiogalactoside (IPTG) for 5 h. The cell pellet was resuspended in osmotic shock buffer (30 mM Tris-HCl, 2 mM EDTA, 40% sucrose, pH 7.2) followed by centrifugation (9000 rpm, 30 min) and boiling for 10 min (while stirring) for the extraction of the protein from bacterial periplasm. After two steps of precipitation with 35% and 55% of ammonium sulfate, the protein was purified by anion exchange chromatography (HiTrap column, GE Healthcare). AKTA

purification systems (GE Healthcare) were used for monitoring the protein absorbance during chromatography process. The presence of rec-αSyn was monitored during all the purification steps by gel electrophoresis (SDS-PAGE). The purity of the final product was confirmed by Western blotting and mass spectroscopy. Fractions containing α-synuclein were dialyzed into water, quantified by measuring the absorbance at 280 nm, lyophilized (FreeZone 2.5 Freeze Dry System, Labconco) and stored at − 80 °C. Before use, rec-αSyn was dissolved in H_2O (at the final concentration of 5 mg/mL) and used to prepare the reaction mix.

3.2.2 *Second study*

Rec-αSyn was produced in the Prion Lab as described in **Paragraph 3.2.1**.

3.2.3 *Third study*

For this study we decided to use rec-αSyn commercially produced from the rPeptide, to minimize the experimental variables that could lead to inconsistencies in the results or conflicting findings.

3.3 *In vitro* generation of rec-αSyn aggregates

3.3.1 *Generation of pre-formed fibrils (PFFs) of rec-αSyn*

Rec-αSyn was thawed and diluted at the final concentration of 140 μM, in a reaction mix composed of 40 mM PBS (pH 8.0), 170 mM NaCl and 10 μM Thioflavin-T (ThT). All reagents used to prepare the reaction mix were filtered through a 0.22 μm filter before use. Reactions were performed in triplicate in a black 96-well optical flat bottom plate (Thermo Fisher Scientific). One-hundred μL of reaction mix was added to each well, together with a 3-mm glass bead (Sigma), required to sustain protein aggregation. The plate was then sealed with a sealing film (Thermo Fisher Scientific), inserted into a Fluoroskan Ascent microplate reader (Thermo Fisher Scientific) and subjected to cycles of shaking (1 min at 600 rpm, single orbital) and incubation (14 min at 42 °C). Fluorescence intensities, expressed as arbitrary units (AU), were taken every 60 min using 450 ± 10 nm (excitation) and 480 ± 10 nm (emission) wavelengths, with a bottom read, to monitor rec-αSyn aggregation. Once reached the fluorescence plateau, PFFs were collected and

characterized by means of biochemical (Western blot) and morphological (transmission electron microscopy, TEM) analyses.

3.3.2 Generation of rec-αSyn aggregates with different morphological features

Rec-αSyn was thawed and diluted to a final concentration of 21 μM in three different aggregation buffers: 1. H2O (αSv1); 2. 5 mM Tris and 100 mM NaCl (αSv2); 3. 5 mM Tris (αSv3). All reagents used to prepare the reaction mixes were filtered through a 0.22 μm filter before use. Reactions were performed in sixfold in a black 96-well optical flat bottom plate (Thermo Fisher Scientific) using the Fluoroskan Ascent microplate reader (Thermo Fisher Scientific). One hundred microliters of reaction mix was added to each well, together with a 3-mm glass bead (Sigma), required to sustain protein aggregation. The plate was sealed with a sealing film (Thermo Fisher Scientific) and subjected to continuous shaking (600 rpm, single orbital) at 37°C. An additional well was prepared for each buffer and supplemented with 10 μM Thioflavin-T (ThT) to monitor rec-αSyn aggregation. Fluorescence intensities, expressed as AU, were taken every 60 min using 450 ± 10 nm (excitation) and 480 ± 10 nm (emission) wavelengths, with a bottom read, to monitor rec-αSyn aggregation. Once reached the fluorescence plateau, rec-αSyn aggregates were collected and characterized by means of biochemical (Western blot, dot blot, dye-binding assay) and morphological (TEM) analyses.

3.4 Preparation of brain samples for biochemical and RT-QuIC analyses

Frontal cortices of patients with neuropathologically confirmed diagnoses of Frontotemporal Dementia with parkinsonism-17 associated with P301L tau mutation (FTDP17, n = 1), PSP (n = 1), CBD (n = 1) and Non Demented Patient (NDP, n = 1); pons of patient with neuropathologically confirmed diagnosis of PD (n = 1); cerebellum of patient with neuropathologically confirmed diagnosis of MSA (n = 1) were homogenized in PBS (pH 7.4, Sigma) at 10% (weight/volume), using a glass potter homogenizer. Samples were centrifuged (Eppendorf Centrifuge) at 800 × g, for 1 min at 4 °C, in order to remove cellular debris. Supernatants were collected and stored at − 20 °C for further biochemical and RT-QuIC analyses.

For RT-QuIC analysis, serial dilutions of PD, MSA and FTDP-17 brain homogenates were prepared in PBS.

3.5 Extraction of soluble and insoluble α-synuclein from brains

Approximately 0.3 g of frozen brain tissues were homogenized 10% (weight/volume) in TBS buffer (supplemented with protease inhibitors and phosphatase inhibitors), using a Tissue Lyser (Qiagen) with a steel bead, for 1 min at maximum speed. The homogenate was then clarified by centrifugation at 1000 x g for 5 min at 4 °C. Supernatants were transferred to polycarbonate centrifuge tubes and centrifuged at 100000 x g (Beckman Coulter Optima MAX) for 1 h at 4 °C. Resulting supernatants were collected as TBS-soluble fraction (soluble α-synuclein) while pellets were washed with 5 volumes of TBS and centrifuged at 100000 x g for 15 min at 4 °C. Pellets were then suspended in TBS buffer supplemented with SDS (5% final dilution) and sonicated (8 min at 500 W). Final solution was centrifuged at 100000 x g for 30 min at 25 °C. Supernatant was collected as SDS soluble fraction (detergent-soluble α-synuclein) while pellets were washed with 5 volumes of TBS-SDS buffer and centrifuged at 100000 x g for 15 min at 25 °C. Pellets were then suspended in 50 µL of TBS-SDS buffer supplemented with urea (8 M final concentration), sonicated for 5 min at 500 W, diluted 1:1 with TBS buffer and collected as urea soluble fraction (insoluble α-synuclein).

3.6 Collection and preparation of olfactory mucosa samples for RT-QuIC analysis

OM samples were collected before the COVID-19 pandemic with non-invasive procedures from extensively characterized patients. Before collection, the nasal cavity was treated with a topical anesthetic (Ecocain, Molteni Dental) for 10 min and, with the use of a special cotton swab (referred to as brush, FLOQSwabsTM Copan Italia, Brescia, Italy), OM were collected between the septum and the middle turbinate. After collection, cotton swabs were immersed in saline solution and olfactory cells separated from the brushes by vigorous vortexing. Cells were finally pelleted at 800 × g for 20 min at 4 °C. The supernatants were removed, and

approximately 6 µg of the pellets were collected with the use of inoculating loops. Such material was then transferred into a tube containing 50 µL of PBS and used for RT-QuIC analyses. For the inter-laboratory assessment, the OM samples were divided into two aliquots, one for ITA-lab and the other for USA-lab analyses, and were blindly tested by both laboratories. OM samples were prepared as previously described.

3.7 RT-QuIC analysis of αSyn aggregates

3.7.1 PFFs RT-QuIC

The solution containing *in vitro* generated PFFs was sonicated for 3 min at 500 W and serially diluted (from 10^{-1} to 10^{-12} volume/volume) in its own reaction buffer. Five µL of the following dilutions: undiluted, 10^{-3}, 10^{-6}, 10^{-9}, 10^{-12} was added to 95 µL of reaction mix and subjected to RT-QuIC analysis. Reaction mix was composed as follow: rec-αSyn diluted in 40 mM PBS (pH 8.0), 170 mM NaCl and 10 µM ThioflavinT (ThT) at the final concentration of 140 µM. All reagents used for the preparation of the reaction mix were filtered through a 0.22 µm filter before the addition of αSyn aggregates. All RT-QuIC reactions were performed in triplicate in a black 96-well optical flat bottom plate (Thermo Fisher Scientific) using the Fluoroskan Ascent microplate reader (Thermo Fisher Scientific). Samples underwent to cycles of shaking (1 min at 600 rpm, single orbital) and incubation (14 min at 42 °C). Fluorescent intensities, expressed as AU, were taken every 30 min using 450 ± 10 nm (excitation) and 480 ± 10 nm (emission) wave-lengths, with a bottom read. The addition of a 3-mm glass bead (Sigma) was necessary to sustain protein aggregation.

3.7.2 rec-αSyn aggregates RT-QuIC

αSv1, αSv2, and αSv3 were serially diluted (volume/volume) in PBS (1.5 µg, 1.5 ng, 1.5 pg, 1.5 fg, and 1.5 ag) and 5 µL of pure or diluted samples was added to 95 µL of RT-QuIC reaction mix prepared as follow: rec-αSyn diluted in 40 mM PBS (pH 8.0), 170 mM NaCl and 10 µM ThT at the final concentration of 14 µM. All the reagents were filtered through a 0.22 µm filter before use. Reactions were performed in triplicate in a black 96-well optical flat bottom plate (Thermo

Fisher Scientific). Each well contained 100 µL of final reaction's volume. The plate was sealed with a sealing film (Thermo Fisher Scientific), inserted into a Fluoroskan Ascent microplate reader (Thermo Fisher Scientific) and subjected to cycles of shaking (1 min at 600 rpm, single orbital) and incubation (14 min at 42 °C). Fluorescent intensities, expressed as AU, were taken every 30 min using 450 ± 10 nm (excitation) and 480 ± 10 nm (emission) wave-lengths, with a bottom read. The addition of a 3-mm glass bead (Sigma) was required to promote protein aggregation. Final reaction products were named RQ-αSv1, RQ-αSv2 and RQ-αSv3. As control, unseeded RT-QuIC reactions (RQ-no seed) were performed.

3.8 RT-QuIC analysis of brain homogenates

3.8.1 First study

Ten % brain homogenates (BH) from patients with PD, MSA, PSP, CBD, FTDP-17 and NDP were diluted at 10^{-3} volume/volume in PBS. Samples were sonicated (3 min at 500 W) and 2 µL was then supplemented to 98 µL of RT-QuIC reaction mix prepared as follow: rec-αSyn diluted in 40 mM PBS (pH 8.0), 170 mM NaCl and 10 µM ThT at the final concentration of 70 µM. Reactions were performed in triplicate in a black 96-well optical flat bottom plate (Thermo Scientific). Each well contained 100 µL of final reaction's volume. The plate was sealed with a sealing film (Thermo Fisher Scientific), inserted into a Fluoroskan Ascent microplate reader (Thermo Fisher Scientific) and subjected to cycles of shaking (1 min at 600 rpm, single orbital) and incubation (29 min at 42 °C). Fluorescent intensities, expressed as arbitrary units (AU), were taken every 30 min using 450 ± 10 nm (excitation) and 480 ± 10 nm (emission) wave-lengths, with a bottom read. The addition of a 3-mm glass bead (Sigma) was required to promote protein aggregation. A sample was considered positive if at least 2 out 3 replicates crossed a threshold of fluorescence set at 500 AU. We have then calculated the average fluorescence intensity of the two or three replicates that crossed this threshold and plotted resulting values in a graph against time. If only one (or none) of the replicates crossed the threshold, we considered the sample as

negative and we calculated the average fluorescence intensity of the two (or three) replicates that remained below such threshold.

3.8.2 Third study

Ten % BH from patients with PD, MSA-P, MSA-C and from a patient not affected by α-synucleinopathy (NAS) were diluted at 10^{-12} volume/volume in PBS. Each well was preloaded with two low-binding silica beads (0.8 mm, OPS Diagnostics). Rec-αSyn, purchased from rPeptide, was reconstituted in water and filtered with 100 kDa filters immediately before use. For each well, 1 µl of each BH was added to 49 µL of reaction mix prepared as follow: rec-αSyn diluted in 40 mM HEPES (pH 8.0), 170 mM sodium citrate, and 20 µM ThT, at the final concentration of 14 µM. The plate was incubated at 42 °C in a BMG FluoSTAR OMEGA microplate reader (BMG Labtech) and subjected to cycles of shaking and incubation (1 min each). Fluorescence intensities of ThT, expressed as AU, were taken every 30 min using 450 ± 10 nm (excitation) and 480 ± 10 nm (emission) wave-lengths, with a bottom read. Reactions were performed in quadruplicates and a sample was considered able to induce seeding activity when at least two out of four replicates crossed the threshold of fluorescence set at 30,000 AU before 13 h. In this case, the sample was considered positive. For each positive sample, we have calculated the average fluorescence intensity of the replicates that crossed the fluorescence thresholds and plotted the results in a graph against time.

3.9 RT-QuIC analysis of olfactory mucosa

3.9.1 First study

Two µL of OM sample prepared as previously described was added to 98 µL of the reaction mix prepared as follow: rec-αSyn diluted in 40 mM PBS (pH 8.0), 170 mM NaCl and 10 µM Thioflavin-T (ThT) at the final concentration of 140 µM. All the reagents were filtered through a 0.22 µm filter before use. Reactions were performed in triplicate in a black 96-well optical flat bottom plate (Thermo Fisher Scientific). Each well contained 100 µL of final reaction's volume. The plate was sealed with a sealing film (Thermo Fisher Scientific), inserted into a Fluoroskan

Ascent microplate reader (Thermo Fisher Scientific) and subjected to cycles of shaking (1 min at 600 rpm, single orbital) and incubation (14 min at 42 °C). Fluorescent intensities, expressed as AU, were taken every 30 min using 450 ± 10 nm (excitation) and 480 ± 10 nm (emission) wavelengths, with a bottom read. The addition of a 3-mm glass bead (Sigma) was required to promote protein aggregation. A sample was considered positive if at least 2 out 3 replicates crossed a threshold of fluorescence set at 6 AU within a certain period of time set at 120 h. We have then calculated the average fluorescence intensity of the two or three replicates that crossed this threshold of fluorescence and plotted resulting values in a graph against time. If only one (or none) of the replicates crossed the threshold, we considered the sample as negative and we calculated the average fluorescence intensity of the two (or three) replicates that remained below such threshold.

3.9.2 Second study

Two µL of OM sample prepared as previously described was added to 98 µL of the reaction mix prepared as follow: rec-αSyn diluted in 40 mM PBS (pH 8.0), 170 mM NaCl and 10 µM ThT at the final concentration of 14 µM. All the reagents were filtered through a 0.22 µm filter before use. Reactions were performed in triplicate in a black 96-well optical flat bottom plate (Thermo Fisher Scientific). Each well contained 100 µL of final reaction's volume. The plate was sealed with a sealing film (Thermo Fisher Scientific), inserted into a Fluoroskan Ascent microplate reader (Thermo Fisher Scientific) and subjected to cycles of shaking (1 min at 600 rpm, single orbital) and incubation (14 min at 42 °C). Fluorescent intensities, expressed as arbitrary units (AU), were taken every 30 min using 450 ± 10 nm (excitation) and 480 ± 10 nm (emission) wavelengths, with a bottom read. The addition of a 3-mm glass bead (Sigma) was required to promote protein aggregation. Final reaction products were named RQ-MSA1, RQ-MSA2, RQ-PD1, RQ-PD2 and RQ-CTRL.

3.9.3 Third study

The RT-QuIC protocol for OM samples analysis was modified from that of the previous studies with the consideration of salt effects on RT-QuIC reactivity as recently described. In brief,

RT-QuIC analyses were performed using 384-well optical flat bottom plates (Thermo Fisher Scientific). Each well was preloaded with two low-binding silica beads (0.8 mm, OPS Diagnostics). Rec-αSyn, purchased from rPeptide, was reconstituted in water and filtered with 100 kDa filters immediately before use. For each well, 1 µL of OM samples was added to 49 µL of RT-QuIC reaction mix that was composed of: rec-αSyn diluted in 40 mM HEPES (pH 8.0), 170 mM sodium citrate, and 20 µM ThT, at the final concentration of 14 µM. Each sample was analyzed in quadruplicate and at least three times in both labs. The plates were incubated at 42 °C in a BMG FluoSTAR OMEGA microplate reader (BMG Labtech) and subjected to cycles of shaking and incubation (1 min each). Fluorescence intensities of ThT, expressed as AU, were taken every 30 min using 450 ± 10 nm (excitation) and 480 ± 10 nm (emission) wave-lengths, with a bottom read. A sample was considered able to induce seeding activity when at least two out of four replicates crossed the threshold of fluorescence set at 30,000 AU before 13 h at ITA-lab or 22.5 h at USA-lab. In this case, the sample was considered positive. For each positive sample, we have calculated the average fluorescence intensity of the replicates that crossed the fluorescence thresholds and plotted the results in a graph against time. Results were correlated with demographic and clinical data.

3.10 RT-QuIC analysis of SH-SY5Y cell lysates stimulated with RQ-MSA, RQ-PD, αSv1, αSv2 or αSv3

SH-SY5Y cells stimulated with RQ-MSA, RQ-PD, αSv1, αSv2 or αSv3 were lysed as described in **Paragraph 3.12** and analyzed by RT-QuIC. Five µL of each lysate, named CS-RQ-MSA, CS-RQ-PD, CS-αS1, CS-αS2 or CS-αS3, respectively, was added to 95 µL of RT-QuIC reaction mix prepared as follow: rec-αSyn diluted in 40 mM PBS (pH 8.0), 170 mM NaCl and 10 µM ThT at the final concentration of 14 µM. All the reagents were filtered through a 0.22 µm filter before use. Reactions were performed in triplicate in a black 96-well optical flat bottom plate (Thermo Fisher Scientific). Each well contained 100 µL of final reaction's volume. The plate was sealed with a sealing film (Thermo Fisher Scientific), inserted into a Fluoroskan Ascent microplate

reader (Thermo Fisher Scientific) and subjected to cycles of shaking (1 min at 600 rpm, single orbital) and incubation (14 min at 42 °C). Fluorescent intensities, expressed as AU, were taken every 30 min using 450 ± 10 nm (excitation) and 480 ± 10 nm (emission) wave-lengths, with a bottom read. The addition of a 3-mm glass bead (Sigma) was required to promote protein aggregation. Final reaction products were named RQ-CS-RQ-MSA1, RQ-CS-RQ-MSA2, RQ-CS-RQ-PD1, RQ-CS-RQ-PD2, RQ-CS-αS1, RQ-CS-αS2 and RQ-CS-αS3.

3.11 Dye-binding assay

To perform the dye-binding assay, samples were prepared without ThT. Samples were then diluted to a final concentration of 5 μM in PBS and divided in different aliquots that were incubated with different dyes (at room temperature, in the dark): 10 μM ThT, 10 μM 4,40 -bis-1-anilinonaphthalene8-sulfonate (Bis-ANS), 5 μM Congo red, Amytracker 480 (1:800 in H_2O), Amytracker 520 (1:800 in H_2O), Amytracker 540 (1:800 in H_2O), Amytracker 630 (1:800 in H_2O) and Amytracker 680 (1:800 in H_2O). After 30 min, samples were added to a black 384-well optical flat bottom plate (Thermo Fisher Scientific). This latter was sealed with a sealing film (Thermo Fisher Scientific) and inserted in a ClarioSTAR microplate reader (BMG Labtech). The fluorescence values were recorded using the appropriate wavelengths: 448/482 nm exc/emi for ThT, 400/505 nm exc/emi for Bis-ANS, 544/620 exc/emi for Congo red, 430/480 nm exc/emi for Amytracker 480, 470/520 nm exc/emi for Amytracker 520, 470/540 nm exc/emi for Amytracker 540, 510/630 nm exc/emi for Amytracker 630 and 540/680 nm exc/emi for Amytracker 680.

3.12 Cell culture and stimulation

Undifferentiated SH-SY5Y neuroblastoma cells were maintained in Dulbecco's Modified Eagle Medium (DMEM) with 2 mM L-glutamine, 1X penicillin/streptomycin, and supplemented with 10% Fetal Calf Serum (FCS) at 37 °C, 5% CO_2. Differentiation of SH-SY5Y cells into neuron-like cells was achieved by 10 μM trans-retinoic acid in DMEM 1% FCS, for 7 days, and seeded

on 24 well-plates for molecular biology analysis, lysate preparation (250,000 cells/well), and for immunofluorescence analysis (70,000 cells/well). Cells were exposed to RQ-MSA1, RQ-MSA2, RQ-PD1, RQ-PD2, αSv1, αSv2, αSv3, RQ-αSv1, RQ-αSv2, RQ-αSv3 and related controls (final concentration 2.5 μM) for 24 h. For lysate preparation, SH-SY5Y cells were detached with PBS by scraping. Supernatants were centrifuged at 10000 rpm for 5 min and stored at −80 °C.

3.13 RT-qPCR analysis

cDNA was synthesized from total RNA (TRIzol, Thermo Fisher Scientific) using random hexamers, and reverse transcriptase (SuperScript VILO cDNA Synthesis Kit, Thermo Fisher Scientific). Real-time quantitative PCR (RT-qPCR) for TLR2 (Hs02621280_s1), TLR6 (Hs01039989_s1), TRAF6 (Hs00939742_g1), IL6 (Hs00174131_m1), NLRP3 (Hs00918080_g1), SOD2 (Hs00167309_m1) expression was performed using Assays-on-Demand Gene Expression assay (Thermo Fisher Scientific). GAPDH (Hs02758991_G1) was used as housekeeping endogenous gene. Target mRNA expression was calculated as mean 2-ΔCtx100 value, in which ΔCt is the difference between target and housekeeping Ct. Real-time PCR reactions were performed in duplicate using ViiA7 Real-Time PCR System (Thermo Fisher Scientific), according to the manufacturer's instructions.

3.14 Confocal microscopy analysis

Neuron-like SH-SY5Y cells, seeded on 13 mm coverslips and exposed to RQ-MSA1, RQ-MSA2, RQ-PD1, RQ-PD2, αSv1, αSv2, αSv3, RQ- αSv1, RQαSv2, RQ-αSv3 and related controls for 24 h, were fixed with 4% paraformaldehyde in PBS (pH 7.0), permeabilized with 0.5% Triton-X100 in PBS, and incubated for 1 h in PBS 5%-BSA 2% NGS (blocking solution). TLR2 expression was detected with the mouse monoclonal antibody anti-TLR2 (TL2.1, Invitrogen) and α-synuclein was detected with the mouse monoclonal antibody 4D6 (Abcam), followed by Alexa Fluor-555 donkey anti-mouse secondary antibody (Thermo Fisher Scientific). Alexa Fluor 488® phalloidin (Thermo Fisher Scientific) was used to stain F-actin (cytoskeleton). Nuclei were stained

with 40,6-diamidino-2-phenylindole (DAPI) (Thermo Fisher Scientific). Isotype control antibodies were used as negative controls (non-specific background). Maximum projection images from 10-slice Z-stack (300 nm step size) were acquired via confocal microscopy (C1/TE2000-E microscope; Nikon) using 40× (NA 1.30) and 100× (NA 1.40) oil objectives; at least 5 adjacent image fields were analyzed. Parameters for image acquisition were not modified to allow the comparison of fluorescence intensity as a measure of relative quantification. Image analysis was performed with Image J and FIJI software.

3.15 NO release analysis

NO production was determined by measuring the accumulation of nitrite in the culture medium. Nitrite was assayed colorimetrically by a diazotization reaction using the Griess reagent, composed of a 1:1 mixture of 1% sulfanilamide in 5% orthophosphoric acid and 0.1% naphtylethylenediamine dihydrochloride in water. One hundred µL of culture medium was mixed to 100 µL of Griess reagent in a 96-multiwell plate and the O.D. at 550 nm was measured within 10 min. The nitrite concentration in the samples was interpolated from a $NaNO_2$ standard curve ranging from 0 to 100 µM. The limits of detection and quantification were 0.25 and 0.7 µM, respectively.

3.16 Multiparametric assay

A Bio-Plex ProTM Human Cytokine 27-plex Immunoassay 96-well kit (Bio-Rad Laboratory) was used to measure the concentration of pro- and anti-inflammatory cytokines, chemokines and growth factors in cells stimulated with αSv1, αSv2 and αSv3. The immunoassay includes: gamma interferon (IFNγ), interleukin-1β (IL1β), IL1 receptor antagonist (IL1ra), interleukin-2 (IL2), IL4, IL6, IL9, IL15, IL17, tumor necrosis factor-alpha (TNFα), interferon gamma-induced protein 10 (IP10).

3.17 Proteinase K digestion

3.17.1 PK digestion of RT-QuIC products derived from seeding with BH and OM (protocol used for the First study)

Eight µL of final RT-QuIC products was treated with PK 100 µg/mL at 37 °C for 60 min under shaking (500 rpm). PK activity was stopped by the addition of LDS loading buffer and boiling at 100 °C for 10 min. Western blot analyses were then performed.

3.17.2 PK digestion of rec-αSyn aggregates and their RT-QuIC products

Eight µL of αSv1, αSv2 or αSv3 and all RT-QuIC products was subjected to limited proteolytic digestion with PK at the final concentration of 10 and 50 µg/mL, respectively. Digestions were performed under shaking (500 rpm), at 37 °C for 60 min. PK activity was stopped by the addition of LDS-PAGE loading buffer and boiling of the samples at 100 ◦C for 10 min. Western blot analyses were then performed.

3.17.3 PK digestion of RT-QuIC products derived from seeding with OM (protocol used for the Third study)

Eight µL of final RT-QuIC products was treated with PK 2.5 mg/mL at 37 °C for 60 min, under shaking (500 rpm). PK activity was stopped by the addition of LDS-PAGE loading buffer and boiling of the samples at 100 ◦C for 10 min. Western blot analyses were then performed.

3.18 Western blotting

Brain extracts (containing either soluble or insoluble αSyn), rec-αSyn aggregates and RT-QuIC products were supplemented with LDS loading buffer, heated at 100 °C for 10 min and loaded into 12% Bolt Bis-Tris Plus gels (Invitrogen). Proteins were separated by means of SDS-PAGE and then transferred onto Polyvinylidene difluoride (PVDF) membranes (Immobilon-P, Millipore). Membranes were first incubated with paraformaldehyde (0.4% in PBS) for 30 min (under shaking) at room temperature or directly blocked with 5% (weight/volume) non-fat dry milk (prepared in Tris-HCl with 0.05% Tween-20) for 1 h at room temperature under shaking. PVDF membranes were incubated with different primary antibody to αSyn (monoclonal 4D6

Invitrogen: epitopes 124–134; polyclonal AB5038 EMD Millipore: epitopes 111–131; monoclonal 5C2 Novus Biologicals: epitopes 61–95; polyclonal AS08 358 Agrisera: epitopes 1–15) overnight at 4 °C under shaking. After washing 3 times with TBST, membranes were incubated with the secondary antibody conjugated with horseradish peroxidase (Amersham donkey against rabbit IgG-HRP, diluted 1:2000 in TBST supplemented with 5% non-fat dry), subjected again to 3 washes with TBST and developed with chemiluminescent system (ECL Prime, cytiva). Reactions were visualized using a G:BOX Chemi Syngene system (Syngene).

3.19 Dot blot analysis

3.19.1 Second study

Two µL of each αSyn aggregates or final RT-QuIC products was diluted with 100 µL of PBS containing 0.1% Tween-20. Two µL of the diluted samples were loaded onto nitrocellulose membranes (0.2 µm pore) and, after 30 min, the membranes were blocked with non-fat dry milk (5% in TBST) for 60 min (under shaking) at room temperature. Membranes were then incubated with a rabbit monoclonal αSyn filament-specific antibody (Abcam ab209538, MJFR-14-6-4-2, diluted 1:5000 in 5% BSA-PBS) for 60 min (under shaking) at room temperature. After washing 3 times with TBST, the membranes were incubated with the secondary antibody (Amersham donkey against rabbit IgG-HRP, diluted 1:10,000 in 5% BSA-PBS) for 60 min at room temperature. After 3 washes in TBST, membranes were developed with chemiluminescent system (ECL Prime) and reactions were visualized using a G:BOX Chemi Syngene system. The densitometric quantitation of the individual dots was performed with ImageJ software (v1.48).

3.19.2 Third study

Two µL of final RT-QuIC products was diluted with 500 µL of PBS containing 0.1% Tween-20. One hundred µL of the diluted samples were loaded onto a nitrocellulose membrane (0.2 µm pore) assembled in a Bio-Rad 96-well Bio-Dot apparatus per manufacturer's protocol. The membrane was blocked for 1 h at room temperature with 5% bovine serum albumin (BSA) made in PBS (5% BSA-PBS). The membrane was then incubated for 1 h with a rabbit monoclonal

αSyn filament-specific antibody (Abcam ab209538, diluted 1:5,000 in 5% BSA-PBS) or a rabbit polyclonal total αSyn antibody (Millipore Ab5038, diluted 1:1,000 in 5% BSA-PBS). After washing 3 times with Tris-buffered saline containing 0.1% Tween-20 (TBST-0.1), the membrane was incubated for 1 h with a secondary antibody (Amersham donkey against rabbit IgG-HRP, diluted 1: 10,000 in 5% BSA-PBS). Following three washes with TBST0.1, the immunoreactivity on the dot-blotted membrane was developed with the enhanced chemiluminescence reagents (ECL, Amersham). The densitometric quantitation of the individual dots was performed with the Epson Perfection V600 photo scanner (Epson Scan Utility v3.9.2).

3.20 Transmission electron microscopy analyses

Ten µL of αSyn aggregates or RT-QuIC products was dropped onto 200- mesh Formvar-carbon coated nickel grids for 30 min and the remaining drop was blotted dry using filter papers. The grids were subsequently stained with 25% Uranyl Acetate Replacement (UAR, negative staining) for 10 min, the solution was removed using filter papers and the grids were air-dried for 15 min before the analyses. Images were recorded at 120 kV with a FEI Tecnai Spirit, equipped with an Olimpus Megaview G2 camera.

3.21 Statistical analyses

TEM images were analyzed with the Gwyddion software for measuring the distances between over-twists occurring in the same amyloid fibril. Final values were compared with a double-tailed unpaired t-test (Mann-Whitney U test) performed using the Prism software (GraphPad v5.0). Graphic representations of RT-QuIC kinetics (based on ThT signals) were also obtained with the Prism software (GraphPad v5.0). Densitometric analysis of PK-resistant RT-QuIC products was performed using ImageJ software (v1.48) and final values were compared using a double-tailed unpaired t-test (Mann-Whitney U test). Graphic representations of densitometric analysis were performed using the Prism software (GraphPad). Data related to cell analyses were expressed as the mean ± SD of two independent experiments. One-way ANOVA

test, followed by Dunnett's multiple comparison test, was used to evaluate statistical differences; p-values were corrected for multiple comparisons. $p < 0.05$ was considered statistically significant. RT-QuIC kinetics were represented using the Prism software (GraphPad v5.0) on a graph where mean fluorescence values were plotted against time. Associations between variables were investigated through t-test or Mann-Whitney test, Chi-square or Fisher exact test, as appropriate. Dot blot results and PK resistance profiles of RT-QuIC products generated by PD and MSA were analyzed through repeated measure analysis of variance (ANOVA). Kappa statistic with the corresponding 95% confidence interval (CI) was calculated to assess interrater agreement between ITA-lab and USA-lab.

4 RESULTS

4.1 First study

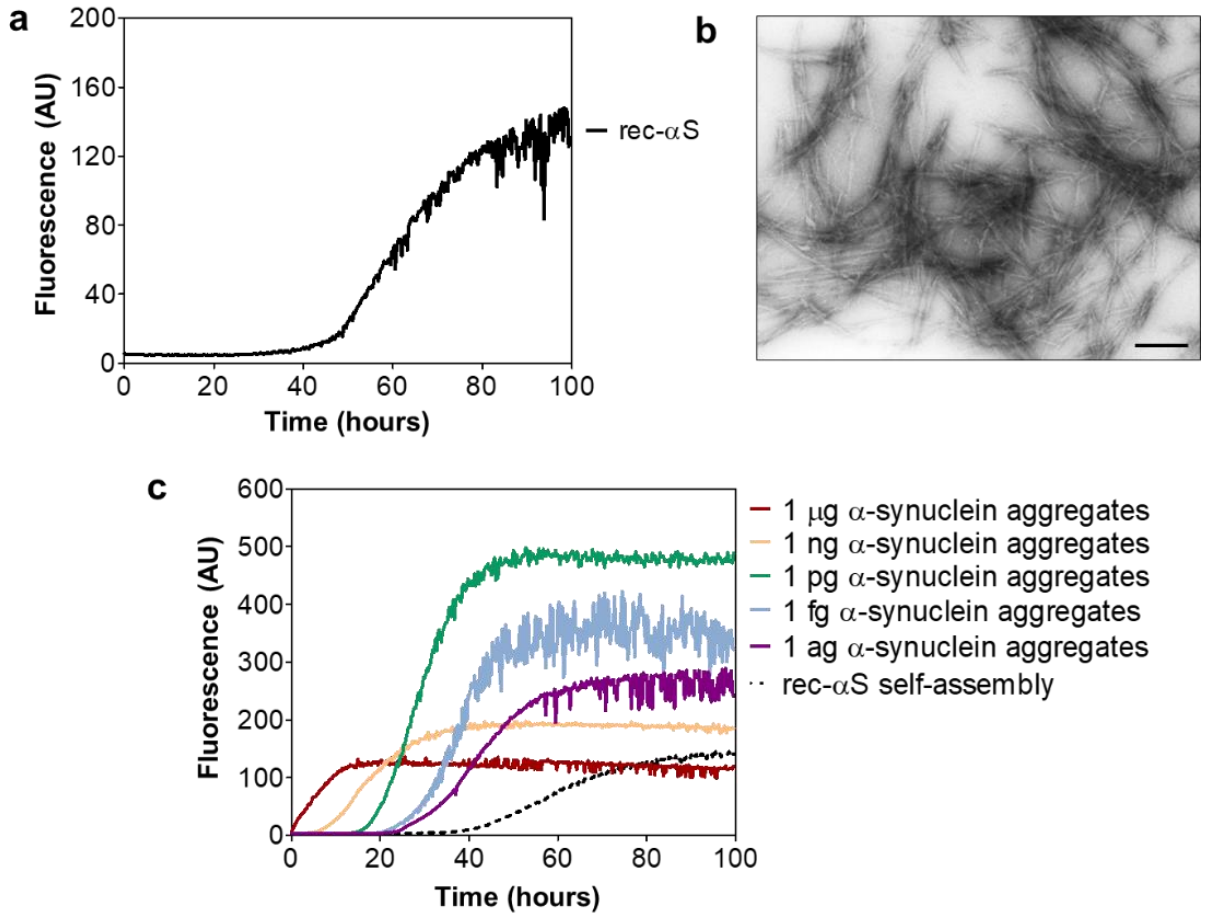

Figure 4.1 RT-QuIC analysis of *in vitro* generated **αSyn** aggregates. **a** *In vitro* generation of **αSyn** aggregates (artificial seeds). rec-**α**Syn was induced to aggregate by alternating cycles of incubation and shaking. Average ThT fluorescence intensity was plotted against time; **b** TEM analysis of final **α**Syn aggregates. Amyloid fibrils were efficiently generated *in vitro* under well-controlled experimental conditions. Scale bar: 500nm; **c** Assessment of the RT-QuIC detection limits. Serial dilutions of the artificial seeds previously produced were analyzed by means of RT-QuIC. All dilutions efficiently accelerated the kinetics of rec-**α**Syn aggregation. Average ThT fluorescence intensity was plotted against time. Self-assembly refers to unseeded rec-**α**Syn reactions.

4.1.1 In vitro generated α-synuclein PFFs efficiently seeded RT-QuIC reaction

We first generated in vitro PFFs of rec-**α**Syn by subjecting the protein to cycles of shaking (1 min) and incubation (14 min). The kinetics of rec-**α**Syn aggregation was reproducible over time

and, after a lag phase of about 40 h, there was a rapid increase in ThT signal that reached a plateau at around 100 h (**Figure 4.1a**).

Final products, collected after 100 h, were analyzed by TEM which confirmed the presence of α-synuclein aggregates, mostly in the form of amyloid fibrils (**Figure 4.1b**). PFFs were then serially diluted and added at the beginning of a new RT-QuIC assay performed using fresh rec-αSyn as reaction's substrate. Results of these experiments demonstrate that even the lowest dilution (which extrapolates to approximately 1 attogram of aggregated protein) was able to efficiently accelerate the kinetics of rec-αSyn aggregation, mostly in a dose-dependent manner (**Figure 4.1c**).

4.1.2 Brain homogenates of patients with α-synucleinopathies efficiently seeded RT-QuIC reaction

Considering the high level of RT-QuIC sensitivity in detecting extremely low amounts of PFFs, we decided to verify its ability to detect pathological α-synuclein aggregates present in brain samples of patients with PD and MSA. Firstly, we have subjected the brains of patients with MSA, PD, PSP, CBD, FTDP-17 and NDP to serial steps of high-speed centrifugation, in order to separate soluble and insoluble (mostly aggregated) α-synuclein species. By means of Western blot we confirmed the presence of aggregated forms of α-synuclein (urea fraction) only in brain homogenates of patients with PD and MSA, while no aggregates were detected in brains of patients with FTDP-17, PSP, CBD and NDP (**Figure 4.2a**). Then, the same brain homogenates were diluted until 10^{-3} and analyzed by RT-QuIC which showed that all of them were able to increase the kinetics of rec-αSyn aggregation but those of PD and MSA reached higher fluorescence intensities (always above 1000 AU) compared to PSP, CBD, FTDP-17 and NDP (that never crossed 500 AU). Thus, considering a threshold of 500 AU we were able to discriminate brain homogenates of patients with PD and MSA from all the others (**Figure 4.2b**). We then considered the fact that the amount of pathological α-synuclein eventually present in OM samples of PD and MSA patients is much lower than that present in the 10^{-3} dilution of brain homogenates previously tested by means of RT-QuIC, so we have performed additional

experiments using lower dilutions (10^{-6} and 10^{-9}) of PD and MSA samples. These dilutions were estimated to contain picograms (10^{-3}), femtograms (10^{-6}) and attograms (10^{-9}) of pathological α-synuclein and they all efficiently increased the kinetics of rec-αSyn aggregation. Notably, dilutions of FTDP-17 brain homogenates were used as controls and promoted rec-αSyn aggregation with less efficiency and lower fluorescence intensity (lower than 500 AU) than those of PD and MSA (Figure 4.2c).

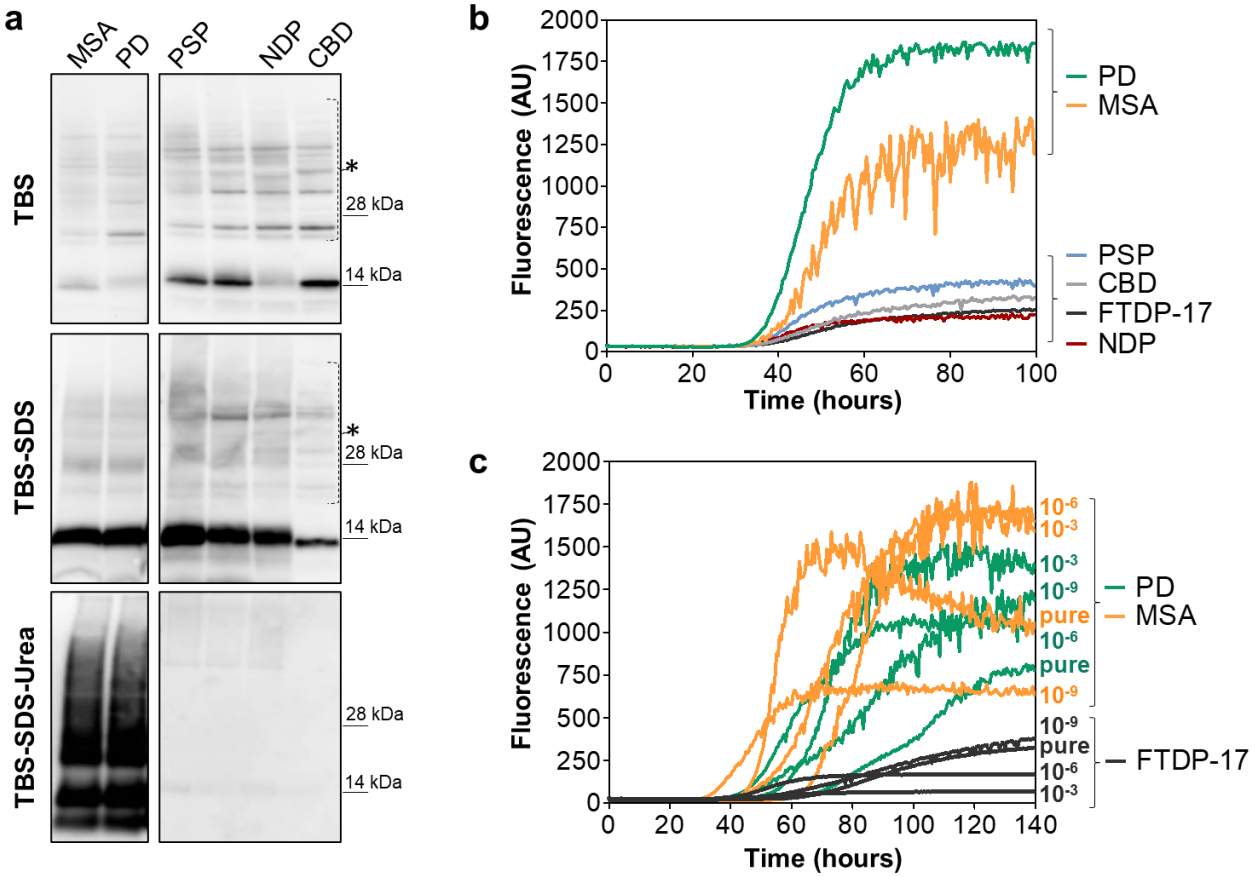

Figure 4.2 RT-QuIC analysis of brain homogenates of patients with PD and neurodegenerative parkinsonisms. **a** Extraction of soluble and insoluble αSyn fractions from BH of patients with PD, MSA, PSP, CBD, FTDP-17 or NDP control. Western blot analyses confirmed the presence of insoluble αSyn only in PD and MSA samples. Blots were immunostained with the AS08 358 antibody. Numbers in the right indicate the position of molecular weights. Asterisks indicate unspecific binding. **b** RT-QuIC analysis of BH samples. Two µL of sonicated BH collected from PD, MSA, PSP, CBD, FTDP-17 and NDP patients was added to rec-αSyn substrate and analyzed by means of RT-QuIC. PD and MSA samples efficiently induced rec-αSyn aggregation that reached higher levels of fluorescence intensities compared to those of PSP, CBD, FTDP-17 and NDP. Average ThT fluorescence intensity was plotted against time. **c** Assessment of the RT-QuIC detection limits. Serial dilutions (undiluted, 10^{-3}, 10^{-6}, 10^{-9}) of sonicated BH collected from PD, MSA and FTDP-17 subjects were analyzed by means of RT-QuIC. All dilutions efficiently induced rec-αSyn aggregation but those of FTDP-17 were characterized by lower fluorescence intensities compared to those of PD and MSA. Average ThT fluorescence intensity was plotted against time.

4.1.3 *Analysis of final RT-QuIC products seeded with different brain homogenates did not show biochemical differences*

In light of the fact that it is known that different strains of α-synuclein (responsible for PD and MSA) could force the same substrate to acquire distinct abnormal conformations, we decided to perform biochemical analysis of the final reaction products seeded with PD, MSA and FTDP-17, by analyzing them by Western blot, after PK digestion (100 μg/mL for 60 min at 37 °C). Regardless of the brain homogenate used to seed the reaction, all α-synuclein aggregates showed similar electrophoretic mobility and banding profile. Therefore, PK digestion alone was not able to demonstrate whether different seeds could imprint their specific conformations to rec-αSyn. Although characterized by low fluorescence intensity, also FTDP-17 brain homogenate revealed the presence of PK-resistant α-synuclein aggregates whose biochemical profile was similar to those of PD and MSA (Figure 4.3).

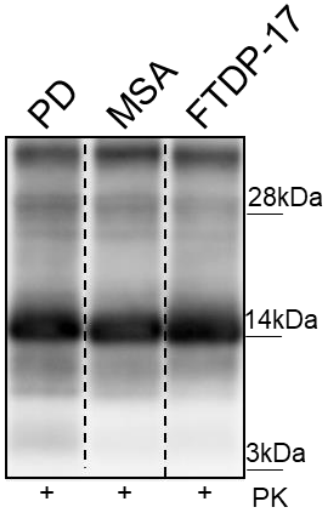

Figure 4.3 Western blot analyses of RT-QuIC aggregates seeded with 10^{-3} dilutions of BH of PD, MSA and FTDP-17 subjects. Samples show the same banding profile. Blots were immunostained with the AS08 358 antibody. Numbers in the right indicate the position of molecular weights. Dashed lines indicate cropped images from separate gels.

4.1.4 *OM samples of patients with a clinical diagnosis of PD or MSA efficiently seeded RT-QuIC reaction.*

OM samples collected from patients with a clinical diagnosis of PD (n = 18), MSA (n = 11), CBD (n = 6) and PSP (n = 12) were blindly analyzed by means of RT-QuIC to investigate their effects on the kinetics of rec-αSyn aggregation. We have then set thresholds of time (120 h) and fluorescence intensity (6 AU) (as described in materials and methods), in order to exclude any background signal, and we have found that 10 out of 18 samples of PD and 9 out of 11 samples of MSA were able to efficiently accelerate rec-αSyn aggregation. Similarly, 1 out of 6 samples of patients with CBD and 2 out of 12 samples of patients with PSP were able to trigger rec-αSyn aggregation. Hence, we have observed α-synuclein seeding activity in 19 out of 29 samples belonging to patients with probable α-synuclein pathology but also in 3 out of 18 samples belonging to patients with probable tauopathies. This may be due to the fact that CBD or PSP can be caused by distinct abnormal strains of tau able to cross-seed the aggregation of α-synuclein with different efficiency. Otherwise, such seeding activity might suggest that these diseases have been misdiagnosed or they might have been correctly diagnosed but characterized by an incidental Lewy body deposition. Notably, we did not find any correlation between positive RT-QuIC results and other clinical evaluations (especially disease duration and age at disease onset) (Figure 4.4).

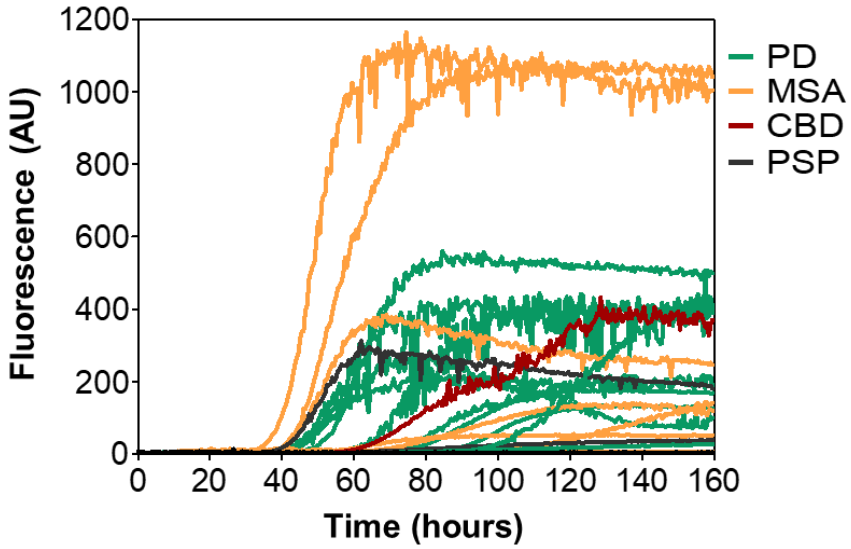

Figure 4.4 RT-QuIC analysis of OM samples collected from patients with PD and neurodegenerative parkinsonisms. Two μL of OM collected from PD (n = 18), MSA (n = 11), CBD (n = 6) and PSP (n = 12) was added to rec-αSyn substrate and analyzed by means of RT-QuIC. 10/18 samples of PD, 9/11 samples of MSA, 1/6 sample of CBD and 2/12 samples of PSP induced the aggregation of the substrate. Average ThT fluorescence intensity was plotted against time.

4.1.5 OM samples of PD or MSA patients induced the formation of α-synuclein aggregates characterized by different biochemical features.

Also in this case, after the RT-QuIC assay, final reaction products seeded with OM samples of PD or MSA were collected and subjected to PK digestion (100 μg/mL for 60 min at 37 °C), to deepen if samples belonging to patients with different forms of synucleinopathy would be able to infer to the substrate specific biochemical properties. Digested samples were then analyzed by means of Western blot with the use of antibodies directed against different epitopes (C-terminal, Non-Amyloid-β Component (NAC) core and N-terminal part) of the protein. This enabled us to demonstrate that PK treatment efficiently removed the C-terminal part of the protein, while leaving a more resistant core composed of the NAC region and the most N-terminal part of α-synuclein, spanning from residues 1 to 15. Western blot analyses with anti-C-terminal antibodies (4D6, AB5038) and anti-NAC antibody (5C2) did not provide informative data other than demonstrating the presence of a PK-resistant core (**Figure 4.5a**). In contrast, analyses with the antibody against the most N-terminal part of the protein demonstrated the presence of important and reproducible differences between samples seeded with olfactory mucosa of PD or MSA patients. In general, we have noted a higher resistance to PK digestion of all RT-QuIC products seeded with MSA samples compared to those seeded with PD. Densitometric analysis performed in triplicate on 4 PD and 4 MSA seeded samples confirmed that these differences were statistically significant ($p = 0.0061$) (**Figure 4.5c**). Additionally, samples seeded with PD were characterized by the presence of a PK-resistant band migrating between 6 and 8 kDa, while samples seeded with MSA showed three PK-resistant bands, two migrating between 6 and 8 kDa, and a third one migrating at around 22 kDa (**Figure 4.5d**). OM that did not induce α-synuclein aggregation, comprising some cases of PD or MSA and almost all PSP and CBD samples, were completely digested by PK and did not show any resistant band (**Figure 4.5e**). Some PSP and CBD samples induced α-synuclein aggregation and showed a PK-resistant α-synuclein banding profile typical of those observed in MSA seeded reactions (**Figure 4.5b**).

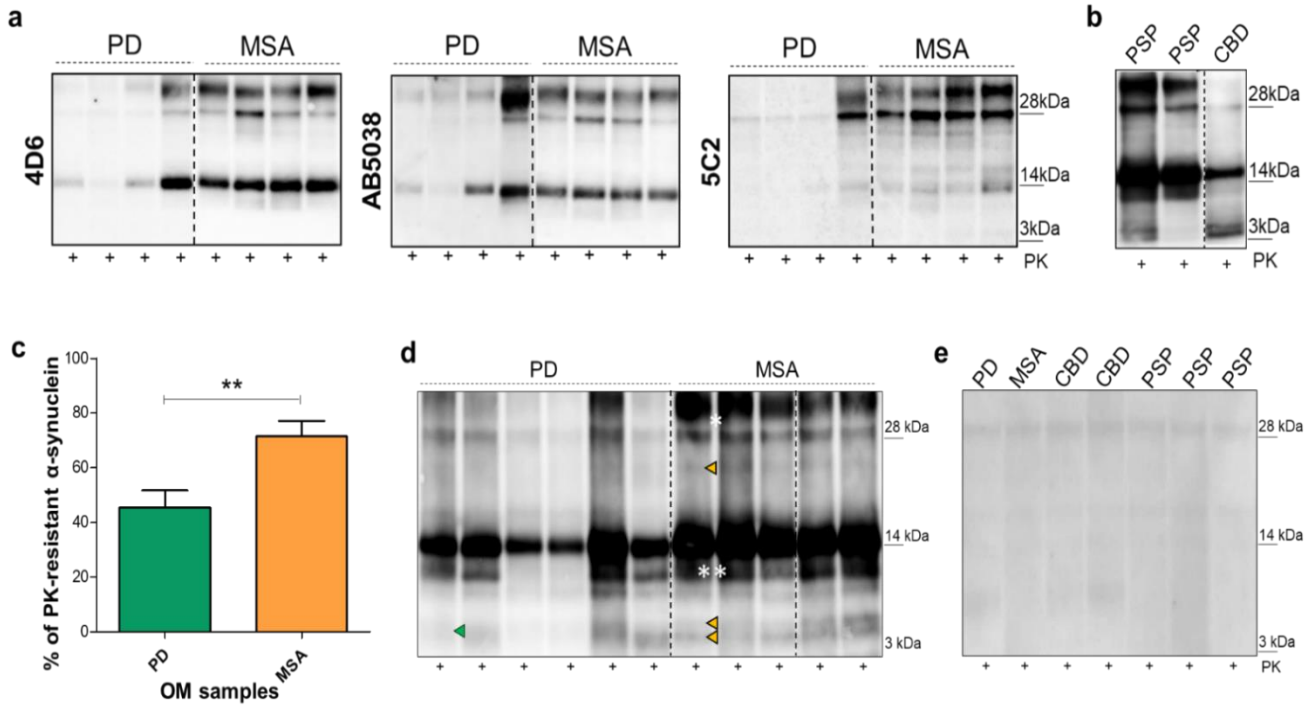

Figure 4.5 Biochemical analyses of RT-QuIC products of OM samples (representative image). Ten µL of final RT-QuIC products were digested with PK and analyzed by means of Western blot. **a** Epitope mapping of RT-QuIC aggregates seeded with OM samples of patients with PD and MSA. C-terminal (4D6 and AB5038) antibodies did not detect any typical PK-resistant αSyn band associated with PD or MSA, while the NAC antibody (5C2) detected a faint PK-resistant αSyn, especially in MSA seeded samples. Numbers in the right indicate the position of molecular weights. **b** Western blot analyses of RT-QuIC aggregates seeded with OM samples of patients with tauopathies that induced rec-αSyn aggregation. Samples show a banding profile comparable to that of MSA seeded RT-QuIC reactions. Blots were immunostained with the AS08 358 antibody. Numbers in the right indicate the position of molecular weights. **c** Densitometric analysis of RT-QuIC products seeded with PD (n = 4) or MSA (n = 4) samples. Three replicates per sample were subjected to PK treatment (100 µg/mL, 37 °C, 60 min) and immunostained with the AS08 358 antibody before quantification. This analysis confirmed that differences in PK resistance between PD and MSA samples were statistically significant ($p = 0.0061$). **d** Biochemical analyses of RT-QuIC products of OM samples collected from PD and MSA patients that induced rec-αSyn aggregation. Green arrows indicate peculiar bands of RT-QuIC products seeded with PD samples. One band migrating at around 6–8 kDa is found in these samples. Orange arrows indicate peculiar band of RT-QuIC products seeded with MSA samples. Two bands are detected at around 6–8 kDa and a third band is detected at around 22 kDa. Blots were immunostained with the AS08 358 antibody. One asterisk (*) indicates the presence of aggregated species of αSyn, while two asterisks (**) indicate partially digested protein. Numbers in the right indicate the position of molecular weights. **e** Biochemical analyses of RT-QuIC products of OM samples collected from PD, MSA, CBD and PSP patients that did not induce rec-αSyn aggregation. Ten µL of final RT-QuIC products were digested with PK and analyzed by means of Western blot and revealed the lack of PK-resistant bands. Blots were immunostained with the AS08 358 antibody. Numbers in the right indicate the position of molecular weights. Dashed lines in **a**, **b** and **d** indicate cropped images from separate gels.

4.1.6 *OM samples of PD or MSA patients induced the formation of α-synuclein aggregates characterized by different structural features*

Since we have observed the presence of specific biochemical patterns in the RT-QuIC reaction products, we have integrated Western blot analysis with TEM analysis, to verify whether the differences in PK-resistant fragments were associated with morphological characteristics. Thus, we have analyzed the structural features of aggregated rec-αSyn obtained at the end of the RT-QuIC assays seeded either with OM samples of PD (n = 5) or MSA (n = 5) patients. The shape, number and length of 50 fibrils per patient were analyzed, with special focus on the presence and the distance between consecutive over-twists present in the same fibril. The data of the 250 fibrils per pathology were pooled together for each pathology (PD or MSA) and showed that the same αSyn substrate was surprisingly able to acquire different structural features when seeded with two distinct strains of αSyn.

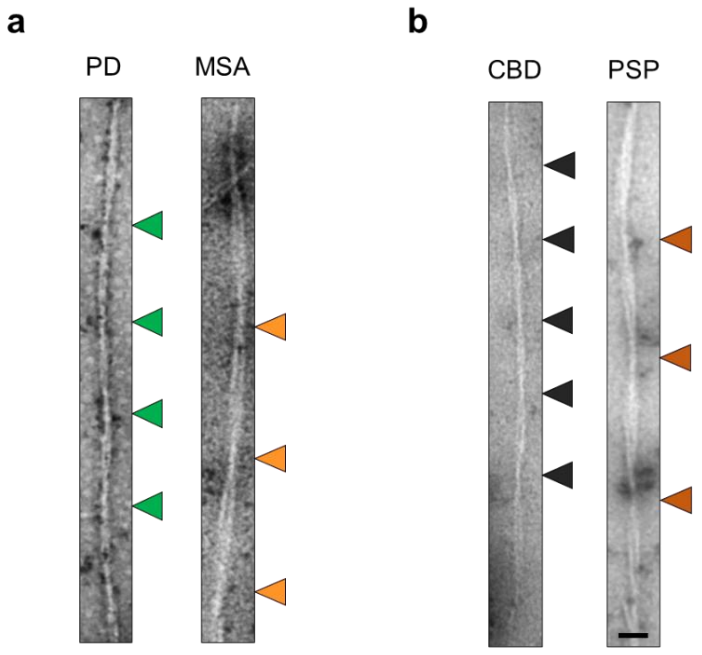

Figure 4.6 Representative TEM images of RT-QuIC products seeded with OM samples. **a** Measurements of the distance between over-twists in final RT-QuIC fibrils seeded with samples of PD (n = 5) and samples of MSA (n = 5). As shown, the distance between over-twists in αSyn fibrils obtained from RT-QuIC products seeded with OM of MSA patients (orange arrows) was about 142 ± 1.3 nm (mean ± standard error of the mean) while that of PD patients (green arrows) was shorter and about 131 ± 1.1 nm and such differences were statistically significant ($p < 0.0001$, Mann-Withney U test). Scale bar: 35 nm. **b** Measurements of the distance between over-twists in final RT-QuIC products seeded with CBD (n = 1) and PSP (n = 1) samples. As shown, the distance between over-twists in αSyn fibrils obtained from RT-QuIC products seeded with OM of CBD (black arrows) and PSP (brown arrows) patients was about 115 ± 1.7 nm (mean ± standard error of the mean) and 155 ± 1.5 nm, respectively. Scale bar: 35 nm.

In particular, we have observed that the distance between overtwists in α-synuclein fibrils obtained from RT-QuIC products seeded with OM of MSA patients was about 142 ± 1.3 nm (mean ± standard error of the mean) while that of PD patients was shorter and about 131 ± 1.1 nm and such differences were statistically significant ($p < 0.0001$, Mann-Withney U test) and reproducible over time and within pathologies (**Figure 4.6a**). We have finally analyzed the RT-QuIC aggregates induced by some PSP or CBD samples and observed that the distance between over-twists was different from those of MSA or PD samples. In particular, those of PSP patients were at about 155 ± 1.5 nm, while those of CBD were at about 115 ± 1.7 nm (**Figure 4.6b**).

4.2 Second study

4.2.1 RT-QuIC analysis of OM samples and biochemical characterization of reaction products

For this study, we have collected OM from MSA (n=2) and PD (n=2) patients, named OM-MSA1, OM-MSA2, OM-PD1 and OMPD2, respectively. Samples were processed and analyzed by RT-QuIC, together with a healthy subject (HC). All the OM induced an efficient RT-QuIC seeding activity while that of HC (OM-HC) did not (**Figure 4.7a**). Final reaction products were then digested with PK and analyzed by Western blot using the AS08 358 antibody. As observed in the *First study*, the RT-QuIC products generated by OM-MSA (RQ-MSA1 and RQ-MSA2) were considerably more resistant to proteolytic digestion than those generated by OM-PD (RQ-PD1 and RQ-PD2) (**Figure 4.7b**). We also performed dot blot analysis on final RT-QuIC products, using the MJFR antibody, which recognizes fibrillary forms of αSyn. Results showed higher signal intensity in RQ-MSA1 and RQ-MSA2 samples than in RQ-PD1 and RQ-PD2, thus suggesting that the aggregates possessed distinct morphological properties (**Figure 4.7c**).

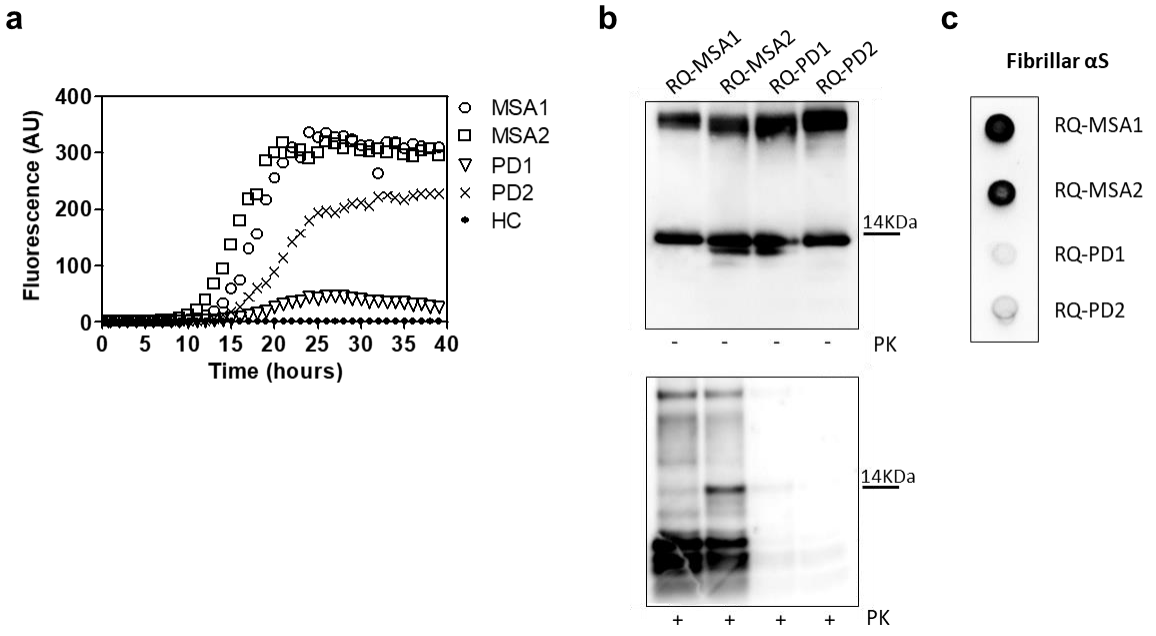

Figure 4.7 a RT-QuIC analysis of OM-MSA and OM-PD samples. OM-MSA1, OM-MSA2, OM-PD1 and OM-PD2 induced a seeding activity while OM-HC did not. Curves represented in the graph were obtained by plotting the average fluorescence intensities of each sample against time. **b** Western blot analysis of untreated or PK digested RT-QuIC products, collected at 40 hours. RQ-MSA1, RQ-MSA2, RQ-PD1 and RQ-PD2 showed similar signal intensities before digestion. RQ-MSA1 and RQ-MSA2 were more resistant to PK digestion than RQ-PD1 and RQ-PD2. Blots were immunostained with the AS08 358 antibody. Number on the right indicates the molecular weight. **c** Dot blot analysis of RT-QuIC products, collected at 40 hours. Using the αSyn filament-specific MJFR antibody RQ-MSA1 and RQ-MSA2 showed a more intense signal than RQ-PD1 and RQ-PD2.

4.2.2 Inflammatory profile of neuronal-like SH-SY5Y cells exposed to RT-QuIC products generated by OM-MSA and OM-PD

Since we have confirmed the results of our previous study, we performed again RT-QuIC reactions in the absence of ThT and final aggregates (RQ-MSA1, RQ-MSA2, RQ-PD1 and RQPD2) were used to stimulate differentiated SH-SY5Y cells for 24 h. After this time, we observed the induction of intracellular αSyn aggregation. The results obtained from RQ-MSA1 and RQ-MSA2 were mediated and collectively named RQ-MSA while those obtained from RQ-PD1 and RQ-PD2 were mediated and collectively named RQ-PD. In particular, by immunofluorescence analysis, we have observed that cells cultured with RQ-MSA and RQ-PD showed the presence of clusters of αSyn aggregates mainly localized in the cytoplasm, whereas cells exposed to unseeded RT-QuIC reaction mix (RQ-no seed) were characterized by a diffuse pattern of αSyn expression.

The distribution and amount of αSyn deposits were similar between RQ-MSA and RQ-PD exposed SHSY5Y cells and no alterations in the structure of the cytoskeleton were observed, as confirmed by F-actin staining (**Figure 4.8**).

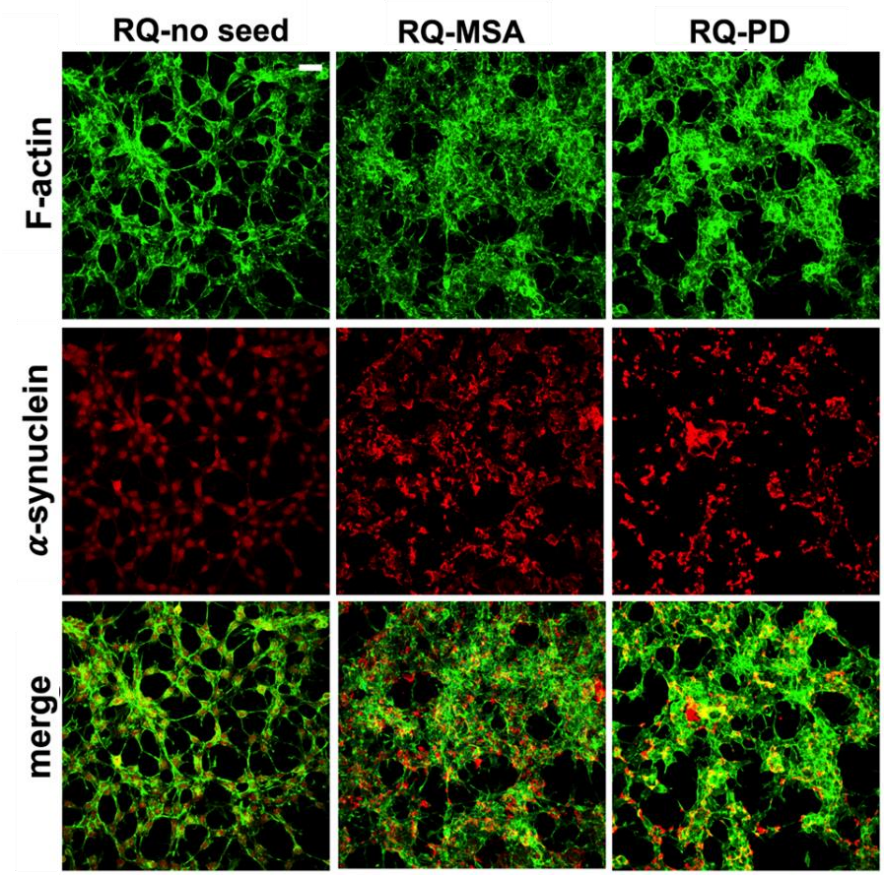

Figure 4.8 Intracellular αSyn aggregates in human differentiated neuroblastoma cells (SH-SY5Y) stimulated with RQ-MSA and RQ-PD. Representative pictures of SH-SY5Y cells incubated with RQ-MSA, RQ-PD (2.5 μM) or the unseeded RT-QuIC reaction mix (RQ-no seed) were stained with mouse monoclonal antibody against αSyn (4D6), followed by Alexa Fluor-555 donkey anti-mouse secondary Abs (red) to show the presence of intracellular aggregates of *α*Syn. SH-SY5Y cells were counterstained with fluorescently-conjugated Alexa-Fluor 488-Phalloidin (green) to highlight the thin neurite-like cytoplasmic structures (cell-to-cell contacts) denoted by F-actin filaments. Scale bar = 25μm.

Moreover, we analyzed the inflammatory effect of such aggregates on cells by means of RT-qPCR and we observed that SH-SY5Y cells exposed to RQ-PD and RQ-MSA showed an increase in transcription levels of inflammatory mediators, including TLR2, TLR6, TRAF6, IL6, NLRP3 inflammasome, and SOD2. In particular, cells stimulated with RQ-MSA showed a significantly higher expression levels for TLR2 (RQ-MSA vs. RQ-no seed: $p = 0.005$; RQ-MSA vs. RQ-PD: $p = 0.01$) (**Figure 4.9a**), TRAF6 (RQ-MSA vs. RQ-no seed: $p < 0.0001$; RQ-MSA vs. RQ-

PD: p < 0.0001) (**Figure 4.9c**), IL6 (RQ-MSA vs. RQ-no seed: p = 0.008; RQ-MSA vs. RQ-PD: p = 0.001) (**Figure 4.9d**), NLRP3 (RQ-MSA vs. RQ-no seed: p = 0.008; RQ-MSA vs. RQ-PD: p = 0.003) (**Figure 4.9e**), and SOD2 (RQ-MSA vs. RQ-no seed: p = 0.01; RQ-MSA vs. RQ-PD: p = 0.0042) (**Figure 4.9f**) than those stimulated with RQ-PD and RQ-no seed. Although upregulated, TLR6 expression levels did not reach statistical significance (**Figure 4.9b**).

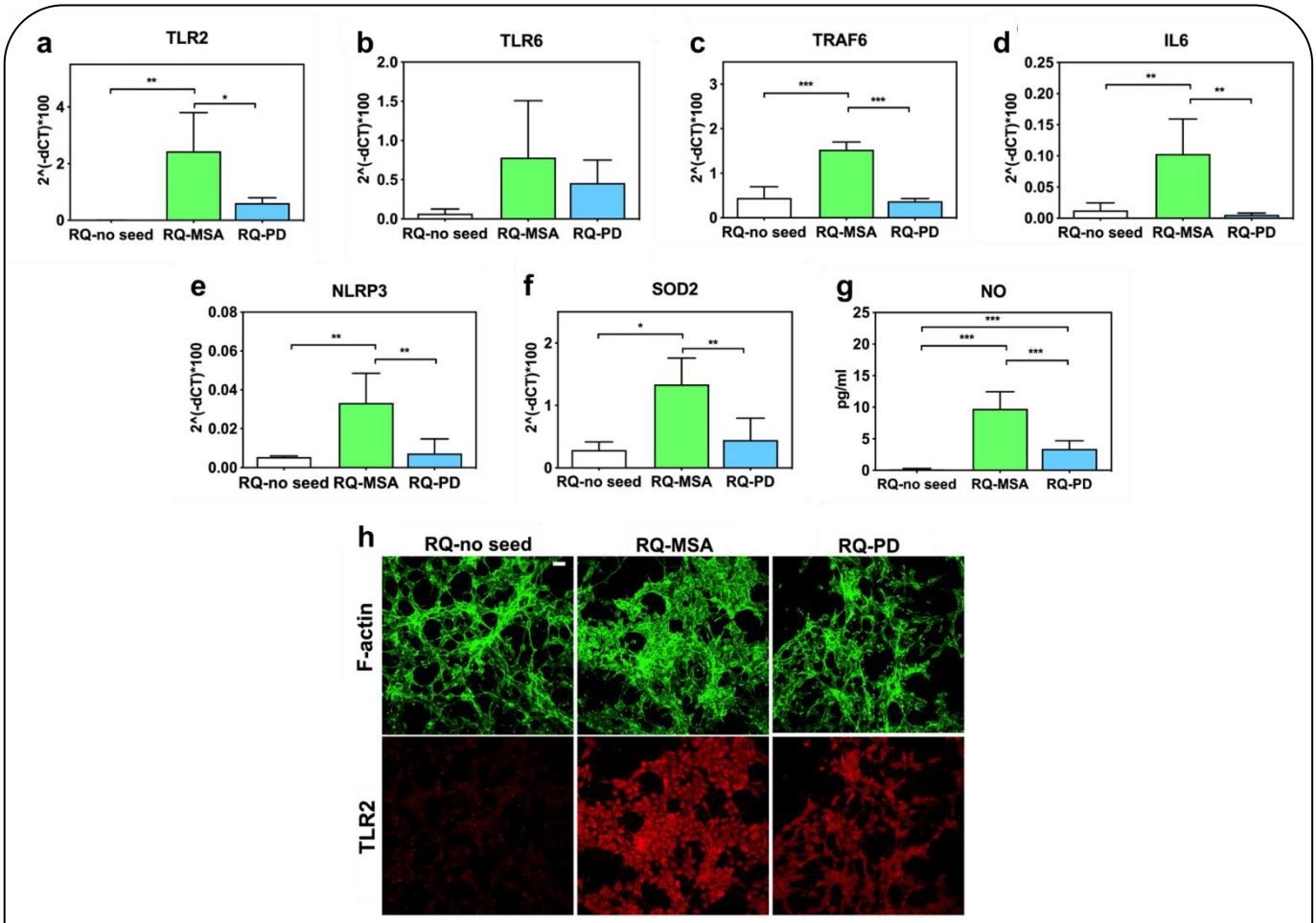

Figure 4.9 Analysis of inflammatory molecules in differentiated SH-SY5Y cells stimulated with RQ-MSA, RQ-PD and RQ-no seed. RT-qPCR analysis of TLR2 (**a**), TLR6 (**b**), TRAF6 (**c**), IL6 (**d**), NLRP3 (**e**), SOD2 (**f**) transcripts in SH-SY5Y exposed to RQ-MSA, RQ-PD (2.5 μM), and RQ-no seed for 24 hours (mean ± SD). (**g**) NO release (mean ± SD) quantification through Griess' reaction in the supernatants of cells stimulated with RQ-MSA, RQ-PD and RQ-no seed. Statistical significance was assessed by one-way ANOVA test with Dunnett's multiple comparison test. Corrected p-values are reported in the results section. **h** Confocal microscopy analysis showed increased TLR2 expression (red) in SH-SY5Y exposed to RQ-MSA and RQ-PD. Counterstaining with Alexa-Fluor 488-Phalloidin (green) was performed to monitor the cytoskeleton structure that appeared preserved in all experimental conditions. Scale bar = 25 μm.

We have also evaluated the levels of nitrites and nitrates (generally referred to as NO) in culture supernatants and found a significant increase of NO release in cells exposed to both RQ-

MSA and RQ-PD compared to unseeded RT-QuIC reaction mix (RQ-MSA vs. RQ-no seed: $p < 0.0001$; RQ-MSA vs. RQ-PD: $p < 0.001$; RQ-PD vs. RQ-no seed: $p = 0.004$) (**Figure 4.9g**). The increased TLR2 expression in RQ-MSA and RQ-PD stimulated cells was further confirmed by immunofluorescence analysis (**Figure 4.9h**).

4.2.3 Generation and morphological characterization of recombinant α-synuclein aggregates

To better investigate whether the αSyn^D strains responsible for MSA and PD might have influenced the distinctive biochemical properties of RQ-MSA and RQ-PD, we decided to generate three different artificial αSyn amyloid fibrils, named αSv1, αSv2 and αSv3. These aggregates were produced starting from rec-αSyn that was incubated in three different buffers without ThT (**Table 4.1**). To monitor the formation of αSyn fibrils in each experimental condition, a group of samples was supplemented with ThT (**Figure 4.10a**). At the end of the aggregation (monitored by ThT), samples were extensively characterized from a biochemical and morphological point of view. In particular, αSv1 fibrils mostly aggregated side-by-side, were sensitive to PK treatment and barely recognized by the MJFR antibody. In contrast, αSv2 fibrils were generally longer than those of αSv1 and did not aggregate side-by-side but formed a net-like structure. In addition, over-twists were detectable at regular intervals in most of the fibrils. These aggregates were partially resistant to proteolytic digestion and four PK-resistant bands (migrating between 3 and 14 kDa) were detected by Wb. The MJFR antibody well-interacted with the sample. Finally, αSv3 fibrils aggregated either side-by-side or by forming a net-like structure and most of them showed the presence of over-twists. We have also observed the presence of some amorphous material that was not found in the other samples (**see arrows in Figure 4.10d**). αSv3 was less resistant to enzymatic digestion than αSv2 and two PK-resistant bands were observed at Wb, always migrating between 3 and 14 kDa. In this case, the MJFR antibody did not interact with the fibrils (**Figure 10b-d**).

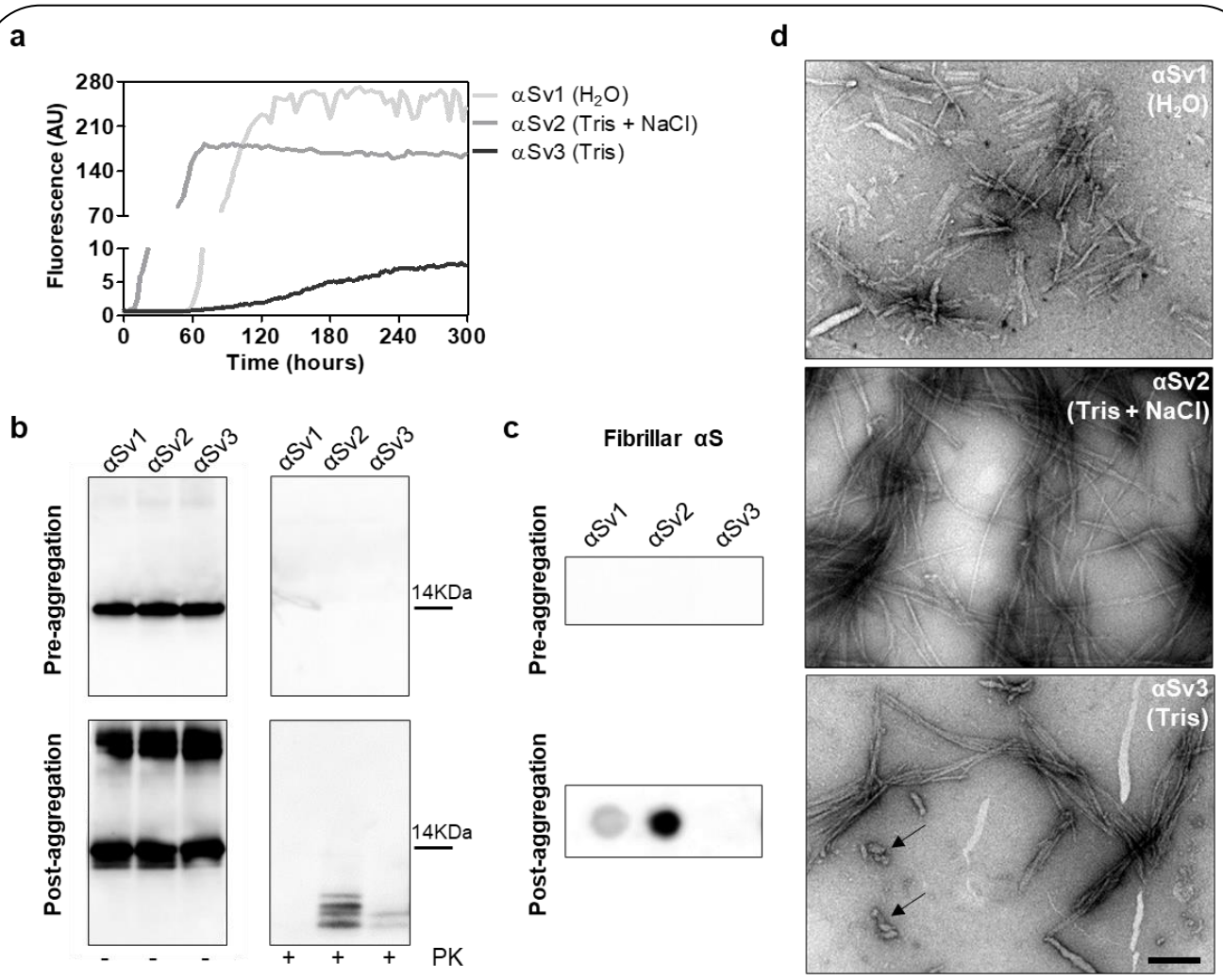

Figure 4.10 a Kinetics of αSv1, αSv2 and αSv3 aggregation. Rec-αSyn was induced to aggregate in H_2O (αSv1, light grey line), 5 mM Tris and 100 mM NaCl (αSv2, dark grey line) or 5 mM Tris (αSv3, black line), under continuous shaking, and the aggregation was monitored with the use of ThT. Curves represented in the graph were obtained by plotting the average fluorescence intensities of each sample against time. **b** Western blot analysis of untreated or PK digested αSv1, αSv2 and αSv3. Before aggregation, the rec-αSyn was completely digested, regardless of the reaction buffer. After aggregation, αSv1 was completely digested by PK, αSv2 showed four PK-resistant bands while αSv3 showed two PK-resistant bands. Samples were immunoblotted with the AS08 358 antibody. Number on the right indicates the molecular weight. **c** Dot blot analysis of αSv1, αSv2 and αSv3 using MJFR antibody. As expected, before aggregation, MJFR did not recognize αSyn fibrils. After aggregation, αSv1 and αSv2 fibrils were recognized by MJFR (although with different affinity) while αSv3 fibrils did not. **d** TEM analysis of αSv1, αSv2 and αSv3. TEM analysis showed that αSv1, αSv2 and αSv3 possessed different morphological features. Arrows indicate amorphous material found together with αSv3 fibrils. Scale bar = 200 nm.

The differences in PK resistance properties, biochemical profiles, affinity toward the MJFR antibody, and TEM findings of αSv1, αSv2 and αSv3 demonstrated that we efficiently generated distinct artificial aggregates of αSyn. Finally, αSv1, αSv2 and αSv3 were incubated

with eight fluorescent probes which differently interacted with the aggregates, hence confirming that they acquired distinct morphological properties (**Figure 4.11**).

αSyn variant	Aggregation buffer	Biochemical properties of the fibrils	Morphological properties of the fibrils		
			Length	Over-twists	Note
αSv1	H_2O	Completely digested by PK	Short	No	Arranged side-by-side
αSv2	5 mM Tris + 100 mM NaCl	Partially resistant to digestion (4 PK resistant bands detected)	Long	Yes, although few fibrils without over-twists were also found	Arranged in a net-like structure
αSv3	5 mM Tris	Partially resistant to digestion (2 PK resistant bands detected)	Mainly short	Yes, although several fibrils without over-twists were also found	Arranged either side-by-side or in a net-like structure. Presence of amorphous material

Table 4.1 Summary of the characteristics of recombinant α-synuclein variants.

4.2.4 RT-QuIC analysis of recombinant α-synuclein aggregates and characterization of final reaction products

After having been thoroughly characterized, αSv1, αSv2 and αSv3 were subjected to RT-QuIC analysis to test whether they could transmit their specific morphological features to the reaction substrate. We observed that all aggregates induced a seeding activity, even when tested at very low dilutions (**Figure 4.12a,d**). This finding showed that traces of αSv1, αSv2 and αSv3 triggered rec-αSyn aggregation with an efficiency similar to that of OM samples. However, although the αSv1, αSv2 and αSv3 were characterized by distinctive features, their RT-QuIC reaction products (named RQ-αSv1, RQ-αSv2 and RQ-αSv3, respectively) did not retain these properties and showed similar PK resistant bands at Wb.

Furthermore, aggregates were also found in RQ-no seed and their biochemical properties were comparable to those of RQ-αSv1, RQ-αSv2 and RQ-αSv3 (**Figure 4.12b**). In particular, we observed 4 bands in each sample, migrating between 3 and 14 kDa. In addition, the MJFR antibody recognized with similar affinity RQ-αSv1, RQ-αSv2, RQ-αSv3 and RQ-no seed (**Figure 4.12c**).

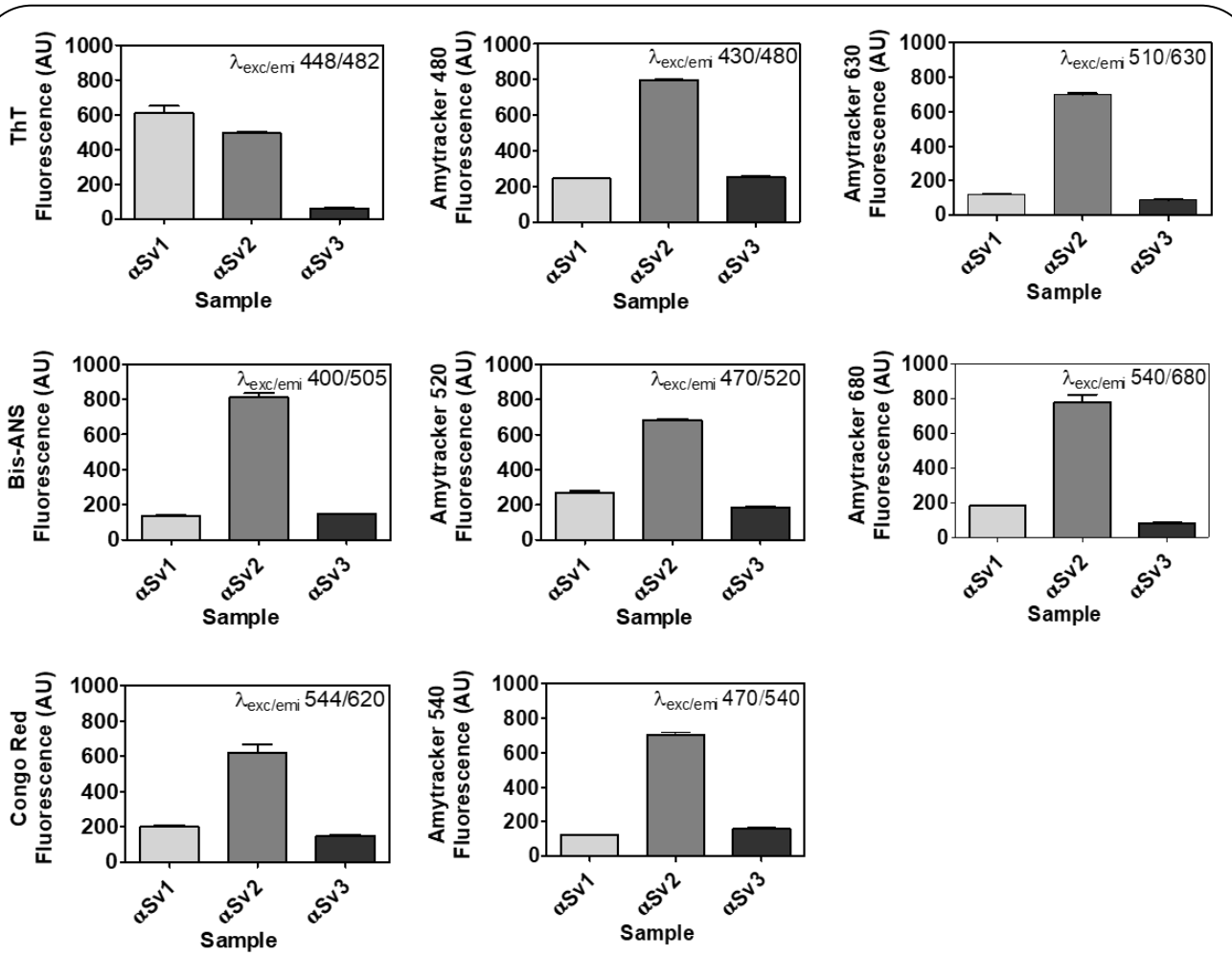

Figure 4.11 Dye-binding assay of rec-αSyn aggregates. Once generated, αSv1, αSv2 and αSv3 were incubated with ThT, Bis-ANS, Congo red, Amytracker 480, Amytracker 520, Amytracker 540, Amytracker 630, Amytracker 680. αSv1 interacted with higer efficiency with ThT than αSv2 and αSv3. αSv2 interacted with higher efficiency with all the other fluorophores while αSv3 weakly interacted with all the fluorescent probes.

Therefore, while OM-MSA and OM-PD samples were able to generate RT-QuIC products with distinctive properties, the *in vitro* generated αSv1, αSv2 and αSv3, although characterized by different morphological features, did not. For this reason, we hypothesized that only the αSyn^{D} strains present in OM samples and likely other tissue factors (e.g. microbiota) could markedly influence the misfolding process of rec-αSyn and the biochemical and morphological features of the RT-QuIC products. Hence, αSv1, αSv2 and αSv3 produced from rec-αSyn, lacked peculiar features which are present in the natural αSyn strains (e.g. phosphorylation) that could play a role in this process.

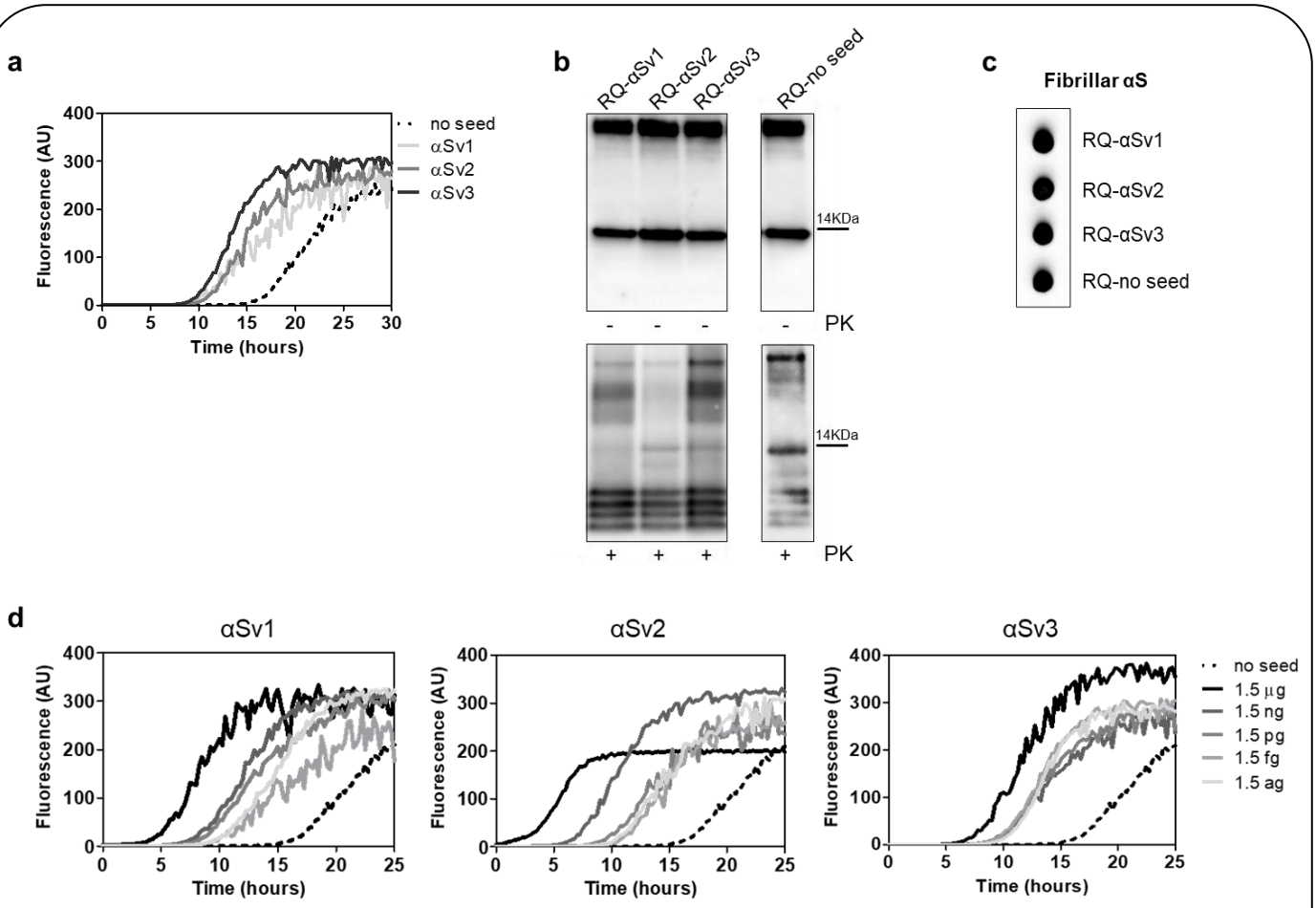

Figure 4.12 a RT-QuIC analysis of αSv1, αSv2 and αSv3. Minute amounts (1.5 ag) of αSv1, αSv2 and αSv3 were tested in RT-QuIC and induced an efficient seeding activity, with respect to the control (no seed). Curves represented in the graph were obtained by plotting the average fluorescence intensities of each sample against time. **b** Western blot analysis of untreated or PK digested RT-QuIC products, collected at 30 hours. RQ-αSv1, RQ-αSv2, RQ-αSv3 and RQ-no seed showed similar signal intensities before digestion. After PK treatment, all samples showed similar resistance to digestion and comparable biochemical profiles (AS08 358 antibody). Number on the right indicates the molecular weight. **c** Dot blot analysis of RT-QuIC products, collected at 30 hours. Dot blot analysis performed using the MJFR antibody showed the presence of a strong signal in all samples. **d** RT-QuIC analysis of serial dilutions of αSv1, αSv2 and αSv3. All dilutions were able to induced an efficient seeding activity by RT-QuIC. Curves represented in the graph were obtained by plotting the average fluorescence intensities of each sample against time.

4.2.5 Inflammatory profile of SH-SY5Y cells exposed to αSv1, αSv2, αSv3 and their RT-QuIC reaction products

Since RQ-MSA and RQ-PD induced distinct inflammatory responses in neuron-like SH-SY5Y cells, we also evaluated the inflammatory effects of αSv1, αSv2, αSv3 and their RT-QuIC reaction products in the same cellular model, with the aim to deepen if there is any correlation between the biochemical/morphological features of the αSyn aggregates and the inflammatory

responses observed in cells. For this reason, we performed RT-qPCR analyses of selected inflammatory mRNAs in cells exposed to αSv1, αSv2, and αSv3 or to their reaction buffers (devoid of rec-αSyn) as controls (**Figure 4.13**). The analysis showed differential expression of TLR2, TLR6, TRAF6 and IL6 transcripts. Since SH-SY5Y cells stimulated with all three control buffers showed analogous responses, the H_2O condition was chosen as representative control (CTRL). In particular, the expression of TLR2 was significantly higher in cells exposed to αSv3 than those exposed to αSv1 and αSv2 (αSv3 vs αSv2: $p<0.0001$; αSv3 vs αSv1: $p<0.0001$) or control (αSv3 vs CTRL: $p<0.0001$) (**Figure 4.13a**) and this increase was also confirmed at protein level by confocal microscopy analysis (**Figure 4.13f, red color**). The expression of TLR6 was found higher in cells exposed to αSv2 and αSv3 than those exposed to αSv1 or CTRL and these differences were statistically significant (αSv1 vs αSv2: $p=0.002$; αSv1 vs αSv3: $p<0.0001$; αSv2 vs αSv3: $p=0.03$; αSv2 vs CTRL: $p= 0.003$; αSv3 vs CTRL: $p<0.0001$) (**Figure 4.13b**). With respect to the cells challenged with control buffers, the expression of TRAF6 was significantly higher only in those exposed to αSv2 and a statistically significant difference was also found between αSv2 and αSv3 stimulated cells ($p=0.017$) or CTRL ($p=0.013$) (**Figure 4.13c**). Finally, a statistically significant increase of IL6 was observed in all stimulated cells compared to controls (αSv1 vs CTRL: $p=0.0002$; αSv2 vs CTRL: $p<0.0001$; αSv3 vs CTRL: $p=0.007$). Among challenged cells, a statistically significant difference was observed only between αSv2 and αSv3 ($p=0.0007$) (**Figure 4.13d**). Moreover, we have assessed the production of NO (**Figure 4.13e**) which was found increased with respect to the controls but not significantly different among αSv1, αSv2, αSv3 (αSv1 vs CTRL: $p=0.0002$; αSv2 vs CTRL: $p<0.0001$; αSv3 vs CTRL: $p=0.0004$). No alterations in the structure of the cytoskeleton of stimulated cells were detected, as confirmed by F-actin staining (**Figure 4.13f, green color**).

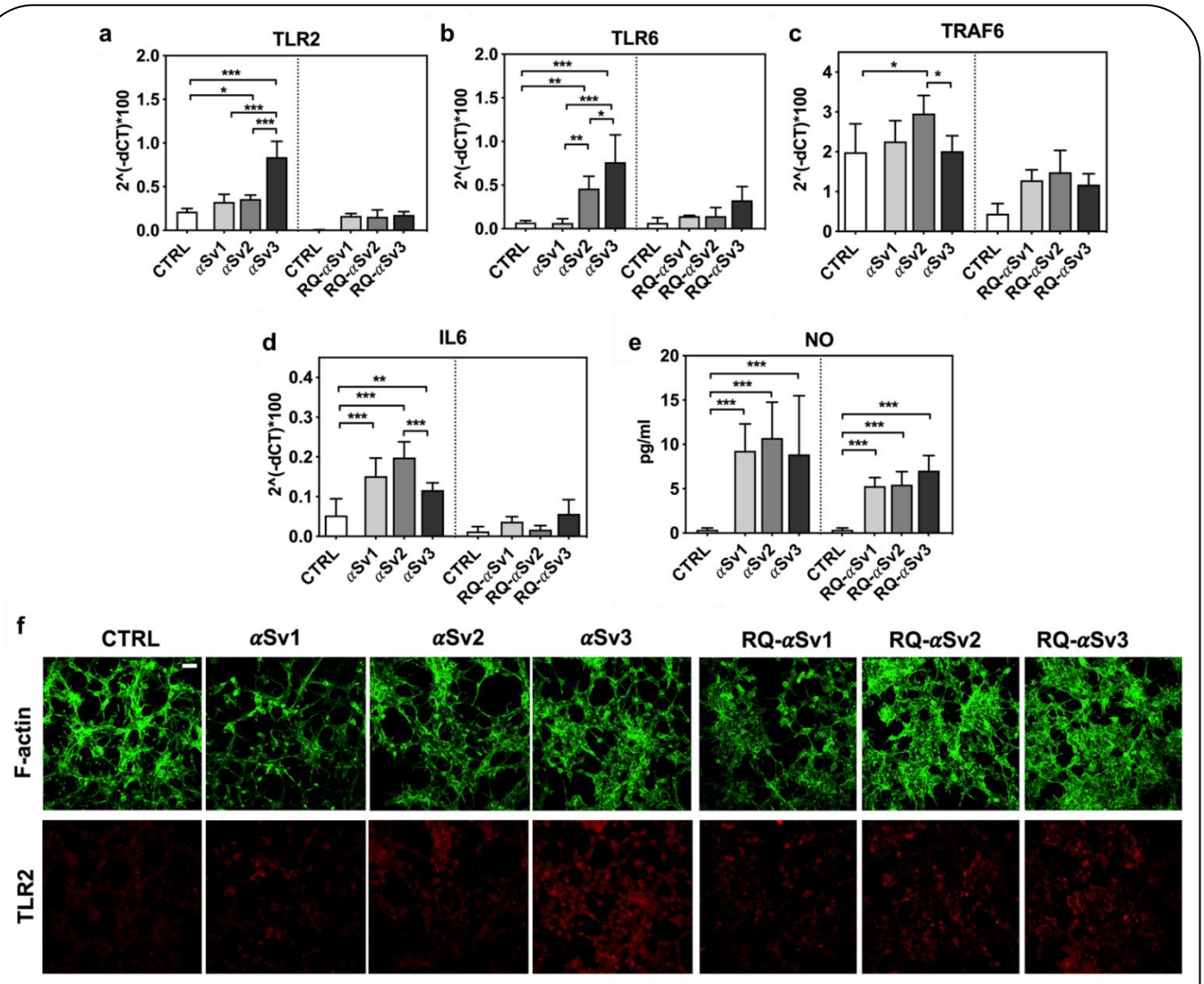

Figure 4.13 Analysis of inflammatory molecules in differentiated SH-SY5Y cells stimulated with αSv1, αSv2, αSv3 and their RT-QuIC reaction products (RQ-αSv1, RQ-αSv2, and RQ-αSv3). RT-qPCR analysis of TLR2 (**a**), TLR6 (**b**), TRAF6 (**c**), IL6 (**d**) showed an upregulation of the inflammatory mediators transcript levels in cells stimulated with αSv1, αSv2, αSv3 but not in those stimulated with RQ-αSv1, RQ-αSv2, and RQ-αSv3. **e** NO quantification in the supernatants of cells stimulated with αSv1, αSv2, αSv3, RQ-αSv1, RQ-αSv2, and RQ-αSv3 and related control buffers. A significant increase in NO release was found only in αSv1, αSv2, αSv3, RQ-αSv1, RQ-αSv2, and RQ-αSv3 stimulated cells. Values are expressed as mean ± SD. Statistical significance was assessed by one-way ANOVA test with Dunnett's multiple comparison test. Corrected p-values are reported in the results section. **f** Immunofluorescence analysis of TLR2 expression (red) in SH-SY5Y treated cells or in control condition showing an increase in protein expression in all SH-SY5Y stimulated cells that was more intense in those challenged with αSv3. Counterstaining with Alexa-Fluor 488-Phalloidin (green) was performed to monitor the cytoskeleton structure. Bar scale = 25μm.

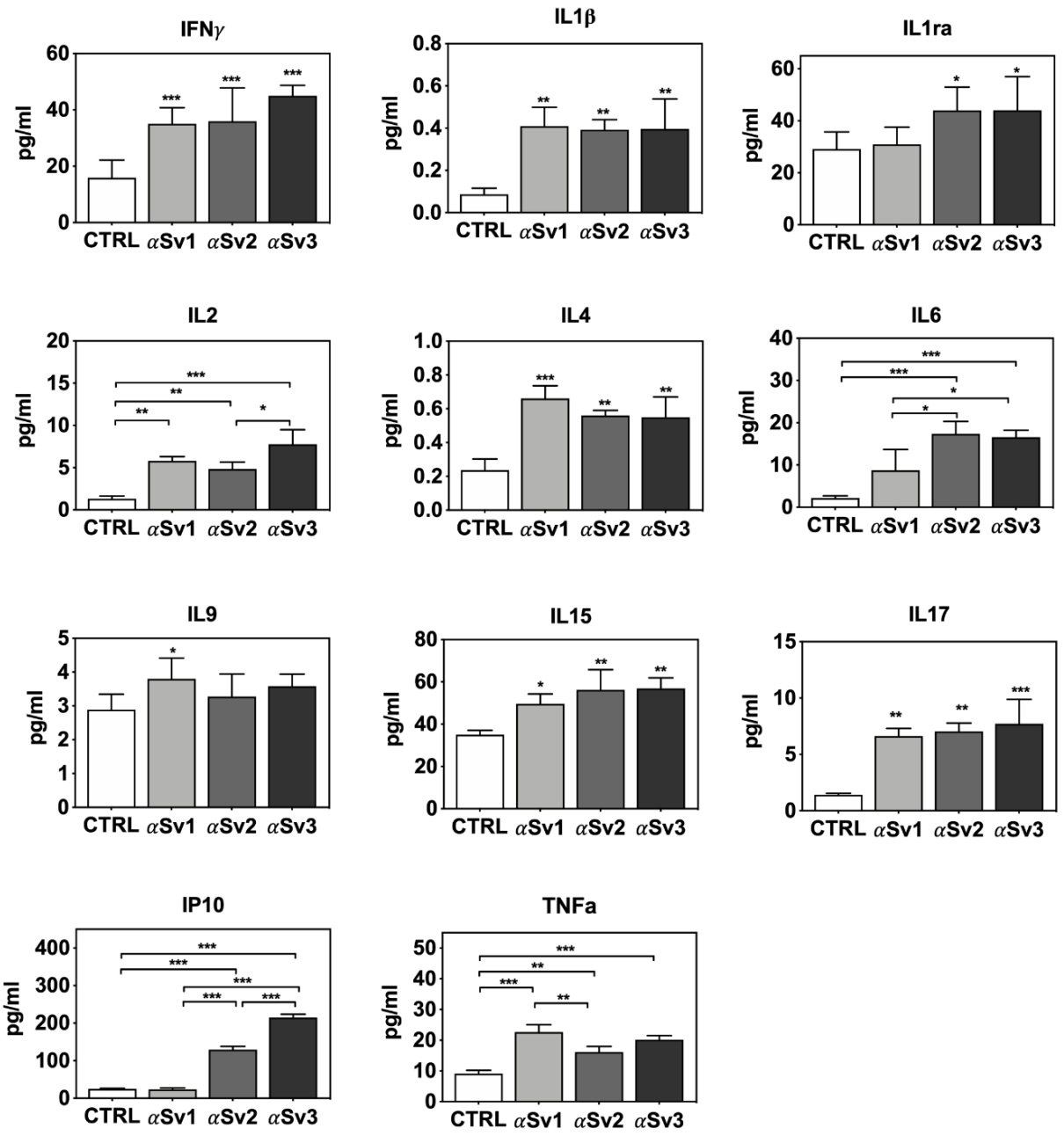

Figure 4.14 Multiparametric analysis of inflammatory mediator production from stimulated SH-SY5Y. Immune mediator quantification in the supernatants of SH-SY5Y incubated with αSv1, αSv2, αSv3 (2.5 μM for 24 hours), and control buffer medium. Among the 27 molecules analyzed, the serum concentration levels of 11 cytokines was found statistically significant: IFNγ (αSv1 vs control: p=0.0008; αSv2 vs control: p=0.0005; αSv3 vs control: p<0.0001); IL1β (αSv1 vs control: p=0.0052; αSv2 vs control: p=0.0070; αSv3 vs control: p=0.0066); ILra (αSv2 vs control: p=0.04; aSv3 vs control: p=0.03); IL2 (αSv1 vs control: p=0.0015; αSv2 vs control: p=0.0067; αSv3 vs control: p=0.0001; αSv2 vs αSv3: p=0.02); IL4 (αSv1 vs control: p=0.0005; αSv2 vs control: p=0.0028; αSv3 vs control: p=0.0034); IL6 (αSv2 vs control: p=0.0007; αSv3 vs control: p=0.001; αSv1 vs αSv2: p=0.02; αSv1 vs αSv3: p=0.03); IL9 (αSv1 vs control: p=0.02); IL15 (αSv1 vs control: p=0.04; αSv2 vs control: p=0.006; αSv3 vs control: p=0.0051); IL17 (αSv1 vs control: p=0.0017; αSv2 vs control: p=0.0011; αSv3 vs control: p=0.0005); IP10 (αSv2 vs control: p<0.0001; αSv3 vs control: p<0.0001; αSv1 vs αSv2: p<0.0001; αSv1 vs αSv3: p<0.0001; αSv2 vs αSv3: p<0.0001); TNFα (αSv1 vs control: p<0.0001; αSv2 vs control: p=0.0028; αSv3 vs control: p=0.0002; αSv1 vs αSv2: p=0.0052). Statistical significance was assessed by one-way ANOVA test with Dunnett's multiple comparison test. * p ≤ 0.05, ** p ≤ 0.01, *** p ≤ 0.001.

We have also analyzed a panel of pro-inflammatory mediators via multiparametric assays in the supernatants of stimulated cells and found a general upregulation of IFNγ, IL1β, IL1ra, IL2, IL4, IL6 IL9, IL15, IL17, IP10 and TNFα with respect to CTRL (**Figure 4.14**).

Finally, accumulation of **αSyn** was observed in all stimulated cells, and the highest signal intensity was observed in those challenged with αSv3 (**Figure 4.15, red color**). Regarding the cells stimulated with RQ-αSv1, RQ-αSv2, RQ-αSv3, respectively, we have found analogous expression levels of inflammatory mediators, including TLR2, TLR6, TRAF6, and IL6 that were higher than those of cells stimulated with CTRL (**Figure 4.13**). However, these differences did not reach a statistical significance. In contrast, we have observed a significantly higher production of NO in cells stimulated with RQ-αSv1, RQ-αSv2, and RQ-αSv3 compared to the control (RQ-αSv1 vs CTRL: $p<0.0001$; RQ-αSv2 vs CTRL: $p<0.0001$; RQ-αSv3 vs CTRL: $p<0.0001$).

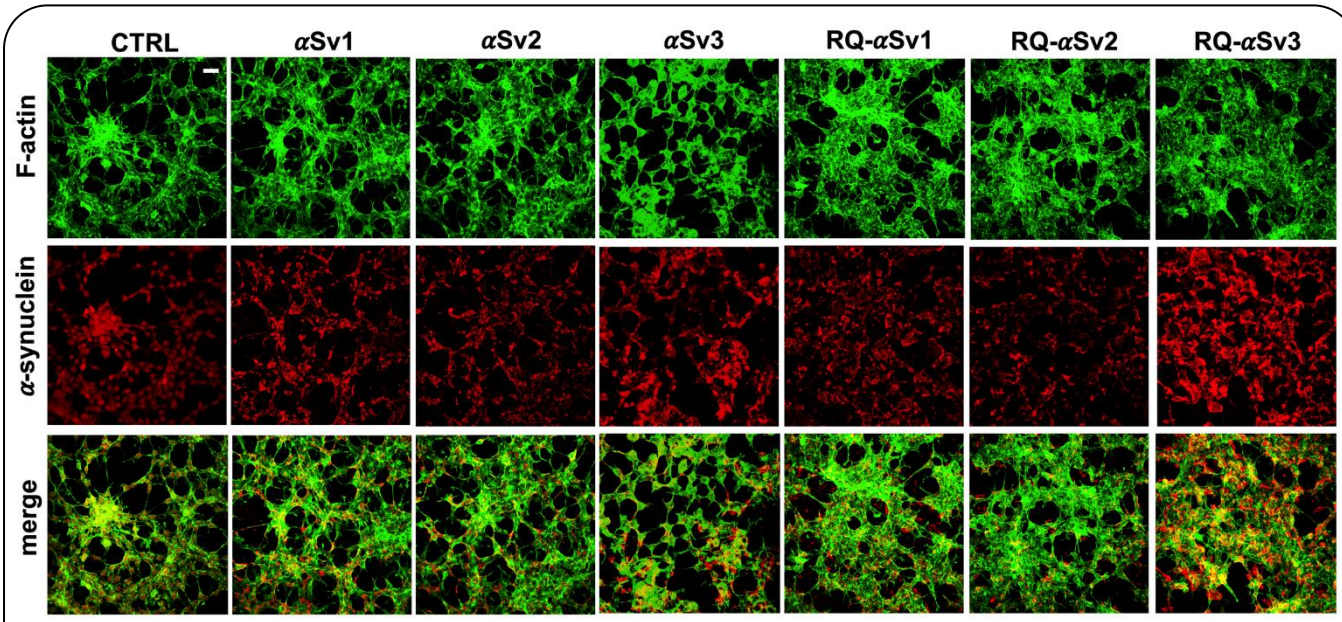

Figure 4.15 Intracellular αSyn aggregates in SH-SY5Y cells stimulated with αSv1, αSv2, αSv3 and their RT-QuIC reaction products (RQ-αSv1, RQ-αSv2, and RQ-αSv3). SH-SY5Y cells, stimulated with αSv1, αSv2, αSv3, RQ-αSv1, RQ-αSv2, RQ-αSv3 (2.5 μM for 24 hours) and control (CTRL), were stained for αSyn (red) to visualize the cellular aggregates. With respect to CTRL, all stimulated SH-SY5Y cells showed clusters of αSyn aggregates that were more abundant in those challenged with both αSv3 and RQ-αSv3. Cells were counterstained with Alexa-Fluor 488-Phalloidin (green) to highlight the thin neurite-like cytoplasmic structures (cell-to-cell contacts) denoted by F-actin filaments. The cytoskeleton of the cells was preserved, regardless of the presence of αSyn aggregates. Scale bar = 25μm.

However, although we did not observe significantly different inflammatory responses in cells stimulated with RQ-αSv1, RQ-αSv2, and RQ-αSv3, immunofluorescence analysis revealed that cells stimulated with RQ-αSv3 showed higher amount of αSyn aggregates than the others. Remarkably, higher accumulation of αSyn was also observed in cells stimulated with αSv3 (**Figure 4.15, red color**). Thus, even if the biochemical profiles of αSv3 and RQ-αSv3 differed between each other, both samples showed stronger seeding activity for αSyn when challenged in SH-SY5Y cells.

4.2.6 RT-QuIC analysis of lysates from cells stimulated with αSv1, αSv2, αSv3 and RQ-MSA and RQ-PD

We hypothesized that the lack of biochemical differences among RQ-αSv1, RQ-αSv2, RQ-αSv3 could be due to the artificial nature of αSv1, αSv2, and αSv3, as previously mentioned. For this reason, we decided to subject to RT-QuIC analysis the αSyn aggregates formed in SH-SY5Y cells stimulated with αSv1, αSv2, αSv3 (CS-αSv1, CS-αSv2, and CS-αSv3, respectively), assuming that their composition might be more similar to that of the natural αSyn^{D} strains (e.g. presence of phosphorylation). Indeed, it has already been shown that the stimulation of SH-SY5Y cells with PFFs induced intracellular accumulation of phosphorylated αSyn, which is similar to that aggregating in the brains of patients with α-synucleinopathies [224]. All samples induced an efficient seeding activity with respect to the control (CS-CTRL). Notably, the kinetics of rec-αSyn aggregation stimulated by αSv3 (**Figure 4.10a**) and CS-αSv3 were found to be less efficient compared to the other samples (**Figure 4.16a**). Also in this case, final RT-QuIC products (named RQ-CS-αSv1, RQ-CS-αSv2, RQ-CS-αSv3 and RQ-CS-CTRL) were subjected to Wb analysis after PK digestion and showed the presence of three PK resistant bands, thus confirming the lack of biochemical differences among specimens (**Figure 4.16b**). Dot blot analysis revealed that the MJFR antibody was able to bind all the aggregates with similar affinity, sustaining that they all possessed similar morphological properties (**Figure 4.16c**). These findings demonstrate that even the αSyn aggregates produced in cells were not able to imprint distinctive features to the RT-

QuIC products. However, we have noticed a difference between the biochemical profiles of RQ-αSv1, RQ-αSv2, RQ-αSv3 (Figure 4.10a) and those of CS-αSv1, CS-αSv2 and CS-αSv3 (Figure 4.16b).

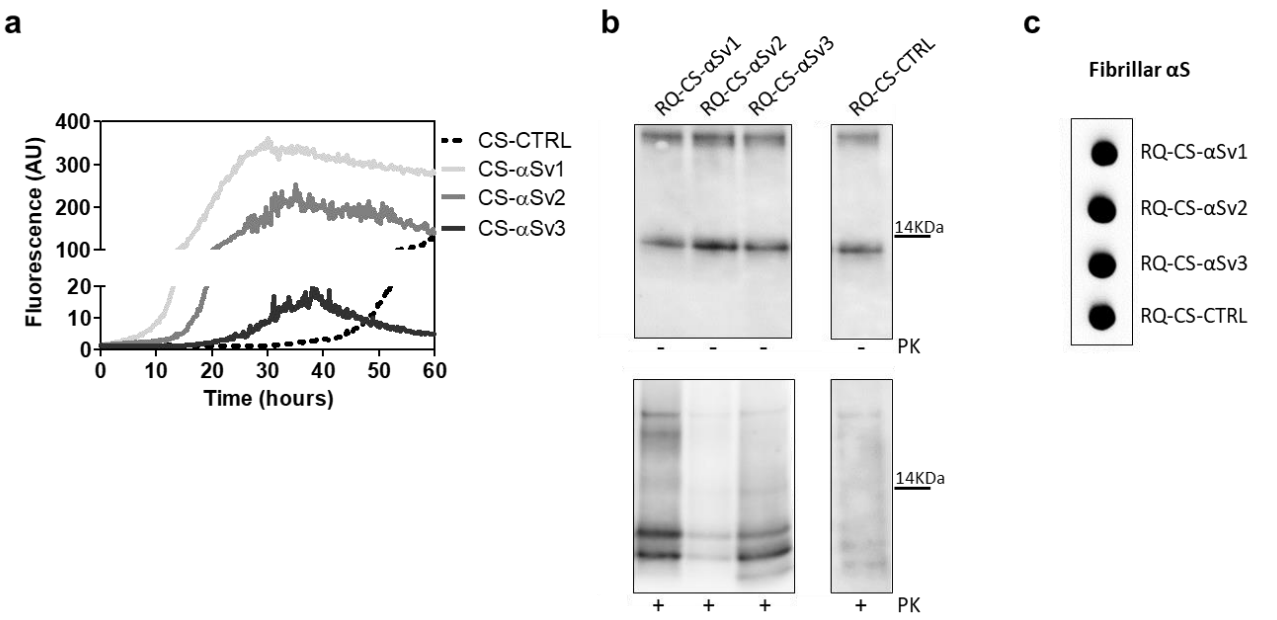

Figure 4.16 a RT-QuIC analysis of CS-αSv1, CS-αSv2 and CS-αSv3. All samples triggered a seeding activity when tested by RT-QuIC. Curves represented in the graph were obtained by plotting the average fluorescence intensities of each sample against time. **b** Western blot analysis of untreated or PK digested RT-QuIC products, collected at 60 hours. Undigested samples showed the same biochemical profiles. PK treatment of RT-QuIC products (RQ-CS-αSv1, RQ-CS-αSv2 and RQ-CS-αSv3 and RQ-CS-CTRL) showed that the samples were characterized by similar biochemical profiles, resulting in the formation of three PK resistant bands migrating between 3 and 14 kDa. Membranes were immunoblotted with the AS08 358 antibody. Number on the right indicates the molecular weight. **c** Dot blot analysis of RT-QuIC products, collected at 60 hours. Dot blot analysis performed using the MJFR antibody showed the presence of a strong signal in all the samples.

Finally, we have decided to test whether the lysates of cells stimulated with RQ-MSA and RQ-PD were still able to trigger rec-αSyn aggregation by RT-QuIC and investigate their biochemical properties. As control, we have used cells stimulated with unseeded RT-QuIC reaction mix. These samples were named CS-RQ-MSA, CS-RQ-PD and CS-RQ-CTRL, respectively and, except the control, efficiently seeded the aggregation of rec-αSyn (Figure 4.17a). Surprisingly, the biochemical profiles of the RT-QuIC products were similar among each-others but those generated by CS-RQ-MSA were more resistant than those generated by CS-RQ-PD.

Such a different sensitivity toward PK digestion of MSA and PD generated samples was also observed in RQ-MSA and RQ-PD (**Figure 4.17b**).

However, the biochemical profiles of resulting RT-QuIC products obtained from both experimental conditions have changed, suggesting that the passage in cells might have further modified the αSyn^{D} strain properties of MSA and PD. Finally, dot blot analysis revealed that the MJFR antibody was able to bind all the aggregates with similar affinity (**Figure 4.17c**).

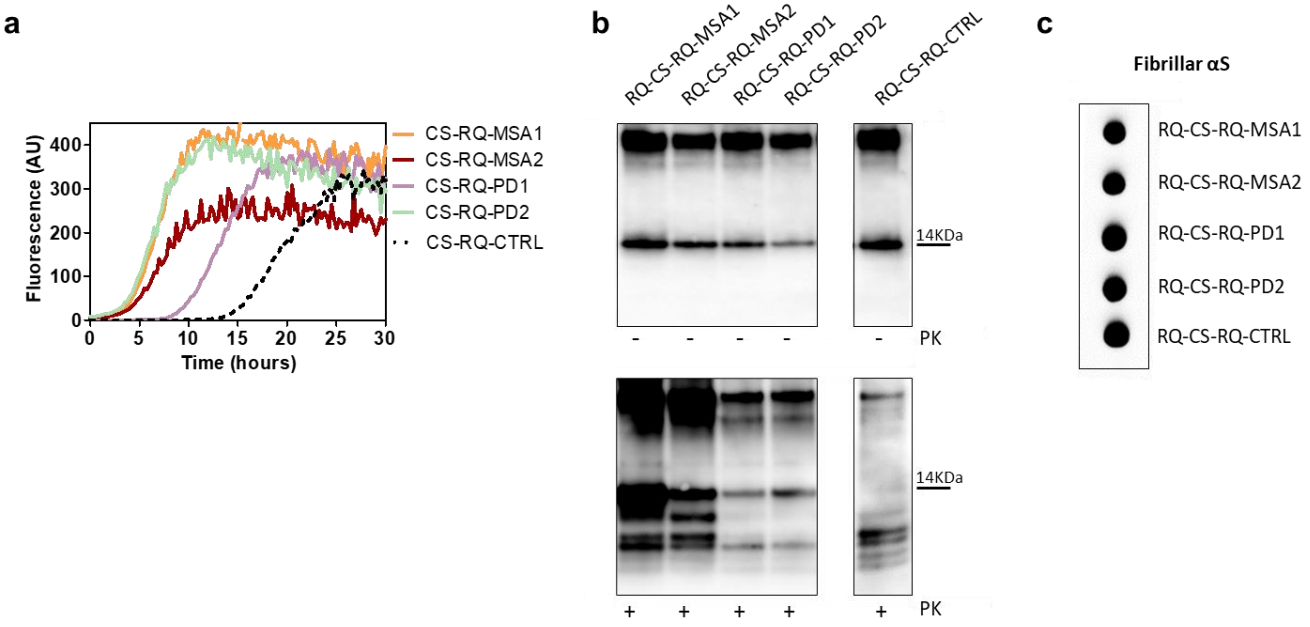

Figure 4.17 a RT-QuIC analysis of CS-RQ-MSA and CS-RQ-PD. All samples were tested by RT-QuIC and induced an efficient seeding activity with respect to the control (CS-RQ-CTRL). Curves represented in the graph were obtained by plotting the average fluorescence intensities of each sample against time. **b** Western blot analysis of untreated or PK digested RT-QuIC products, collected at 30 hours. Undigested samples showed the same biochemical profiles. Western blot analysis of PK digested RQ-CS-RQ-MSA1 and RQ-CS-RQ-MSA2 showed higher resistance to proteolytic digestion than RQ-CS-RQ-PD1 and RQ-CS-RQ-PD2. Membranes were immunoblotted with the AS08 358 antibody. Number on the right indicates the molecular weight. **c** Dot blot analysis of RT-QuIC products, collected at 30 hours. Dot blot analysis performed using the MJFR antibody showed the presence of a strong signal in all samples.

4.3 Third study

4.3.1 Efficient RT-QuIC seeding activity was observed in BH of PD, MSA-P and MSA-C patients but not in those of NAS control

First of all, we validated the new optimized RT-QuIC protocol by testing the brain homogenates of autopsy-confirmed cases of PD (n = 1), MSA-P (n = 1), and MSA-C (n = 1) as sources of different αSyn^D strains. The BH of a patient not affected by α-synucleinopathy (NAS) was used as control. The results indicate that PD, MSA-P, and MSA-C were able to induce RT-QuIC seeding activity before the time threshold set at 13 h while that of the patient with NAS did not (Figure 4.18).

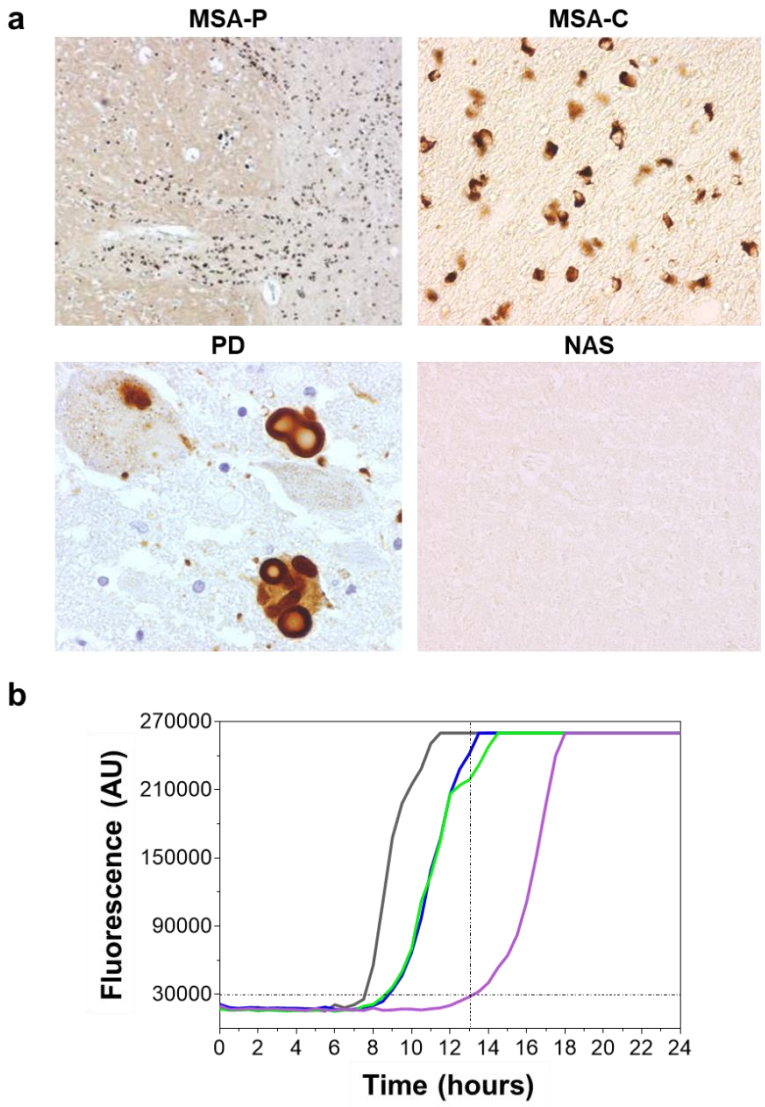

Figure 4.18 RT-QuIC analysis of brain homogenates of patients with PD, MSA-P, MSA-C and NAS. **a** Immunohistochemical analysis revealed the presence of distinct αSyn^D aggregates in the brain of tested patients, except for NAS. MSA-P and NAS images were taken using 10x magnification. MSA-C and PD images were taken using 40x magnification. **b** One µl of each BH was added to 49 µL of reaction mix and subjected to RT-QuIC analysis. The results indicate that PD (light green line), MSA-P (blue line), and MSA-C (grey line) induced RT-QuIC seeding activity before the time threshold set at 13 h while that of the patient with NAS (purple line) did not. Each sample was analyzed in quadruplicate. Curves represented in the graph were obtained by plotting the average fluorescence intensities of each sample against time.

4.3.2 *Efficient RT-QuIC seeding activity was observed in OM of PD and MSA-P patients but not in those of MSA-C patients*

As the protocol seemed to be extremely sensitive, both labs (ITA-lab and USA-lab) performed blind RT-QuIC analyses of OM samples collected from PD (% mean MDS-UPDRS Gain 30.1), MSA-P (% mean MDS-UPDRS Gain 13.3), MSA-C (% mean MDS-UPDRS Gain 17.6) patients as well as HS. According to lab-specific time thresholds, we observed that the OM of the same PD patients (9/13) and MSA-P patients (18/20) consistently induced a seeding activity for rec-αSyn thus yielding a 100% interlaboratory reproducibility of the results (**Figure 4.19a,b,c,d**). Notably, at ITA-lab the OM of PD patients induced faster rec-αSyn aggregation compared to those of MSA-P and the time to threshold (mean ± standard deviation) of PD (9.31 ± 1.19 h) was statistically different from that of MSA-P (10.54 ± 1.17 h) (t-test, $p = 0.0170$). In contrast, at USA-lab the time to threshold of PD and MSA-P samples (15.93 ± 4.41 h and 17.23 ± 3.29 h, respectively) was not statistically different (t-test, $p = 0.3944$). Similarly, both laboratories did not observe differences in the average fluorescence values reached by PD and MSA-P at the time thresholds (**Figure 4.20**). With respect to the clinical diagnosis, we obtained a 90% sensitivity of RT-QuIC seeding activity in OM samples of patients with MSA-P while that of PD patients was 69% (slightly higher than that of the *First study*). Surprisingly, except for one OM at USA-lab, none of the MSA-C samples induced RT-QuIC seeding activity, leading to a 90% interrater agreement of results (IAR) (**Figure 4.19e,f**). Thus, the opposite RT-QuIC analytical responsiveness of MSA-C and MSA-P, constantly observed in both laboratories, enabled efficient discrimination between disease phenotypes. Finally, none of the OM collected from HS induced seeding activity, except for one sample at USA-lab (**Figure 4.19g,h**). This yielded a 91% IAR between laboratories. Taken together, these data led to an overall 96% IAR between ITA-lab and USA-lab (Kappa = 0.93, 95% CI 0.83–1.00). Thus, the optimized RT-QuIC analyses enabled high levels of discrimination between: (i) MSA-P and MSA-C (chi-square test, $p < 0.001$ based on both ITA-lab and USA-lab findings), (ii) MSA-P and HS (chi-square test, $p < 0.001$ based on both ITA-lab and USA-lab findings), and (iii) PD and HS (chi-square test, $p \leq 0.001$ and $p = 0.003$ based on ITA-lab and

USA-lab findings, respectively) with a specificity of 91%. Notably, repeated cycles of freezing and thawing of the OM samples did not affect their RT-QuIC behavior.

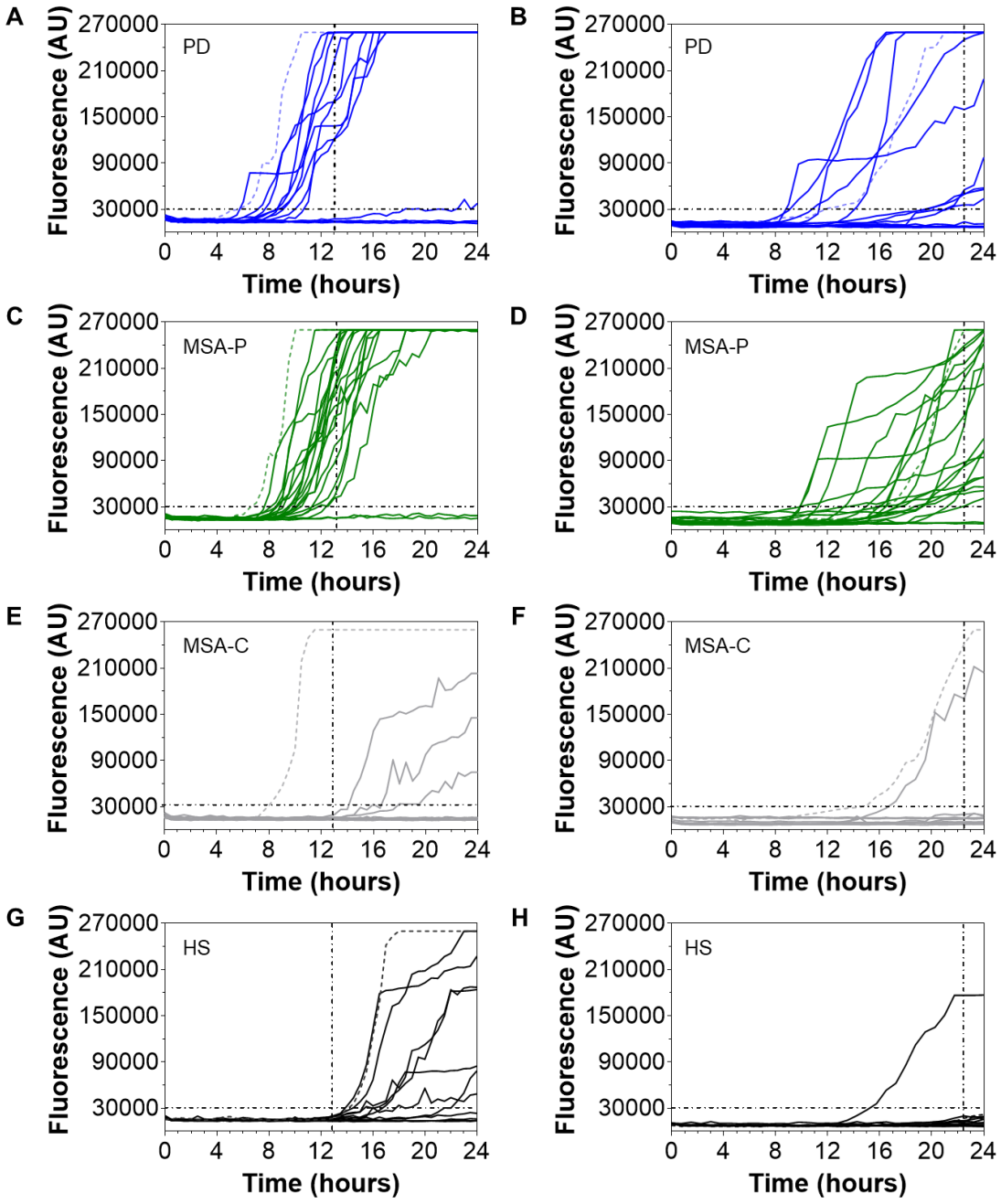

Figure 4.19 Evaluation of RT-QuIC seeding activity triggered by the OM of patients with PD, MSA-P, MSA-C, and HS. RT-QuIC seeding activity of αSyn^{D} was observed in 9/13 OM samples of the same PD patients (**a** and **b**) and 18/20 of the same MSA-P patients (**c** and **d**) analyzed at ITA-lab (**a** and **c**) and USA-lab (**b** and **d**). None of the samples collected from MSA-C (**e**) or HS (**g**) induced a seeding activity at ITA-lab, while 1/10 OM sample collected from MSA-C patients (**f**) and 1/11 sample collected from HS (**h**) induced a seeding activity at USA-lab. Samples were analyzed at least three times in quadruplicate. Curves represented in the graphs were obtained by plotting the average fluorescence intensities of each sample against time. The BH of PD (dashed curves in **a** and **b**), MSA-P (dashed curves in **c** and **d**) and MSA-C (dashed curves in **e** and **f**) patients were diluted until 10^{-4} and used as positive controls. The BH of a patient not affected by α-synucleinopathy (dashed curves in **g** and **h**) was diluted until 10^{-4} and used as negative control.

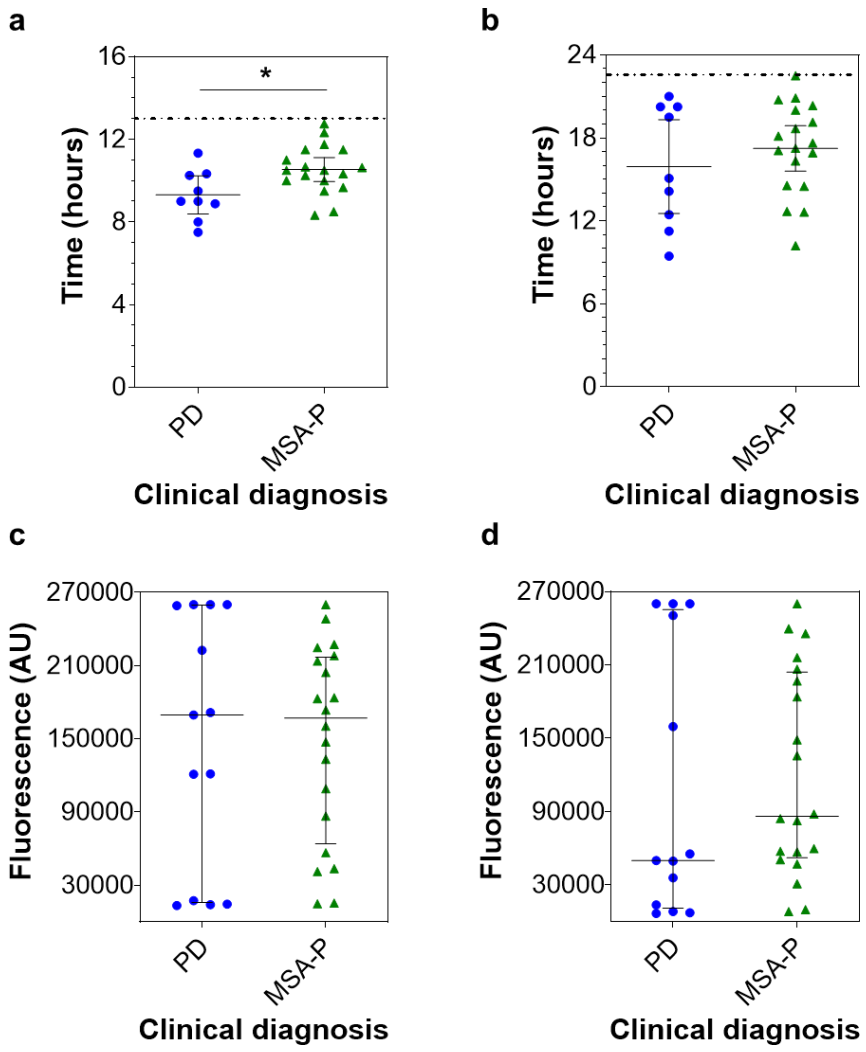

Figure 4.20 Time to threshold and mean fluorescence at time threshold obtained at ITA-lab and USA-lab. At (**a**) ITA-lab, time to threshold was significantly shorter in reactions seeded with OM samples of PD compared to that of MSA-P (unpaired t-test, p = 0.017) while at (**b**) USA-lab they were comparable (unpaired t-test, p = 0.3944). No significant differences in the average of fluorescence values reached by PD and MSA samples at the time threshold were observed in both (**c**) ITA-lab (146,494 ± 103,670 AU and 147,298 ± 80,123 AU, respectively; Mann-Whitney test, p = 0.9853) and (**d**) USA-lab (108,961 ± 110,426 AU and 119,929 ± 83,655 AU, respectively; Mann-Whitney test, p = 0.4279). In **a** and **b**, means with 95% CI are shown. In **c** and **d**, medians with interquartile range are shown.

4.3.3 RT-QuIC seeding activity of OM samples significantly correlated with patient rigidity and postural instability

We then performed association analyses between RT-QuIC seeding activity in PD and MSA-P patients and several clinical parameters: sex, cerebellar syndrome, MRI putamen strie, MRI middle cerebellar peduncle, MRI cerebellum, family history of parkinsonisms, bradykinesia, rigidity, tremor, postural instability, gait freezing, RBD, early gait ataxia, gait ataxia, limb ataxia, cerebellar dysartria, hyposmia, autonomic failure, orthostatic hypotension and other

cardiovascular dysautonomic symptoms, urinary disfunction and other dysautonomia, MRI atrophy, age at brushing, disease duration at sampling, beneficial levodopa (L-DOPA) response UPDRS, MDS-UPDRS-III OFF (**Table 4.2**). We found a significant positive association between RT-QuIC seeding activity and rigidity (seeding activity was present in 89.7% or 25.0% of patients with vs without rigidity, Fisher exact test, p = 0.014) and postural instability (seeding activity was present in 95.0% or 61.5% of patients with vs without postural instability, Fisher exact test, p = 0.025). Furthermore, there was a trend toward greater seeding activity prevalence, albeit not statistically significant, in patients with bradykinesia compared to those without symptoms (86.7% vs 33.3%, Fisher exact test, p = 0.078). Finally, an inverse, although not statistically significant, association was observed between seeding activity and disease duration (7.8 vs 5.4 years in patients without vs with seeding activity respectively, t-test, p = 0.19). Similar results were also observed considering separately PD and MSA-P patients groups.

Clinical/demographic parameter	RT-QuIC seeding activity		p-value*
	Positive	Negative	
Sex – n (%)			1
Male	16 (84.21)	3 (15.79)	
Female	11 (78.57)	3 (21.43)	
Cerebellar syndrome – n (%)			1
Yes	5 (83.33)	1 (16.67)	
No	22 (81.48)	5 (18.52)	
MRI putamen strie – n (%)			1
Yes	9 (81.82)	2 (18.18)	
No	18 (81.82)	4 (18.18)	
MRI middle cerebellar peduncle – n (%)			1
Yes	4 (100)	0 (0)	
No	23 (79.31)	6 (20.69)	
MRI cerebellum – n (%)			0.58
Yes	5 (71.43)	2 (28.57)	
No	22 (84.62)	4 (15.38)	
Family history of parkinsonisms – n (%)			1
Yes	2 (66.67)	1 (33.33)	
No	25 (83.33)	5 (16.67)	
Bradykinesia – n (%)			0.08
Yes	26 (86.67)	4 (13.33)	
No	1 (33.33)	2 (66.67)	
Rigidity – n (%)			0.01
Yes	26 (89.66)	3 (10.24)	
No	1 (25.00)	3 (75.00)	
Tremor – n (%)			0.18
Yes	18 (90.00)	2 (10.00)	
No	9 (69.23)	4 (30.77)	

Postural instability – n (%)			0.02
Yes	19 (95.00)	1 (5.00)	
No	8 (61.54)	5 (38.46)	
Gait freezing – n (%)			0.14
Yes	2 (50.00)	2 (50.00)	
No	25 (86.21)	4 (13.79)	
RBD – n (%)			1
Yes	11 (84.62)	2 (15.38)	
No	16 (80.00)	4 (20.00)	
Early gait ataxia (within 3 years of disease onset) – n (%)			1
Yes	1 (100.00)	0 (0.00)	
No	26 (81.25)	6 (18.75)	
Gait ataxia – n (%)			1
Yes	5 (83.33)	1 (16.67)	
No	22 (81.48)	5 (18.52)	
Limb ataxia – n (%)			0.56
Yes	5 (100.00)	0 (0.00)	
No	22 (78.57)	6 (21.43)	
Cerebellar dysartria – n (%)			0.56
Yes	6 (100.00)	0 (0.00)	
No	21 (77.78)	6 (22.22)	
Hyposmia – n (%)			1
Yes	4 (80.00)	1 (20.00)	
No	23 (82.14)	5 (17.86)	
Autonomic failure – n (%)			0.62
Yes	21 (84.00)	4 (16.00)	
No	6 (75.00)	2 (25.00)	
Orthostatic hypotension – n (%)			1
Yes	14 (82.35)	3 (17.65)	
No	13 (86.67)	2 (13.33)	
Other cardiovascular dysautonomic symptoms – n (%)			1
Yes	20 (83.33)	4 (16.67)	
No	7 (77.78)	2 (22.22)	
Urinary disfunction – n (%)			0.29
Yes	23 (85.19)	4 (14.81)	
No	4 (66.67)	2 (33.33)	
Other dysautonomia – n (%)			0.14
Yes	22 (88.00)	3 (12.00)	
No	5 (62.50)	3 (37.50)	
MRI atrophy – n (%)			1
Yes	9 (81.82)	2 (18.18)	
No	17 (80.95)	4 (19.05)	
Age at brushing – mean (SD)	61.22 (7.88)	61.50 (7.82)	0.94
Disease duration at sampling (year) – mean (SD)	5.37 (3.55)	7.83 (6.24)	0.19
Beneficial L-DOPA response UPDRS – mean (SD)	19.52 (10.76)	21.67 (11.06)	0.66
MDS-UPDRS-III OFF – mean (SD)	34.48 (8.87)	36.33 (12.40)	0.67

*p-values from fisher exact test or t-test, as appropriate; SD= standard deviation

Table 4.2 Association analyses between RT-QuIC seeding activity triggered by OM of PD and MSA-P patients and clinical or demographic parameters.

4.3.4 *The biochemical properties of RT-QuIC products enabled an efficient discrimination between α-synucleinopathies*

The RT-QuIC products seeded with OM samples of PD, MSA-P, MSA-C, and HS were subjected to dot blot immunoassay with the MJFR conformation-specific antibody and revealed the presence of filament-specific αSyn only in samples that induced rec-αSyn aggregation, while no significant differences were observed in the total levels of αSyn among different groups. Therefore, the seeding activity of RT-QuIC reactions induced by OM samples from PD and MSA-P can be accounted for by the newly formed αSyn fibrils. In contrast, the lack of seeding activity in OM samples from MSA-C and HS is consistent with the absence of detectable αSyn fibrils following RT-QuIC reactions (**Figure 4.21**).

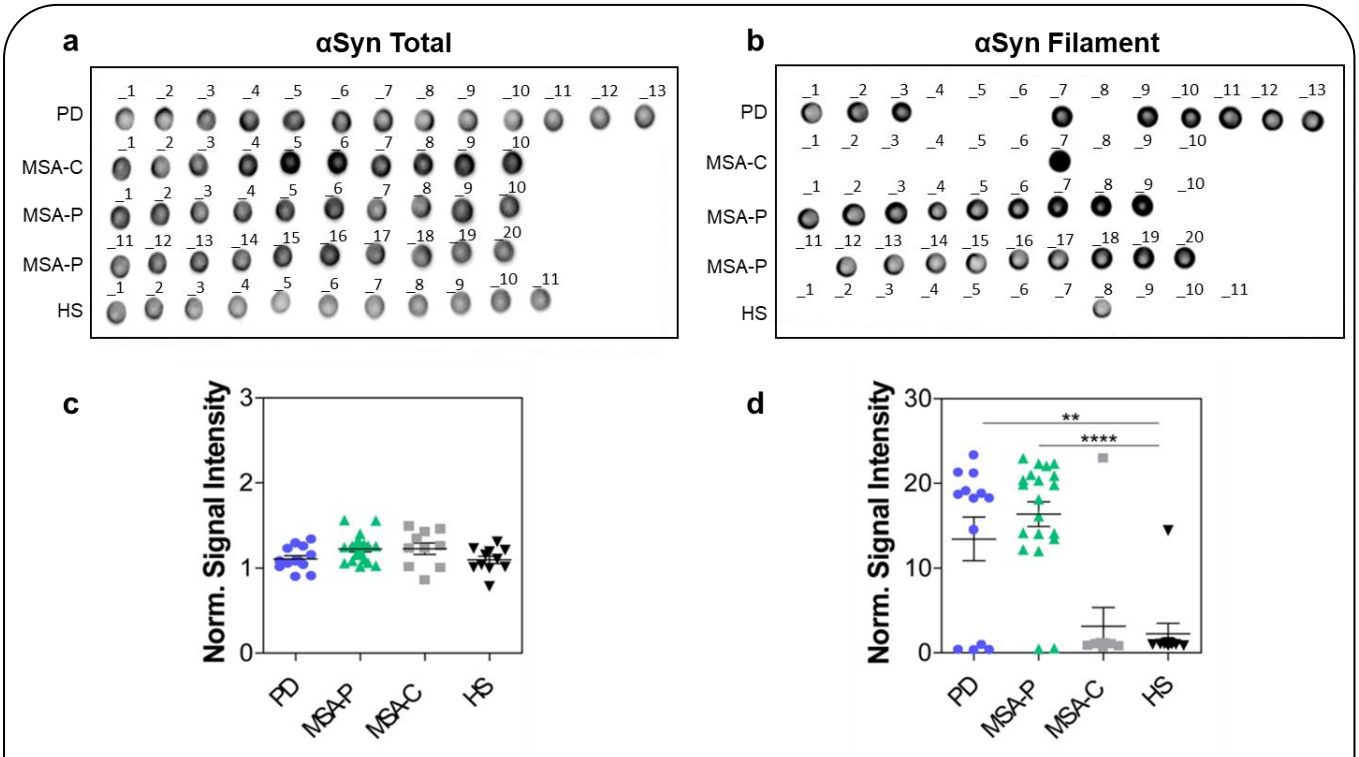

Figure 4.21 Dot blot immunoassay of RT-QuIC products from OM-seeded reactions obtained using an antibody against αSyn filament or antibody against total αSyn. **a** Total αSyn immunoreactivity was observed in all OM samples. **b** αSyn filament immunoreactivity was present only in the products generated by OM samples of PD and MSA-P but was instead absent in those produced by MSA-C and HS. **c** Statistical analysis revealed that total αSyn levels were comparable between groups ($p = 0.0619$, one-way ANOVA). **d** Levels of αSyn filament in RT-QuIC products generated by OM from PD ($p < 0.01$) and MSA-P ($p < 0.0001$) were significantly higher compared to those of MSA-C and HS (one-way ANOVA). The signal intensity of each dot was normalized to that of HS controls (set to the unit of 1) and represented as mean with SD in **c** and **d**. Densitometric analyses in **c** and **d** have been performed on dot blot images of RT-QuIC products generated from PD (n = 13), MSA-P (n = 20), MSA-C (n = 10) and HS (n = 11) OM samples at USA-lab.

The same OM-seeded RT-QuIC products were then subjected to Western blot analysis after PK treatment and showed the presence of PK-resistant bands in 14/18 MSA-P (78%) and 6/9 (67%) PD samples that induced rec-αSyn aggregation. Notably, the bands observed in MSA-P were significantly more resistant to digestion than those observed in PD (Mann-Whitney test, p = 0.0104). This difference is probably due to the likelihood that the rec-αSyn substrate was able to acquire distinct abnormal conformations which partially recapitulated those of the original αSyn^{D} strains responsible for PD and MSA-P. This may result in important differences in the PK resistance of the RT-QuIC reaction products generated from OM samples of PD and MSA-P. None of the samples belonging to MSA-C or HS showed PK-resistant signals (**Figure 4.22**).

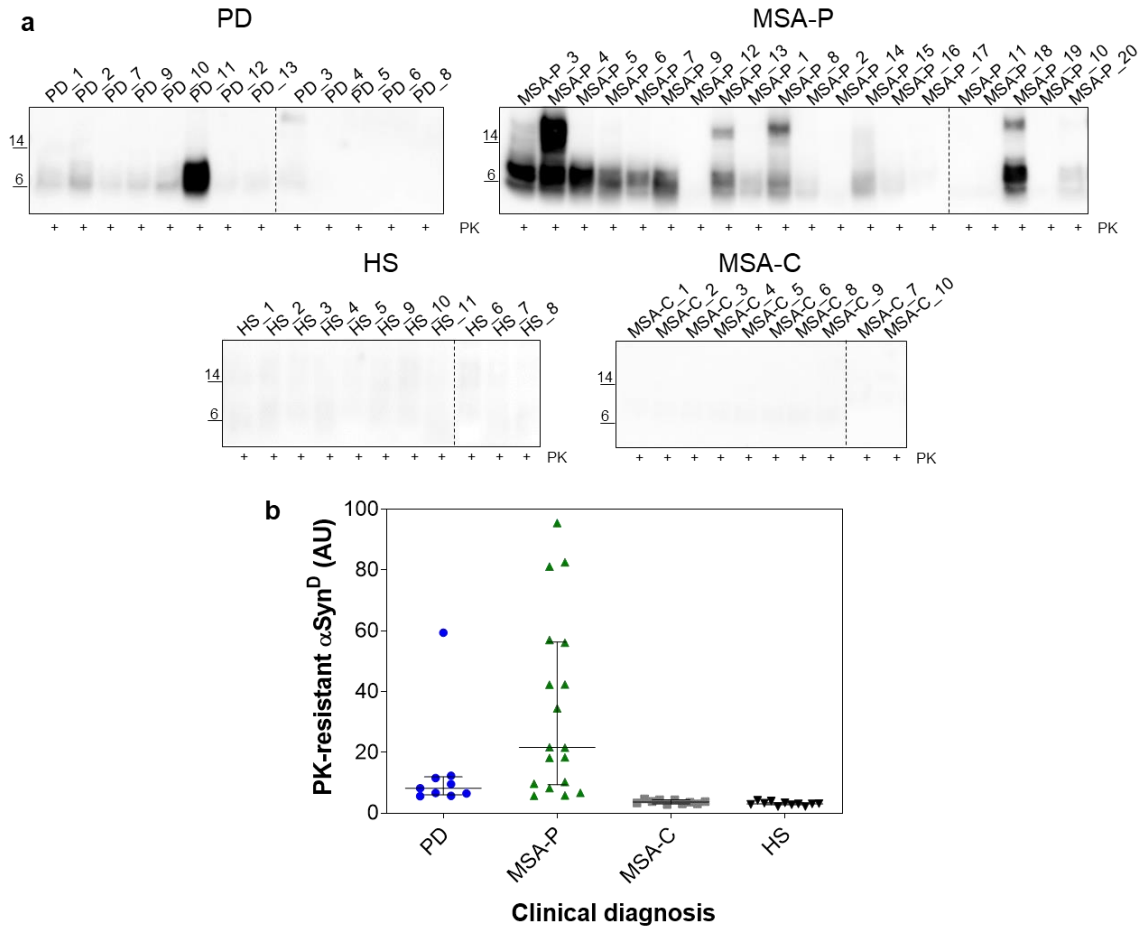

Figure 4.22 a Western blot analyses of RT-QuIC products from OM-seeded reaction showing the presence of PK resistant bands in RT-QuIC end products generated by PD and MSA-P samples. Conversely, no bands were detected in RT-QuIC end products seeded with HS and MSA-C. **b** Statistical analysis revealed that PD generated products were significantly less resistant to PK digestion compared to those generated by MSA-P (Mann-Whitney test p = 0.0104). Median with interquartile range is shown. Densitometric analyses have been performed on Western blot images of RT-QuIC products generated from PD (n = 13), MSA-P (n = 20), MSA-C (n = 10) and HS (n = 11) OM samples at ITA-lab.

Finally, the RT-QuIC products obtained from the analysis of MSA-P and MSA-C samples at ITA-lab (collected at 13 h) were analyzed by TEM and confirmed the presence of amyloid fibrils only in MSA-P samples capable of inducing an efficient seeding activity (except for MSA-P_10 and MSA-P_11 that remained negative by RT-QuIC). The amyloid fibrils were instead not detected in all MSA-C seeded samples (**Figure 4.23**).

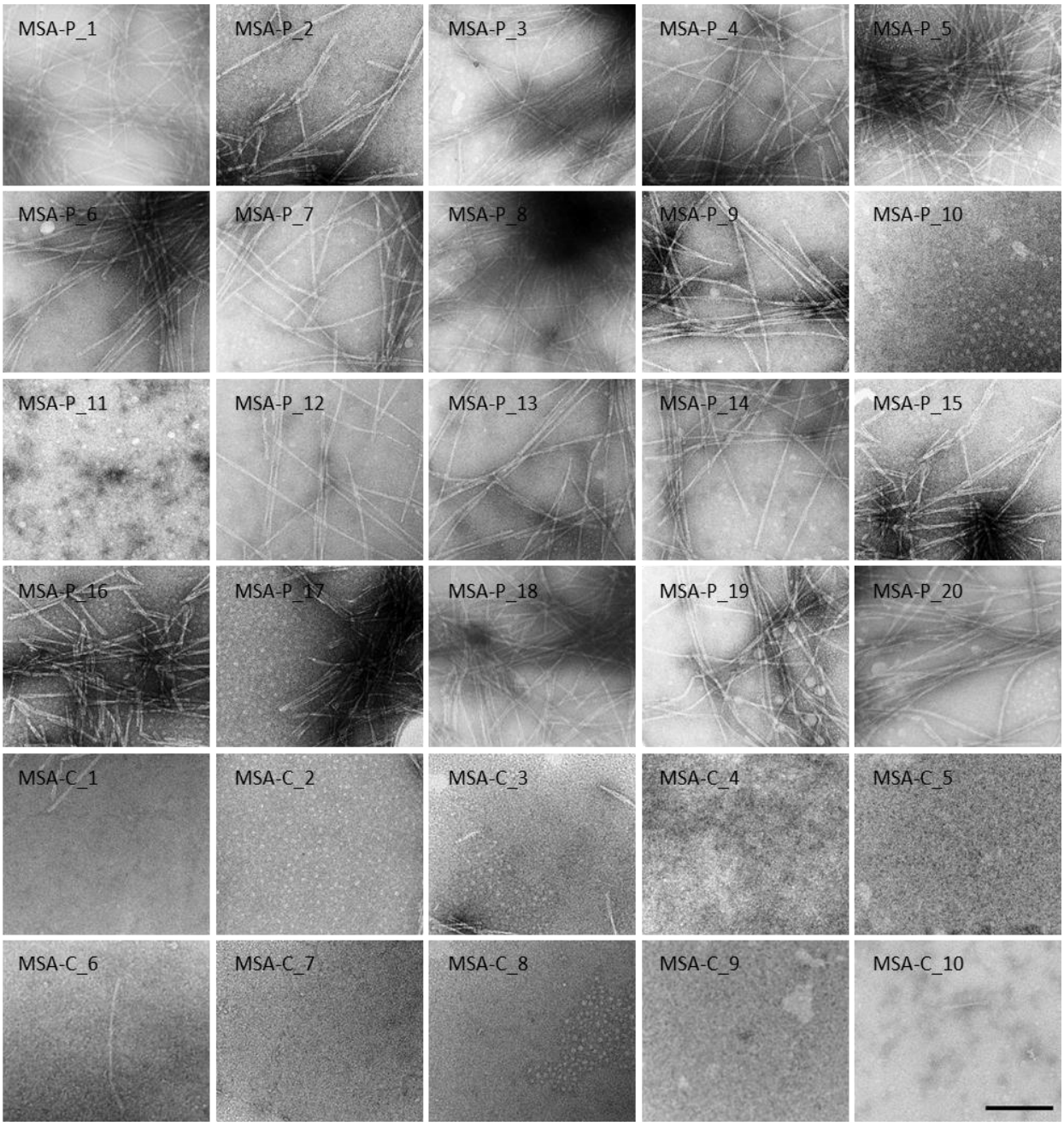

Figure 4.23 Morphological analsysis of RT-QuIC reaction products generated by MSA-P and MSA-C samples at ITA-lab. Rec-αSyn amyloid fibrils were detected in all RT-QuIC products seeded with MSA-P samples, except for MSA-P_10 and MSA-P_11. In constrast, none of the MSA-C samples induced the formation of rec-αSyn fibrils (except for occasional, rare and short aggregates detected in MSA-C_1, MSA-C_3 and MSA-C_6). All TEM images were taken at the same magnification (scale bar: 200 nm).

Similarly, when tested with different fluorescent probes known to bind protein aggregates (dye-binding assay), including ThT, Congo red and amyloid-selective marker Amytracker 630 [225], 18 out of 20 MSA-P seeded samples showed a strong fluorescence signal that was instead very weak or absent in all the other MSA tested samples (MSA-P_10, MSAP_11 and all MSA-C) (Figure 4.24).

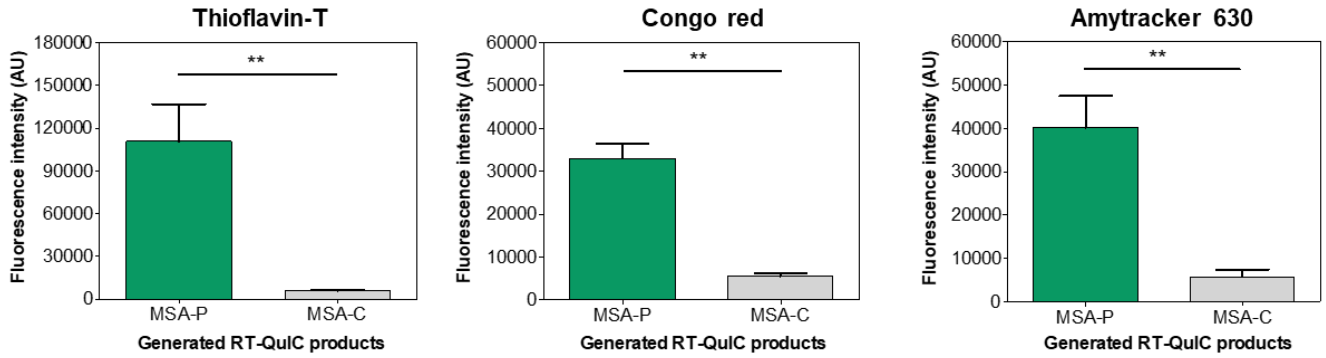

Figure 4.24 Dye-binding assay of RT-QuIC products generated by MSA-P (n = 20) and MSA-C (n = 10) samples at ITA-lab. Regardless of the probe used, all MSA-P samples (except for MSA-P_10 and MSA-P_11) showed strong fluorescent signals while the MSA-C did not. These differences were statistically significant in the case of (i) ThT (t-test p = 0.0063), (ii) Congo red (t-test, p = 0.0018) and (iii) Amytracker 630 (t-test, p = 0.0051). Graphs show the mean values (± SEM) of MSA-P and MSA-C fluorescence signals.

Finally, the epitope mapping study performed on Western blot showed the presence of PK resistant rec-αSyn only in MSA-P samples, thus further supporting these findings (Figure 4.25). Combined together, these results confirmed that there was a good correlation between the RT-QuIC seeding activity and the presence of amyloid fibrils in each sample, and that, in contrast to MSA P, the MSA-C samples did not efficiently trigger rec-αSyn aggregation. Therefore, thanks to the combination of these biochemical and morphological analyses, we were able to validate the RT-QuIC results, recognize PD and MSA-P, and even discriminate MSA-P from MSA-C.

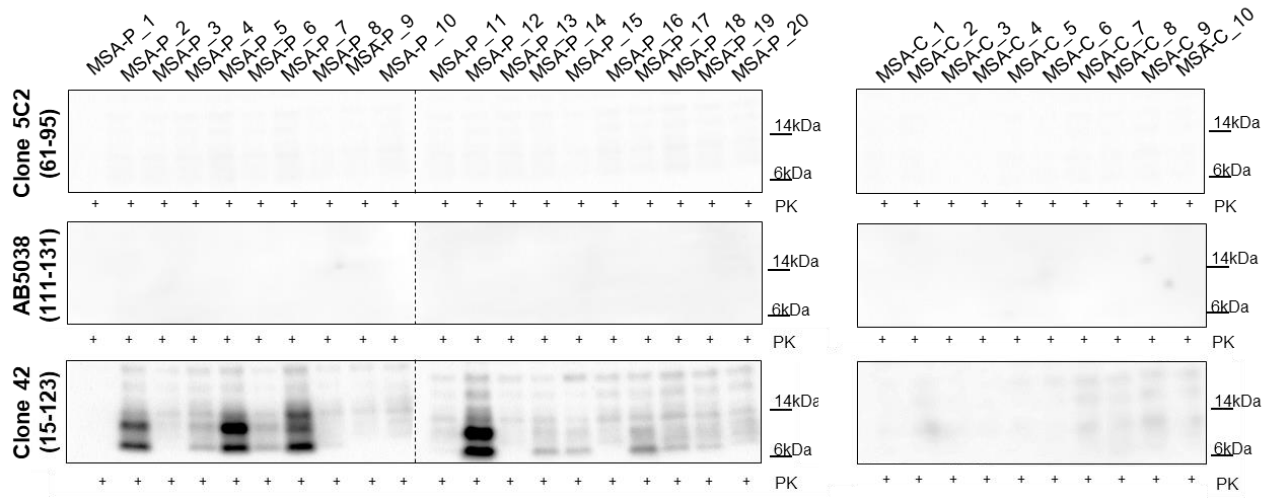

Figure 4.25 Epitope mapping of RT-QuIC products generated by MSA-P (n = 20) and MSA-C (n = 10) samples at ITA-lab. Samples were treated with PK and immunoblotted with 5C2, AB5038 and clone 42. No signals were observed in samples immunoblotted with the AB5038 and the clone 5C2, while with the clone 42, PK resistant bands were specifically detected in RT-QuIC products seeded with MSA-P but not in those seeded with MSA-C samples.

CHAPTER V

5 DISCUSSION

Definite diagnosis of PD or other neurodegenerative parkinsonisms is extremely challenging especially in the early stages of the disease when symptoms might overlap [226]. These diseases are characterized by intracerebral accumulation of disease-specific abnormally folded proteins: α-synuclein in the case of PD and MSA, tau in the case of PSP and CBD.

Misdiagnosis negatively impacts the healthcare system and the life of the patients and could lead to erroneous inclusions in clinical trials. Proper diagnosis can be predictive of treatment responsiveness, indeed, in the early stage, MSA-P patients often respond to levodopa while MSA-C patients do not [227]. It is, therefore, necessary to identify the disease phenotype as early as possible, to provide patients with the most appropriate diagnostic and therapeutic care pathways. The same concept is valid for the other α-synucleinopathies, including PD, where early and accurate diagnosis allows proper treatment initiation and is key to enrollment into neuroprotective clinical trials.

Since the process of intracerebral accumulation of disease-specific abnormally folded proteins begins decades before the appearance of clinical signs of the disease, it is conceivable that the abnormal proteins accumulate also in peripheral tissues and body fluids (e.g. olfactory mucosa, blood and urine) long before disease onset at concentrations well below the detection limits of the classical biochemical diagnostic techniques. With the development of the SAAs, including RT-QuIC, significant progress has been made in the field of α-synucleinopathy diagnosis. For instance, through RT-QuIC analysis, traces of αSyn^{D} were found in the CSF, submandibular gland, and skin of diseased patients [44,67,228,229]. The identification of αSyn^{D} in peripheral tissues may serve as the gold standard for the diagnosis of α-synucleinopathies. For this reason, once optimized and integrated into clinical practice, SAAs have the potential to revolutionize the diagnosis, therapy, and prognostication of these diseases.

In particular, in contrast to CSF collection that can be painful and associated with adverse effects such as headache or cerebrospinal fluid leak, OM samples can be easily and periodically collected with a minimally invasive procedure. Given this evidence and considering the possibility that OM samples may contain misfolded proteins, in 2019, our research group made the first attempt to develop an RT-QuIC protocol for the analysis of OM collected from subjects with PD and MSA, and the results of this work were obtained during the first part of my PhD project (here named *First study*, [230]). As comparison, we have included OM samples from patients with clinical diagnosis of neurodegenerative parkinsonisms associated with tau pathology (PSP and CBD). Although we are aware that numerous data are currently available about RT-QuIC analysis for detecting αSyn^{D} in CSF [180,189,190] the study of OM samples might widen the diagnostic approach to these diseases by the analysis of tissues that can be collected by less invasive procedures. The main objective of our study was to verify whether OM from patients with PD and MSA have a different behavior as seeding activity for αSyn compared to patients with tauopathies. First of all, we have set up the protocol of rec-αSyn aggregation and verified the ability of αSyn aggregates either artificially produced (referred to as artificial seeds) or present in brain samples to accelerate this kinetics. Our results showed an acceleration of rec-αSyn aggregation after the addition of attograms of artificial seeds, thus indicating that RT-QuIC is highly sensitive. The kinetics was also accelerated by the addition of PD, MSA, PSP, CBD, FTDP-17 and NDP brain homogenates, however the fluorescence intensities were significantly higher in reactions seeded with PD or MSA compared to the others. These data suggest that the homologous seeding (ability of abnormally folded αSyn to accelerate the aggregation of rec-αSyn) is more effective than the heterologous one where the kinetics of rec-αSyn aggregation could have been modified by proteins other than αSyn. This phenomenon is also known as cross-seeding effect and, for instance, abnormal forms of tau present in PSP, CBD and FTDP-17 samples could have contributed in stimulating rec-αSyn aggregation. Similarly, other proteins present in NDP sample might have sustained a cross-seeding effect. Since RT-QuIC analyses of brain homogenates enabled us to identify PD and MSA samples, we decided to verify whether

this discrimination could also occur in RT-QuIC reactions seeded with OM collected from patients with clinical diagnosis of PD, MSA, PSP and CBD. Compared to brains, where a faint cross-seeding effect often occurred, OM analysis produced much clear results. Probably OM samples contained fewer factors able to cross-seed rec-αSyn aggregation. PD and MSA samples were characterized by higher rec-αSyn seeding efficiency compared to PSP and CBD. Indeed, almost all MSA samples (9/11) and more than half of PD samples (10/18) were able to induce rec-αSyn aggregation. Probably, the presence of abnormally folded αSyn in these samples was more efficient in stimulating rec-αSyn aggregation (homologous seeding). At difference, CBD and PSP samples did not induce such aggregation, except for 2 out of 12 PSP and 1 out of 6 CBD. These results might have several explanations and here I report some of our hypotheses. First, since these pathologies are clinically diagnosed using criteria whose accuracy is not absolute, it might be that the clinical diagnosis was not correct. Other options to be considered include the fact that some of these diseases might share an incidental Lewy body deposition or that such phenomenon may be neither incidental nor coincidental, thus αSyn represents the unique pathological protein of otherwise usually tau-related clinical phenotypes [231]. Alternatively, some strains of tau might be more effective than others in cross-seed rec-αSyn aggregation, and the efficiency of such phenomenon may be amount-dependent [232–235]. Unfortunately, collection and use of OM samples in the diagnostic field of neurodegenerative diseases is being born in the most recent years and it is not possible to perform retrospective analysis or compare data with neuropathological results to verify the sensitivity of the technique. For this reason, considered the limited number of samples analyzed, we decided not to calculate both sensitivity and specificity of the assay. Indeed, in contrast to prion diseases which have much shorter duration compared to PD and MSA, the autopsy confirmation might take many years. Therefore, we are aimed at collecting data and following up our patients for gathering information to be compared with neuropathological results in the future. Notably, considering the accuracy of the *in vivo* diagnosis, a percentage of the patients of our case series might have been clinically misdiagnosed. Furthermore, regeneration of OM might influence the total amount of pathological

αSyn present in the samples, thus decreasing RT-QuIC sensitivity. Recent evidence demonstrated an important drainage of CSF through the olfactory mucosa [236]. For this reason, our RT-QuIC results might have been influenced by a combination of both OM and CSF and their relative content of abnormally folded proteins. Another important point is that PD is characterized by a remarkable phenotypic heterogeneity that might be associated with different abnormal conformers of αSyn^D [67]. Such strains might possess different seeding properties for rec-αSyn, thus explaining why some PD samples were not detected in our assay, in relation to the low sample size of the subjects evaluated. Moreover, the concomitant presence of other misfolded proteins (e.g. Aβ or tau) in OM samples might have influenced the aggregation properties of rec-αSyn. Recent data from the literature have demonstrated that RT-QuIC might efficiently discriminate between PD and other parkinsonisms [194,237]. In some cases, the same RT-QuIC substrate can acquire distinct abnormal structures if supplemented with different seeds. Hence, we decided to verify whether OM of PD and MSA patients were able to induce the formation of αSyn aggregates characterized by disease-related biochemical and morphological features. Results of these analyses demonstrated that rec-αSyn acquired peculiar features when seeded with PD or MSA samples. In particular, αSyn fibrils produced by MSA showed three PK-resistant bands migrating at around 6–8, and 22 kDa and TEM analysis showed that these fibrils were characterized by the presence of over-twists whose distance was about 141 ± 1.3 nm (mean ± standard error of the mean). In contrast, αSyn fibrils produced by PD samples were significantly less resistant to PK digestion ($p = 0.0061$, Mann-Withney U test) and possessed one faint band migrating at around 6–8 kDa with distances between over-twists of about 131 nm ± 1.1 nm. These structural differences were statistically significant ($p < 0.0001$, Mann-Withney U test) and contribute in demonstrating that PD and MSA are caused by different strains of αSyn^D that could effectively transmit their specific conformations to the same substrate. Moreover, differences in post-translational modifications of αSyn (e.g. phosphorylation) or in the size of the oligomeric αSyn seeds in PD and MSA might have influenced the RT-QuIC kinetics and the abnormal structures acquired by the substrate. The fact that our samples were collected from patients

without neuropathological confirmation represents a relevant but at present not addressable limitation of our study. Vascular leukoencephalopathy was observed in 4 patients, who all received a clinical diagnosis of PD according to Postuma criteria [172]. However, these patients, having evidence of only mild vascular disease and in cerebral regions unlikely associated with motor symptoms, did not meet criteria for vascular parkinsonism [238,239] and were not excluded from the analysis. It is worth noting, however, that removal of these patients from analysis resulted in detection of αSyn seeding activity in 10 out of 14 OM samples, thus reaching an accuracy which is comparable to that of the RT-QuIC analysis of CSF [190,240]. Such observations might be better defined in the future by using OM samples collected from patients neuropathologically verified. However, this study provided the proof-of-concept that OM samples collected from patients with PD and MSA possess seeding activities for αSyn.

After this study, published in 2019, other groups have confirmed our results. For instance, Shahnawaz et al. demonstrated that CSF of PD and MSA patients contains αSyn^{D} strains able to promote the formation of rec-αSyn aggregates with different biochemical and structural properties. In this work, MSA samples produced lower seeding activities and lower fluorescence intensities at the final plateau compared to PD samples. Notably, the analysis of RT-QuIC-derived kinetic parameters enabled discrimination between PD and MSA with an overall sensitivity of 95.4%. The morphological analysis of RT-QuIC reaction products by TEM confirmed the presence of two distinct strains, since fibrils generated from MSA CSF samples were characterized by closer twists as compared to PD [241]. Moreover, Stefani et al. analyzed by RT-QuIC the OM of another coort of PD patients by obtaining values of sensitivity and specificity almost comparable with ours (46.3% and 89.8%, respectively) [242].

Since we have shown that OM samples collected from patients with MSA and PD were able to seed RT-QuIC reaction, leading to the formation of distinct αSyn aggregates that possess specific biochemical and morphological properties, in the second part of my Ph.D. project (here named *Second study*, [243]) we wondered if these aggregates (called RQ-MSA and RQ-PD) could also show particular inflammatory effects on cells. Indeed, we have demonstrated that they

induced different levels of inflammatory responses when challenged in neuronal-like differentiated SH-SY5Y cells. Other than confirming their ability to seed the aggregation of endogenous αSyn, RQ-MSA elicited a significant increase in the transcription levels of several inflammatory mediators, including TLR2, TRAF6, IL6, NLRP3, SOD2 than those activated by RQ-PD and controls. Notably, the level of transcription factors activated in cells stimulated with RQ-PD was slightly higher than that of cells stimulated with control, but this difference was not statistically significant. This indicates that RQ-PD possesses less inflammatory features than RQ-MSA, even though both samples induced a significant increase of NO release in stimulated cells compared to controls. These findings suggested the existence of a link between the morphology of the aggregates and their inflammatory properties. Since the OM samples contain several components, besides αSyn^D, that could have influenced the misfolding of rec-αSyn, we have decided to evaluate to what extent the aberrant structures of αSyn^D could have impacted this process. Hence, we have produced three different aggregates of αSyn (αSv1, αSv2, αSv3) starting from the same rec-αSyn. The aim of this experiment was to generate, in a controlled environment, artificial αSyn seeds, resembling to some extent the αSyn^D strains present in OM, and test their behavior by RT-QuIC without the presence of specific tissue factors. Although capable to efficiently seed rec-αSyn aggregation, αSv1, αSv2, and αSv3 did not transmit their seed-specific properties to the reaction products which showed comparable biochemical properties, instead. Probably, our experimental setting was too artificial to properly recapitulate the phenomenon of the seeding effect exerted by αSyn^D in RT-QuIC. However, when used to stimulate SH-SY5Y cells, αSv1, αSv2, and αSv3 acted on different activators of inflammatory pathways, thus strengthening the existence of a correlation between morphological and inflammatory properties of αSyn fibrils. All stimulated cells showed aggregates of endogenous αSyn that could be more similar to the αSyn^D present in OM samples with respect to the artificial αSv1, αSv2, and αSv3. For this reason, we have lysed the cells and tested the lysates by RT-QuIC to verify whether they could seed the reaction and generate final products eventually showing distinctive biochemical properties. Although the cell-derived aggregates were able to seed the reaction, resulting αSyn

fibrils (named RQ-CS-αSv1, RQ-CS-αSv2, and RQ-CS-αSv3) showed similar biochemical properties. Notably, by comparing the biochemical profiles of the RT-QuIC products generated by αSv1, αSv2, and αSv3 (RQ-αSv1, RQ-αSv2, RQ-αSv3) with those obtained from cells stimulated with them (RQ-CS-αSv1, RQ-CS-αSv2, and RQ-CS-αSv3), we have observed that the number of PK resistant αSyn bands were different. In particular, 4 bands were found in the first case and 3 bands in the second one. This finding indicates that the aggregates generated in cells, hence in a more physiological environment, might have acquired conformations that were slightly different from that of αSv1, αSv2, and αSv3. Therefore, the properties of these αSyn aggregates (e.g. presence of post-translational modifications), the existence of specific cellular components (e.g. different microenvironments), or both, might have influenced the biochemical properties of the final RT-QuIC products further sustaining that they could depend on several factors, not only on the structure and composition of the original αSyn seeds. Unfortunately, we did not have enough OM samples for a direct stimulation of the cells that were stimulated with RQ-MSA and RQ-PD, instead. Cells were then lysed and lysates subjected to RT-QuIC analysis. All samples were able to seed the aggregation of rec-αSyn and final reaction products (RQ-CS-RQ-MSA and RQ-CS-RQ-PD) did not show distinct biochemical profiles but, surprisingly, those generated from RQ-MSA were again more resistant to PK digestion than those generated by RQ-PD. Also in this case, the passage in cells has partially altered the biochemical features of RQ-MSA and RQ-PD. For this reason, passaging of αSyn aggregates in cells might alter their original features, regardless of the origins (artificial vs natural). Our study, although performed on a limited number of samples, showed that there might be an association between the aberrant conformations of the αSyn aggregates and the inflammatory responses that they are capable to induce in SH-SY5Y stimulated cells. It is important to verify whether the inflammatory pathways altered in RQ-MSA and RQ-PD stimulated cells might resemble those eventually altered by αSyn^{D} responsible for MSA and PD. If this was the case, stimulation of cells with OM generated RT-QuIC aggregates can be exploited to study the molecular events associated with αSyn misfolding and aggregation *in vitro* and eventually identify novel disease-specific therapeutic targets. Finally, we have

observed that not only the structure of these aggregates, but also other environmental factors might play a role in modulating the final properties of the RT-QuIC reaction products. Hence, the discovery of specific environmental modulators involved in αSyn^D misfolding in MSA and PD might further help to plan innovative targeted therapies.

The majority of the RT-QuIC studies applied to α-synucleinopathies were based on CSF samples and highlighted that, besides the impressive performance of the technology in detecting traces of αSyn^D, there are important variabilities in the findings that could be associated with the experimental protocol adopted by each laboratory. The use of customized analytical procedures has hampered the possibility to compare the results and evaluate the reliability and the robustness of the assays. For this reason, in the last part of my Ph.D. project (here named *Third study*, [244]) we decided to combine for the first time the expertise of two independent specialized laboratories (ITA-lab and USA-lab) with the aim to explore the interlaboratory reproducibility of RT-QuIC performed on OM samples collected from PD, MSA-C, and MSA-P patients. Both of our laboratories harmonized the analytical procedures by minimizing all the experimental variables that could lead to inconsistencies in the results or conflicting findings (e.g. use of a commercially available rec-αSyn). The final RT-QuIC protocol that has been developed enabled us to reach a very high IAR (96%) between ITA-lab and USA-lab. In particular, the OM of 69% PD patients and 90% MSA-P patients induced RT-QuIC seeding activity with 100% of IAR. In contrast, none of the OM belonging to MSA-C patients and the HS induced RT-QuIC seeding activity at ITA-lab, except for one patient per group at USA-lab, thus leading to 90 and 91% IAR, respectively. We decided to consider non age-matched HS (younger than the patients) for reducing the probability to include subjects at pre-symptomatic stages of α-synucleinopathy, eventually causing positive RT-QuIC results difficult to interpret (e.g. real seeding activity vs false positive signal). Surprisingly, OM collected from MSA-P and MSA-C patients showed totally different behavior, with the latter being almost unresponsive to RT-QuIC. The lack of seeding activity in MSA-C suggests that, although MSA-P and MSA-C belong to the same disease group, they may be caused by distinct αSyn^D strains that possess different tropism for peripheral tissues, including the OM.

In very recent studies, it has been suggested that αSyn^{D} may originate outside the brain, including the nose, the gut and the urogenital tract and then spread to the CNS [37,99,245]. The tissue microenvironment might influence αSyn^{D} properties thus driving its tropism for specific neuroanatomical regions. This might lead to the onset of different forms of MSA and contribute to the phenotypic heterogeneity of α-synucleinopathies. Interesting findings indicate that even different αSyn strains can be found within the same MSA brain [213]. Since the brain homogenates of MSA-C patients were able to induce an efficient RT-QuIC seeding activity using our protocol, we speculate that the αSyn^{D} strain responsible for MSA-C (i) might not be present in the OM (while that associated with MSA-P accumulates in this tissue with greater efficiency), (ii) might be present in the OM but could be subjected to tissue/microenvironment specific changes that make this strain incapable of triggering the seeding activity, or (iii) might be present in the OM but at concentrations which are still too low to induce a detectable seeding activity. Regardless of the reasons which determine this opposite RT-QuIC behavior of MSA-P and MSA-C, the findings can be exploited to efficiently distinguish these different pathologies in living patients. Several research groups have subjected to RT-QuIC analysis the CSF of patients with MSA but controversial results were reported [189,193,194,241,246]. Moreover, except for a few papers, there were no clear indications about the subtypes of MSA examined and whether specific correlations between the disease phenotype and the RT-QuIC outcomes were observed. Interestingly, van Rumund and colleagues reported that only a small group of CSF samples belonging to MSA-P patients were able to induce seeding activity by RT-QuIC, while those belonging to MSA-C patients did not [194]. Although these data refer to a different biological sample, they are in line with those of our OM study and further support the hypothesis that MSA-P and MSA-C may be caused by distinct αSyn^{D} strains with peculiar tropism for CSF, OM, and likely other peripheral tissues. Our findings might also unveil different biological and molecular pathways involved in the disease pathogenesis. Notably, in PD and MSA-P patients we found a positive significant association between RT-QuIC seeding activity and some clinical parameters, including rigidity and postural instability. In contrast, we did not find any correlation between RT-QuIC seeding activity and the

disease duration. Taken together, these data indicate that through a careful combination of aggregation kinetics, biochemical and morphological assays, and clinical information, the RT-QuIC assay of OM can significantly improve the clinical diagnosis of α-synucleinopathies. In particular, the assay may help physicians to identify and stratify patients with PD and MSA and, above all, to specifically recognize MSA-P or MSA-C phenotypes. The high degree of interlaboratory reproducibility strongly supports the reliability and the robustness of the RT-QuIC results. Therefore, the fact that some OM of PD patients and almost all OM of MSA-C patients did not induce RT-QuIC seeding activity does not represent a technical limitation of the assay (e.g. lack of sensitivity). These findings could also not be the result of stochastic events. We rather think that there might be additional significant biological and pathophysiological reasons that cannot be totally understood at present. Overall, the different outcomes obtained from our and other laboratories, from the RT-QuIC amplification of αSyn aggregates from MSA and PD (or DLB) biospecimens may be explained by considering that the elongation of a particular strain may be favored or hindered in different RT-QuIC reaction mixes. Since the chemical environment has been shown to influence the formation and growth of aggregates belonging to different strains [247], it is thus possible that a protocol optimized for the amplification of PD strain may not efficiently work for the detection of MSA and viceversa. In addition to the strain effect, the distribution of misfolded αSyn in peripheral tissues/biofluids may also depend on the type of α-synucleinopathy, making a biomatrix able to reflect ongoing α-synucleinopathy better than another.

Certainly, with our protocol, we can benefit from better recognizing patients with PD, MSA-P, and MSA-C, and potentially identifying heterogeneous pathological subgroups within these diagnoses, to pave the way to tailored treatment regimens. For all these reasons, OM-based RT-QuIC analysis may be a promising candidate as a routine diagnostic test for PD, MSA-P, and MSA-C. Additionally, this assay requires further studies to determine whether it will identify presymptomatic and prodromal PD and MSA patients. If this were the case, RT-QuIC could be helpful to identify subjects at risk of developing the disease and can be particularly important in

this very moment where preliminary studies suggest that the Sars-CoV-2 viral infection seems to influence the vulnerability to PD [248]. Finally, the assay can be exploited to test *in vitro* the efficacy of therapeutic compounds to interfere with the aggregation of αSyn in reactions seeded with patients' biological samples. The fact that few, if any, of the patients included in our work will undergo neuropathological assessment, represents the major limitation of the study that cannot be addressed. As already specified for the *First study*, the lack of OM samples collected from pathologically confirmed cases of PD, MSA-C, and MSA-P hampers the possibility to perform a retrospective analysis for estimating the sensitivity and specificity of the assay. Moreover, the quantity of OM sample collectible from each patient is considerably limited. For this reason, we have decided to perform this preliminary work of protocol set-up and harmonization by involving no more than two specialized laboratories with the aim of having enough material to be accurately and repeatedly analyzed by both groups. As a matter of fact, almost the entire volume of each OM sample included in this work was consumed during the analyses before reaching the conclusion that the samples can be significantly diluted (up to 20X) without affecting the sensitivity and specificity of the RT-QuIC. This observation should be considered for future studies, where newly collected OM can be prepared as described and used to perform multicenter studies for a better assessment of the RT-QuIC performances. The limited number of samples included in this study depends on the fact that MSA is a rare disease and that the COVID-19 pandemic outbreak has imposed severe limitations on OM collection for biosafety reasons. Nevertheless, our exploratory study showed striking differences in RT-QuIC responses between (1) MSA-C and MSA-P, (2) MSA-C and PD, (3) MSA-P and controls, and (4) PD and controls that were faithfully reproducible in both laboratories thus demonstrating that they were not due to merely stochastic events. Although the analytical procedures have been harmonized, two different thresholds of time were set at ITA-lab and USA-lab to discriminate positive and negative samples. Likely, despite using the same instrument (BMG LabTech OMEGA), some conditions may inevitably differ (e.g. the stability of the temperature during the whole analytical process or the mechanism of shaking of the plate) hence promoting the variability in the time

thresholds between labs. In addition, other factors, including the precision of the pipettes or the type of consumables (e.g. tubes) used for the analysis might have favored this discrepancy. Certainly, additional studies would help to define a window of time, instead of a single lab-dependent time threshold, within which the samples can be considered positive. Longitudinal studies using samples collected from larger cohorts of patients are required to definitively evaluate the diagnostic accuracy of OM-αSyn^{D} as a biomarker for PD, MSA-P, MSA-C, and other α-synucleinopathies. However, we believe that these evaluations should be performed at the end of the COVID-19 pandemic since, at present, we do not know whether the potential presence of the Sars-CoV-2 virus in the nasal cavity of either diseased patients or healthy subjects might alter the properties of the OM samples while compromising the RT-QuIC analyses. Finally, additional investigations will also be needed to determine whether this assay could be used as a biomarker to track disease progression and monitor the effect of disease-modifying treatments.

CHAPTER VI

6 CONCLUSIONS

These results represent a starting point for future studies aimed at (i) estimating sensitivity and specificity of RT-QuIC analysis on OM samples useful for PD and MSA diagnosis, (ii) comparing the sensitivity of OM analysis with that of CSF simultaneously collected from the same patient, (iii) integrating RT-QuIC analysis of CSF and OM with other instrumental and biochemical data and verifying whether this can significantly improve the clinical diagnostic accuracy of PD and other neurodegenerative parkinsonisms. Thus, if these observations will be confirmed and extended, RT-QuIC integrated with biochemical and TEM analyses may turn out to be a biomarker for the preclinical diagnosis of PD and MSA, but a process of assay harmonization is urgently needed to minimize the variability or conflicting findings between specialized laboratories.

Moreover, our results suggest that PD, MSA-P, and MSA-C are caused by distinct αSyn^{D} strains that might have peculiar pathological features and tropism for peripheral tissues, including OM, eventually unveiling different biological and molecular pathways involved in the disease pathogenesis. These studies provide evidence that RT-QuIC of OM samples represents a reliable assay that can distinguish patients with MSA-P from those with MSA-C and may limit the negative effects that misdiagnosis produces in terms of costs for the healthcare system and improve overall patient care, treatment, and possible enrollment in future clinical trials.

Moreover, RT-QuIC might offer a great opportunity to test the efficiency of several compounds to interfere with the process of rec-αSyn aggregation triggered by distinct α-synuclein strains, thus laying the foundations for precision medicine.

Finally, given all the results present is this work, we are currently working at different projects:

- We are evaluating if the RT-QuIC products derived from OM of PD and MSA-P patients, other than triggering different inflammatory responses in SH-SY5Y cells, could also be able to induce pathological effects in mouse models;
- We are testing by RT-QuIC skin samples collected from the same patients whose OM we have already analyzed, to evaluate the distribution and the localization of αSyn^D aggregates in different α-synucleinopathies;
- We are working at the optimization of RT-QuIC procedures for the detection of seeding activiry of urine and plasma samples of patients with α-synucleinopathy;
- We are extending RT-QuIC analysis to the OM of patients with DLB, by evaluating the seeding activity for rec-αSyn of these samples in comparison with OM of AD or Frontotemporal dementia, to observe if it is possible to differentiate them. We are conducting these experiments in blind in two different laboratories to assess the IAR;
- We are estending RT-QuIC analysis to the OM of patients with mild or severe GBA mutations (able to induce α-synucleinopathy) to evaluate their seeding activity for rec-αSyn;
- We are evaluating the microbiota present in the olfactory mucosa of patients with PD, MSA, DLB and healthy controls, to deepend the role of the nasal microenvironment on the formation of specific αSyn^D strains.

REFERENCES

1. Ma, Q.L.; Chan, P.; Yoshii, M.; Uéda, K. α-Synuclein Aggregation and Neurodegenerative Diseases. *J. Alzheimer's Dis.* 2003.

2. Ulmer, T.S.; Bax, A.; Cole, N.B.; Nussbaum, R.L. Structure and Dynamics of Micelle-Bound Human α-Synuclein. *J. Biol. Chem.* **2005**, doi:10.1074/jbc.M411805200.

3. Spillantini, M.G.; Schmidt, M.L.; Lee, V.M.Y.; Trojanowski, J.Q.; Jakes, R.; Goedert, M. α-Synuclein in Lewy Bodies [8]. *Nature* 1997, *388*.

4. Vekrellis, K.; Rideout, H.J.; Stefanis, L. Neurobiology of α-Synuclein. *Mol. Neurobiol.* 2004.

5. Lashuel, H.A.; Overk, C.R.; Oueslati, A.; Masliah, E. The Many Faces of α-Synuclein: From Structure and Toxicity to Therapeutic Target. *Nat. Rev. Neurosci.* 2013.

6. Burré, J.; Sharma, M.; Südhof, T.C. Cell Biology and Pathophysiology of α-Synuclein. *Cold Spring Harb. Perspect. Med.* **2018**, doi:10.1101/cshperspect.a024091.

7. Burré, J.; Sharma, M.; Tsetsenis, T.; Buchman, V.; Etherton, M.R.; Südhof, T.C. α-Synuclein Promotes SNARE-Complex Assembly in Vivo and in Vitro. *Science (80-.).* **2010**, doi:10.1126/science.1195227.

8. Lee, A.C.; Harris, J.P.; Atkinson, E.A.; Nithi, K.; Fowler, M.S. Dopamine and the Representation of the Upper Visual Field: Evidence from Vertical Bisection Errors in Unilateral Parkinson's Disease. *Neuropsychologia* **2002**, doi:10.1016/S0028-3932(02)00055-6.

9. Cooper, A.A.; Gitler, A.D.; Cashikar, A.; Haynes, C.M.; Hill, K.J.; Bhullar, B.; Liu, K.; Xu, K.; Strathearn, K.E.; Liu, F.; et al. α-Synuclein Blocks ER-Golgi Traffic and Rab1 Rescues Neuron Loss in Parkinson's Models. *Science (80-.).* **2006**, doi:10.1126/science.1129462.

10. Nemani, V.M.; Lu, W.; Berge, V.; Nakamura, K.; Onoa, B.; Lee, M.K.; Chaudhry, F.A.; Nicoll, R.A.; Edwards, R.H. Increased Expression of α-Synuclein Reduces Neurotransmitter Release by Inhibiting Synaptic Vesicle Reclustering after Endocytosis. *Neuron* **2010**, doi:10.1016/j.neuron.2009.12.023.

11. Reish, H.E.A.; Standaert, D.G. Role of α-Synuclein in Inducing Innate and Adaptive Immunity in Parkinson Disease. *J. Parkinsons. Dis.* 2015.

12. Burré, J.; Sharma, M.; Südhof, T.C. α-Synuclein Assembles into Higher-Order Multimers upon Membrane Binding to Promote SNARE Complex Formation. *Proc. Natl. Acad. Sci. U. S. A.* **2014**, doi:10.1073/pnas.1416598111.

13. Chinta, S.J.; Mallajosyula, J.K.; Rane, A.; Andersen, J.K. Mitochondrial Alpha-Synuclein Accumulation Impairs Complex I Function in Dopaminergic Neurons and Results in Increased Mitophagy in Vivo. *Neurosci. Lett.* **2010**, doi:10.1016/j.neulet.2010.09.061.

14. Devi, L.; Raghavendran, V.; Prabhu, B.M.; Avadhani, N.G.; Anandatheerthavarada, H.K. Mitochondrial Import and Accumulation of α-Synuclein Impair Complex I in Human Dopaminergic Neuronal Cultures and Parkinson Disease Brain. *J. Biol. Chem.* **2008**, doi:10.1074/jbc.M710012200.

15. Luth, E.S.; Stavrovskaya, I.G.; Bartels, T.; Kristal, B.S.; Selkoe, D.J. Soluble, Prefibrillar α-Synuclein Oligomers Promote Complex I-Dependent, Ca2+-Induced Mitochondrial

Dysfunction. *J. Biol. Chem.* **2014**, doi:10.1074/jbc.M113.545749.

16. Li, W.W.; Yang, R.; Guo, J.C.; Ren, H.M.; Zha, X.L.; Cheng, J.S.; Cai, D.F. Localization of α-Synuclein to Mitochondria within Midbrain of Mice. *Neuroreport* **2007**, doi:10.1097/WNR.0b013e3282f03db4.

17. Parihar, M.S.; Parihar, A.; Fujita, M.; Hashimoto, M.; Ghafourifar, P. Mitochondrial Association of Alpha-Synuclein Causes Oxidative Stress. *Cell. Mol. Life Sci.* **2008**, doi:10.1007/s00018-008-7589-1.

18. Jensen, M.B.; Bhatia, V.K.; Jao, C.C.; Rasmussen, J.E.; Pedersen, S.L.; Jensen, K.J.; Langen, R.; Stamou, D. Membrane Curvature Sensing by Amphipathic Helices: A Single Liposome Study Using α-Synuclein and Annexin B12. *J. Biol. Chem.* **2011**, doi:10.1074/jbc.M111.271130.

19. Middleton, E.R.; Rhoades, E. Effects of Curvature and Composition on α-Synuclein Binding to Lipid Vesicles. *Biophys. J.* **2010**, doi:10.1016/j.bpj.2010.07.056.

20. Kubo, S.I.; Nemani, V.M.; Chalkley, R.J.; Anthony, M.D.; Hattori, N.; Mizuno, Y.; Edwards, R.H.; Fortin, D.L. A Combinatorial Code for the Interaction of α-Synuclein with Membranes. *J. Biol. Chem.* **2005**, doi:10.1074/jbc.M504894200.

21. Calì, T.; Ottolini, D.; Negro, A.; Brini, M. α-Synuclein Controls Mitochondrial Calcium Homeostasis by Enhancing Endoplasmic Reticulum-Mitochondria Interactions. *J. Biol. Chem.* **2012**, doi:10.1074/jbc.M111.302794.

22. Chiti, F.; Dobson, C.M. Protein Misfolding, Functional Amyloid, and Human Disease. *Annu. Rev. Biochem.* 2006.

23. Bertoncini, C.W.; Jung, Y.S.; Fernandez, C.O.; Hoyer, W.; Griesinger, C.; Jovin, T.M.; Zweckstetter, M. Release of Long-Range Tertiary Interactions Potentiates Aggregation of Natively Unstructured α-Synuclein. *Proc. Natl. Acad. Sci. U. S. A.* **2005**, doi:10.1073/pnas.0407146102.

24. Upadhyay, A. Structure of Proteins: Evolution with Unsolved Mysteries. *Prog. Biophys. Mol. Biol.* 2019.

25. Chen, B.; Retzlaff, M.; Roos, T.; Frydman, J. Cellular Strategies of Protein Quality Control. *Cold Spring Harb. Perspect. Biol.* **2011**, doi:10.1101/cshperspect.a004374.

26. Soto, C.; Pritzkow, S. Protein Misfolding, Aggregation, and Conformational Strains in Neurodegenerative Diseases. *Nat. Neurosci.* 2018.

27. Pihlstrøm, L.; Wiethoff, S.; Houlden, H. Genetics of Neurodegenerative Diseases: An Overview. In *Handbook of Clinical Neurology*; 2018.

28. Ma, M.R.; Hu, Z.W.; Zhao, Y.F.; Chen, Y.X.; Li, Y.M. Phosphorylation Induces Distinct Alpha-Synuclein Strain Formation. *Sci. Rep.* **2016**, doi:10.1038/srep37130.

29. Beyer, K.; Ariza, A. α-Synuclein Posttranslational Modification and Alternative Splicing as a Trigger for Neurodegeneration. *Mol. Neurobiol.* 2013.

30. Soto, C. Unfolding the Role of Protein Misfolding in Neurodegenerative Diseases. *Nat. Rev. Neurosci.* **2003**, *4*, doi:10.1038/nrn1007.

31. Wood, S.J.; Wypych, J.; Steavenson, S.; Louis, J.-C.; Citron, M.; Biere, A.L. α-Synuclein

Fibrillogenesis Is Nucleation-Dependent. *J. Biol. Chem.* **1999**, doi:10.1074/jbc.274.28.19509.

32. Guo, J.L.; Lee, V.M.Y. Cell-to-Cell Transmission of Pathogenic Proteins in Neurodegenerative Diseases. *Nat. Med.* 2014.

33. Angot, E.; Brundin, P. Dissecting the Potential Molecular Mechanisms Underlying α-Synuclein Cell-to-Cell Transfer in Parkinson's Disease. *Park. Relat. Disord.* **2009**, doi:10.1016/S1353-8020(09)70802-8.

34. Braak, H.; Bohl, J.R.; Müller, C.M.; Rüb, U.; de Vos, R.A.I.; Del Tredici, K. Stanley Fahn Lecture 2005: The Staging Procedure for the Inclusion Body Pathology Associated with Sporadic Parkinson's Disease Reconsidered. *Mov. Disord.* 2006.

35. Pan-Montojo, F.J.; Funk, R.H.W. Oral Administration of Rotenone Using a Gavage and Image Analysis of Alpha-Synuclein Inclusions in the Enteric Nervous System. *J. Vis. Exp.* **2010**, doi:10.3791/2123.

36. Braak, H.; Del Tredici, K.; Rüb, U.; De Vos, R.A.I.; Jansen Steur, E.N.H.; Braak, E. Staging of Brain Pathology Related to Sporadic Parkinson's Disease. *Neurobiol. Aging* **2003**, doi:10.1016/S0197-4580(02)00065-9.

37. Hawkes, C.H.; Del Tredici, K.; Braak, H. Parkinson's Disease: The Dual Hit Theory Revisited. In Proceedings of the Annals of the New York Academy of Sciences; 2009.

38. Kordower, J.H.; Chu, Y.; Hauser, R.A.; Olanow, C.W.; Freeman, T.B. Transplanted Dopaminergic Neurons Develop PD Pathologic Changes: A Second Case Report. *Mov. Disord.* **2008**, doi:10.1002/mds.22369.

39. Li, J.Y.; Englund, E.; Holton, J.L.; Soulet, D.; Hagell, P.; Lees, A.J.; Lashley, T.; Quinn, N.P.; Rehncrona, S.; Björklund, A.; et al. Lewy Bodies in Grafted Neurons in Subjects with Parkinson's Disease Suggest Host-to-Graft Disease Propagation. *Nat. Med.* **2008**, doi:10.1038/nm1746.

40. Mougenot, A.L.; Nicot, S.; Bencsik, A.; Morignat, E.; Verchère, J.; Lakhdar, L.; Legastelois, S.; Baron, T. Prion-like Acceleration of a Synucleinopathy in a Transgenic Mouse Model. *Neurobiol. Aging* **2012**, doi:10.1016/j.neurobiolaging.2011.06.022.

41. Luk, K.C.; Kehm, V.M.; Zhang, B.; O'Brien, P.; Trojanowski, J.Q.; Lee, V.M.Y. Intracerebral Inoculation of Pathological α-Synuclein Initiates a Rapidly Progressive Neurodegenerative α-Synucleinopathy in Mice. *J. Exp. Med.* **2012**, doi:10.1084/jem.20112457.

42. Masuda-Suzukake, M.; Nonaka, T.; Hosokawa, M.; Oikawa, T.; Arai, T.; Akiyama, H.; Mann, D.M.A.; Hasegawa, M. Prion-like Spreading of Pathological α-Synuclein in Brain. *Brain* **2013**, doi:10.1093/brain/awt037.

43. Paumier, K.L.; Luk, K.C.; Manfredsson, F.P.; Kanaan, N.M.; Lipton, J.W.; Collier, T.J.; Steece-Collier, K.; Kemp, C.J.; Celano, S.; Schulz, E.; et al. Intrastriatal Injection of Pre-Formed Mouse α-Synuclein Fibrils into Rats Triggers α-Synuclein Pathology and Bilateral Nigrostriatal Degeneration. *Neurobiol. Dis.* **2015**, doi:10.1016/j.nbd.2015.06.003.

44. Peelaerts, W.; Bousset, L.; Van der Perren, A.; Moskalyuk, A.; Pulizzi, R.; Giugliano, M.; Van den Haute, C.; Melki, R.; Baekelandt, V. α-Synuclein Strains Cause Distinct

Synucleinopathies after Local and Systemic Administration. *Nature* **2015**, *522*, 340–344, doi:10.1038/nature14547.

45. Recasens, A.; Dehay, B.; Bové, J.; Carballo-Carbajal, I.; Dovero, S.; Pérez-Villalba, A.; Fernagut, P.O.; Blesa, J.; Parent, A.; Perier, C.; et al. Lewy Body Extracts from Parkinson Disease Brains Trigger α-Synuclein Pathology and Neurodegeneration in Mice and Monkeys. *Ann. Neurol.* **2014**, doi:10.1002/ana.24066.

46. Vaquer-Alicea, J.; Diamond, M.I. Propagation of Protein Aggregation in Neurodegenerative Diseases. *Annu. Rev. Biochem.* **2019**, doi:10.1146/annurev-biochem-061516-045049.

47. Holmes, B.B.; DeVos, S.L.; Kfoury, N.; Li, M.; Jacks, R.; Yanamandra, K.; Ouidja, M.O.; Brodsky, F.M.; Marasa, J.; Bagchi, D.P.; et al. Heparan Sulfate Proteoglycans Mediate Internalization and Propagation of Specific Proteopathic Seeds. *Proc. Natl. Acad. Sci. U. S. A.* **2013**, doi:10.1073/pnas.1301440110.

48. Lim, Y.J.; Lee, S.J. Are Exosomes the Vehicle for Protein Aggregate Propagation in Neurodegenerative Diseases? *Acta Neuropathol. Commun.* 2017.

49. Yáñez-Mó, M.; Siljander, P.R.M.; Andreu, Z.; Zavec, A.B.; Borràs, F.E.; Buzas, E.I.; Buzas, K.; Casal, E.; Cappello, F.; Carvalho, J.; et al. Biological Properties of Extracellular Vesicles and Their Physiological Functions. *J. Extracell. Vesicles* 2015.

50. Rambaran, R.N.; Serpell, L.C. Amyloid Fibrils: Abnormal Protein Assembly. *Prion* 2008.

51. Conway, K.A.; Rochet, J.C.; Ding, T.T.; Harper, J.D.; Williamson, R.E.; Lansbury, P.T. Accelerated Oligomerization by Parkinson's Disease Linked α-Synuclein Mutants. In Proceedings of the Annals of the New York Academy of Sciences; 2000.

52. Lashuel, H.A.; Petre, B.M.; Wall, J.; Simon, M.; Nowak, R.J.; Walz, T.; Lansbury, P.T. α-Synuclein, Especially the Parkinson's Disease-Associated Mutants, Forms Pore-like Annular and Tubular Protofibrils. *J. Mol. Biol.* **2002**, doi:10.1016/S0022-2836(02)00735-0.

53. Cremades, N.; Cohen, S.I.A.; Deas, E.; Abramov, A.Y.; Chen, A.Y.; Orte, A.; Sandal, M.; Clarke, R.W.; Dunne, P.; Aprile, F.A.; et al. Direct Observation of the Interconversion of Normal and Toxic Forms of α-Synuclein. *Cell* **2012**, doi:10.1016/j.cell.2012.03.037.

54. Ghosh, D.; Singh, P.K.; Sahay, S.; Jha, N.N.; Jacob, R.S.; Sen, S.; Kumar, A.; Riek, R.; Maji, S.K. Structure Based Aggregation Studies Reveal the Presence of Helix-Rich Intermediate during α-Synuclein Aggregation. *Sci. Rep.* **2015**, doi:10.1038/srep09228.

55. Rockenstein, E.; Nuber, S.; Overk, C.R.; Ubhi, K.; Mante, M.; Patrick, C.; Adame, A.; Trejo-Morales, M.; Gerez, J.; Picotti, P.; et al. Accumulation of Oligomer-Prone α-Synuclein Exacerbates Synaptic and Neuronal Degeneration in Vivo. *Brain* **2014**, doi:10.1093/brain/awu057.

56. Campioni, S.; Mannini, B.; Zampagni, M.; Pensalfini, A.; Parrini, C.; Evangelisti, E.; Relini, A.; Stefani, M.; Dobson, C.M.; Cecchi, C.; et al. A Causative Link between the Structure of Aberrant Protein Oligomers and Their Toxicity. *Nat. Chem. Biol.* **2010**, doi:10.1038/nchembio.283.

57. Lindberg, I.; Shorter, J.; Wiseman, R.L.; Chiti, F.; Dickey, C.A.; McLean, P.J. Chaperones in Neurodegeneration. *J. Neurosci.* 2015.

58. Serpell, L.C.; Berriman, J.; Jakes, R.; Goedert, M.; Crowther, R.A. Fiber Diffraction of Synthetic α-Synuclein Filaments Shows Amyloid-like Cross-β Conformation. *Proc. Natl. Acad. Sci. U. S. A.* **2000**, doi:10.1073/pnas.97.9.4897.

59. Celej, M.S.; Sarroukh, R.; Goormaghtigh, E.; Fidelio, G.D.; Ruysschaert, J.M.; Raussens, V. Toxic Prefibrillar α-Synuclein Amyloid Oligomers Adopt a Distinctive Antiparallel β-Sheet Structure. *Biochem. J.* **2012**, doi:10.1042/BJ20111924.

60. Van Raaij, M.E.; Van Gestel, J.; Segers-Nolten, I.M.J.; De Leeuw, S.W.; Subramaniam, V. Concentration Dependence of α-Synuclein Fibril Length Assessed by Quantitative Atomic Force Microscopy and Statistical-Mechanical Theory. *Biophys. J.* **2008**, doi:10.1529/biophysj.107.127464.

61. Sweers, K.; van der Werf, K.; Bennink, M.; Subramaniam, V. Nanomechanical Properties of α-Synuclein Amyloid Fibrils: A Comparative Study by Nanoindentation, Harmonic Force Microscopy, and Peakforce QNM. *Nanoscale Res. Lett.* **2011**, doi:10.1186/1556-276X-6-270.

62. Bousset, L.; Pieri, L.; Ruiz-Arlandis, G.; Gath, J.; Jensen, P.H.; Habenstein, B.; Madiona, K.; Olieric, V.; Böckmann, A.; Meier, B.H.; et al. Structural and Functional Characterization of Two Alpha-Synuclein Strains. *Nat. Commun.* **2013**, doi:10.1038/ncomms3575.

63. Dusa, A.; Kaylor, J.; Edridge, S.; Bodner, N.; Hong, D.P.; Fink, A.L. Characterization of Oligomers during α-Synuclein Aggregation Using Intrinsic Tryptophan Fluorescence. *Biochemistry* **2006**, doi:10.1021/bi051426z.

64. Tanaka, M.; Kim, Y.M.; Lee, G.; Junn, E.; Iwatsubo, T.; Mouradian, M.M. Aggresomes Formed by α-Synuclein and Synphilin-1 Are Cytoprotective. *J. Biol. Chem.* **2004**, doi:10.1074/jbc.M310994200.

65. Peelaerts, W.; Baekelandt, V. α-Synuclein Strains and the Variable Pathologies of Synucleinopathies. *J. Neurochem.* 2016.

66. Peng, C.; Gathagan, R.J.; Lee, V.M.Y. Distinct α-Synuclein Strains and Implications for Heterogeneity among α-Synucleinopathies. *Neurobiol. Dis.* **2018**, *109*, 209–218, doi:10.1016/j.nbd.2017.07.018.

67. Peelaerts, W.; Bousset, L.; Baekelandt, V.; Melki, R. α-Synuclein Strains and Seeding in Parkinson's Disease, Incidental Lewy Body Disease, Dementia with Lewy Bodies and Multiple System Atrophy: Similarities and Differences. *Cell Tissue Res.* **2018**, *373*, 195–212, doi:10.1007/s00441-018-2839-5.

68. Polymeropoulos, M.H.; Lavedan, C.; Leroy, E.; Ide, S.E.; Dehejia, A.; Dutra, A.; Pike, B.; Root, H.; Rubenstein, J.; Boyer, R.; et al. Mutation in the α-Synuclein Gene Identified in Families with Parkinson's Disease. *Science (80-.).* **1997**, doi:10.1126/science.276.5321.2045.

69. Krüger, R.; Kuhn, W.; Müller, T.; Woitalla, D.; Graeber, M.; Kösel, S.; Przuntek, H.; Epplen, J.T.; Schöls, L.; Riess, O. Ala30Pro Mutation in the Gene Encoding α-Synuclein in Parkinson's Disease. *Nat. Genet.* **1998**, doi:10.1038/ng0298-106.

70. Zarranz, J.J.; Alegre, J.; Gómez-Esteban, J.C.; Lezcano, E.; Ros, R.; Ampuero, I.; Vidal, L.; Hoenicka, J.; Rodriguez, O.; Atarés, B.; et al. The New Mutation, E46K, of α-Synuclein Causes Parkinson and Lewy Body Dementia. *Ann. Neurol.* **2004**, doi:10.1002/ana.10795.

71. Spira, P.J.; Sharpe, D.M.; Halliday, G.; Cavanagh, J.; Nicholson, G.A. Clinical and Pathological Features of a Parkinsonian Syndrome in a Family with an Ala53Thr α-Synuclein Mutation. *Ann. Neurol.* **2001**, doi:10.1002/ana.67.

72. Appel-Cresswell, S.; Vilarino-Guell, C.; Encarnacion, M.; Sherman, H.; Yu, I.; Shah, B.; Weir, D.; Thompson, C.; Szu-Tu, C.; Trinh, J.; et al. Alpha-Synuclein p.H50Q, a Novel Pathogenic Mutation for Parkinson's Disease. *Mov. Disord.* **2013**, doi:10.1002/mds.25421.

73. Kiely, A.P.; Asi, Y.T.; Kara, E.; Limousin, P.; Ling, H.; Lewis, P.; Proukakis, C.; Quinn, N.; Lees, A.J.; Hardy, J.; et al. A-Synucleinopathy Associated with G51D SNCA Mutation: A Link between Parkinson's Disease and Multiple System Atrophy? *Acta Neuropathol.* **2013**, doi:10.1007/s00401-013-1096-7.

74. Pasanen, P.; Myllykangas, L.; Siitonen, M.; Raunio, A.; Kaakkola, S.; Lyytinen, J.; Tienari, P.J.; Pöyhönen, M.; Paetau, A. A Novel α-Synuclein Mutation A53E Associated with Atypical Multiple System Atrophy and Parkinson's Disease-Type Pathology. *Neurobiol. Aging* **2014**, doi:10.1016/j.neurobiolaging.2014.03.024.

75. Khalaf, O.; Fauvet, B.; Oueslati, A.; Dikiy, I.; Mahul-Mellier, A.L.; Ruggeri, F.S.; Mbefo, M.K.; Vercruysse, F.; Dietler, G.; Lee, S.J.; et al. The H50Q Mutation Enhances Aα-Synuclein Aggregation, Secretion, and Toxicity. *J. Biol. Chem.* **2014**, doi:10.1074/jbc.M114.553297.

76. Lesage, S.; Anheim, M.; Letournel, F.; Bousset, L.; Honoré, A.; Rozas, N.; Pieri, L.; Madiona, K.; Dürr, A.; Melki, R.; et al. G51D α-Synuclein Mutation Causes a Novel Parkinsonian-Pyramidal Syndrome. *Ann. Neurol.* **2013**, doi:10.1002/ana.23894.

77. Fares, M.B.; Ait-Bouziad, N.; Dikiy, I.; Mbefo, M.K.; Jovičić, A.; Kiely, A.; Holton, J.L.; Lee, S.J.; Gitler, A.D.; Eliezer, D.; et al. The Novel Parkinson's Disease Linked Mutation G51D Attenuates in Vitro Aggregation and Membrane Binding of α-Synuclein, and Enhances Its Secretion and Nuclear Localization in Cells. *Hum. Mol. Genet.* **2014**, doi:10.1093/hmg/ddu165.

78. Rutherford, N.J.; Giasson, B.I. The A53E α-Synuclein Pathological Mutation Demonstrates Reduced Aggregation Propensity in Vitro and in Cell Culture. *Neurosci. Lett.* **2015**, doi:10.1016/j.neulet.2015.04.022.

79. Fredenburg, R.A.; Rospigliosi, C.; Meray, R.K.; Kessler, J.C.; Lashuel, H.A.; Eliezer, D.; Lansbury, P.T. The Impact of the E46K Mutation on the Properties of α-Synuclein in Its Monomelic and Oligomeric States. *Biochemistry* **2007**, doi:10.1021/bi7000246.

80. Jo, E.; Fuller, N.; Rand, R.P.; St George-Hyslop, P.; Fraser, P.E. Defective Membrane Interactions of Familial Parkinson's Disease Mutant A30P α-Synuclein. *J. Mol. Biol.* **2002**, doi:10.1006/jmbi.2001.5269.

81. Choi, W.; Zibaee, S.; Jakes, R.; Serpell, L.C.; Davletov, B.; Anthony Crowther, R.; Goedert, M. Mutation E46K Increases Phospholipid Binding and Assembly into Filaments of Human α-Synuclein. *FEBS Lett.* **2004**, doi:10.1016/j.febslet.2004.09.038.

82. Kim, J.Y.; Illigens, B.M.W.; McCormick, M.P.; Wang, N.; Gibbons, C.H. Alpha-Synuclein in Skin Nerve Fibers as a Biomarker for Alpha-Synucleinopathies. *J. Clin. Neurol.* **2019**, doi:10.3988/jcn.2019.15.2.135.

83. Doppler, K.; Weis, J.; Karl, K.; Ebert, S.; Ebentheuer, J.; Trenkwalder, C.; Klebe, S.;

Volkmann, J.; Sommer, C. Distinctive Distribution of Phospho-Alpha-Synuclein in Dermal Nerves in Multiple System Atrophy. *Mov. Disord.* **2015**, doi:10.1002/mds.26293.

84. Doppler, K. Detection of Dermal Alpha-Synuclein Deposits as a Biomarker for Parkinson's Disease. *J. Parkinsons. Dis.* 2021.

85. Coon, E.A.; Singer, W. Synucleinopathies. *Contin. Lifelong Learn. Neurol.* 2020.

86. Prusiner, S.B.; Woerman, A.L.; Mordes, D.A.; Watts, J.C.; Rampersaud, R.; Berry, D.B.; Patel, S.; Oehler, A.; Lowe, J.K.; Kravitz, S.N.; et al. Evidence for α-Synuclein Prions Causing Multiple System Atrophy in Humans with Parkinsonism. *Proc. Natl. Acad. Sci.* **2015**, *112*, E5308–E5317, doi:10.1073/pnas.1514475112.

87. Yamasaki, T.R.; Holmes, B.B.; Furman, J.L.; Dhavale, D.D.; Su, B.W.; Song, E.-S.; Cairns, N.J.; Kotzbauer, P.T.; Diamond, M.I. Parkinson's Disease and Multiple System Atrophy Have Distinct α-Synuclein Seed Characteristics. *J. Biol. Chem.* **2019**, *294*, 1045–1058, doi:10.1074/jbc.RA118.004471.

88. Guerrero-Ferreira, R.; Taylor, N.M.I.; Mona, D.; Ringler, P.; Lauer, M.E.; Riek, R.; Britschgi, M.; Stahlberg, H. Cryo-EM Structure of Alpha-Synuclein Fibrils. *Elife* **2018**, doi:10.7554/eLife.36402.

89. Yang, Y.; Shi, Y.; Schweighauser, M.; Zhang, X.; Kotecha, A.; Murzin, A.G.; Garringer, H.J.; Cullinane, P.W.; Saito, Y.; Foroud, T.; et al. Structures of α-Synuclein Filaments from Human Brains with Lewy Pathology Ì. *Nature* **2022**, doi:https://doi.org/10.1038/s41586-022-05319-3.

90. Houlden, H.; Singleton, A.B. The Genetics and Neuropathology of Parkinson's Disease. *Acta Neuropathol.* 2012.

91. Wirdefeldt, K.; Adami, H.O.; Cole, P.; Trichopoulos, D.; Mandel, J. Epidemiology and Etiology of Parkinson's Disease: A Review of the Evidence. *Eur. J. Epidemiol.* 2011.

92. Poewe, W.; Seppi, K.; Tanner, C.M.; Halliday, G.M.; Brundin, P.; Volkmann, J.; Schrag, A.E.; Lang, A.E. Parkinson Disease. *Nat. Rev. Dis. Prim.* **2017**, doi:10.1038/nrdp.2017.13.

93. Armstrong, M.J.; Okun, M.S. Diagnosis and Treatment of Parkinson Disease: A Review. *JAMA - J. Am. Med. Assoc.* 2020.

94. Parkinson, J. An Essay on the Shaking Palsy. 1817. *J. Neuropsychiatry Clin. Neurosci.* **2002**, doi:10.1176/jnp.14.2.223.

95. Chou, K.L.; Elm, J.J.; Wielinski, C.L.; Simon, D.K.; Aminoff, M.J.; Christine, C.W.; Liang, G.S.; Hauser, R.A.; Sudarsky, L.; Umeh, C.C.; et al. Factors Associated with Falling in Early, Treated Parkinson's Disease: The NET-PD LS1 Cohort. *J. Neurol. Sci.* **2017**, *377*, doi:10.1016/j.jns.2017.04.011.

96. Pringsheim, T.; Jette, N.; Frolkis, A.; Steeves, T.D.L. The Prevalence of Parkinson's Disease: A Systematic Review and Meta-Analysis. *Mov. Disord.* 2014, *29*.

97. Joseph, A.; Wanono, R.; Flamant, M.; Vidal-Petiot, E. Orthostatic Hypotension: A Review. *Nephrol. Ther.* 2017, *13*.

98. Bloem, B.R.; Okun, M.S.; Klein, C. Parkinson's Disease. *Lancet* 2021.

99. Hawkes, C.H.; Del Tredici, K.; Braak, H. Parkinson's Disease: A Dual-Hit Hypothesis.

Neuropathol. Appl. Neurobiol. 2007.

100. Boeve, B.F. Update on the Diagnosis and Management of Sleep Disturbances in Dementia. *Sleep Med. Clin.* 2008.

101. Postuma, R.B.; Iranzo, A.; Hu, M.; Högl, B.; Boeve, B.F.; Manni, R.; Oertel, W.H.; Arnulf, I.; Ferini-Strambi, L.; Puligheddu, M.; et al. Risk and Predictors of Dementia and Parkinsonism in Idiopathic REM Sleep Behaviour Disorder: A Multicentre Study. *Brain* **2019**, doi:10.1093/brain/awz030.

102. Rizzo, G.; Copetti, M.; Arcuti, S.; Martino, D.; Fontana, A.; Logroscino, G. Accuracy of Clinical Diagnosis of Parkinson Disease. *Neurology* **2016**, doi:10.1212/WNL.0000000000002350.

103. Postuma, R.B.; Berg, D.; Stern, M.; Poewe, W.; Olanow, C.W.; Oertel, W.; Obeso, J.; Marek, K.; Litvan, I.; Lang, A.E.; et al. MDS Clinical Diagnostic Criteria for Parkinson's Disease. *Mov. Disord.* 2015.

104. Suwijn, S.R.; van Boheemen, C.J.M.; de Haan, R.J.; Tissingh, G.; Booij, J.; de Bie, R.M.A. The Diagnostic Accuracy of Dopamine Transporter SPECT Imaging to Detect Nigrostriatal Cell Loss in Patients with Parkinson's Disease or Clinically Uncertain Parkinsonism: A Systematic Review. *EJNMMI Res.* 2015.

105. Lippa, C.F.; Duda, J.E.; Grossman, M.; Hurtig, H.I.; Aarsland, D.; Boeve, B.F.; Brooks, D.J.; Dickson, D.W.; Dubois, B.; Emre, M.; et al. DLB and PDD Boundary Issues: Diagnosis, Treatment, Molecular Pathology, and Biomarkers. *Neurology* **2007**, doi:10.1212/01.wnl.0000256715.13907.d3.

106. Macleod, A.D.; Taylor, K.S.M.; Counsell, C.E. Mortality in Parkinson's Disease: A Systematic Review and Meta-Analysis. *Mov. Disord.* **2014**, doi:10.1002/mds.25898.

107. Pennington, S.; Snell, K.; Lee, M.; Walker, R. The Cause of Death in Idiopathic Parkinson's Disease. *Park. Relat. Disord.* **2010**, doi:10.1016/j.parkreldis.2010.04.010.

108. Müller, T. Catechol-O-Methyltransferase Inhibitors in Parkinson's Disease. *Drugs* 2015.

109. Fox, S.H.; Katzenschlager, R.; Lim, S.Y.; Ravina, B.; Seppi, K.; Coelho, M.; Poewe, W.; Rascol, O.; Goetz, C.G.; Sampaio, C. The Movement Disorder Society Evidence-Based Medicine Review Update: Treatments for the Motor Symptoms of Parkinson's Disease. *Mov. Disord.* **2011**, doi:10.1002/mds.23829.

110. Bratsos, S.P.; Karponis, D.; Saleh, S.N. Efficacy and Safety of Deep Brain Stimulation in the Treatment of Parkinson's Disease: A Systematic Review and Meta-Analysis of Randomized Controlled Trials. *Cureus* **2018**, doi:10.7759/cureus.3474.

111. Perez-Lloret, S.; Rey, M.V.; Pavy-Le Traon, A.; Rascol, O. Emerging Drugs for Autonomic Dysfunction in Parkinson's Disease. *Expert Opin. Emerg. Drugs* 2013.

112. Connolly, B.; Fox, S.H. Treatment of Cognitive, Psychiatric, and Affective Disorders Associated with Parkinson's Disease. *Neurotherapeutics* 2014.

113. Fanciulli, A.; Stankovic, I.; Krismer, F.; Seppi, K.; Levin, J.; Wenning, G.K. Multiple System Atrophy. *Int. Rev. Neurobiol.* **2019**, doi:10.1016/bs.irn.2019.10.004.

114. Köllensperger, M.; Geser, F.; Ndayisaba, J.P.; Boesch, S.; Seppi, K.; Ostergaard, K.;

Dupont, E.; Cardozo, A.; Tolosa, E.; Abele, M.; et al. Presentation, Diagnosis, and Management of Multiple System Atrophy in Europe: Final Analysis of the European Multiple System Atrophy Registry. *Mov. Disord.* **2010**, doi:10.1002/mds.23192.

115. Krismer, F.; Wenning, G.K. Multiple System Atrophy: Insights into a Rare and Debilitating Movement Disorder. *Nat. Rev. Neurol.* 2017.

116. Gilman, S.; Wenning, G.K.; Low, P.A.; Brooks, D.J.; Mathias, C.J.; Trojanowski, J.Q.; Wood, N.W.; Colosimo, C.; Durr, A.; Fowler, C.J.; et al. Second Consensus Statement on the Diagnosis of Multiple System Atrophy. *Neurology* **2008**, *71*, 670–676, doi:10.1212/01.wnl.0000324625.00404.15.

117. Jellinger, K.A. Multiple System Atrophy: An Oligodendroglioneural Synucleinopathy. *J. Alzheimer's Dis.* 2018.

118. Sun, Z.; Jia, D.; Shi, Y.; Hou, X.; Yang, X.; Guo, J.; Li, N.; Wang, J.; Sun, Q.; Zhang, H.; et al. Prediction of Orthostatic Hypotension in Multiple System Atrophy and Parkinson Disease. *Sci. Rep.* **2016**, doi:10.1038/srep21649.

119. Bajaj, S.; Krismer, F.; Palma, J.A.; Wenning, G.K.; Kaufmann, H.; Poewe, W.; Seppi, K. Diffusion-Weighted MRI Distinguishes Parkinson Disease from the Parkinsonian Variant of Multiple System Atrophy: A Systematic Review and Meta-Analysis. *PLoS One* 2017.

120. Gazulla, J.; Errea, J.; Benavente, I.; Tordesillas, C. Improvement of Ataxia in Cortical Cerebellar Atrophy with the Drug Gabapentin [2]. *Clin. Neuropharmacol.* 2003.

121. Iranzo, A. Sleep and Breathing in Multiple System Atrophy. *Curr. Treat. Options Neurol.* 2007.

122. Eichhorn, T.E.; Oertel, W.H. Macrogol 3350/Electrolyte Improves Constipation in Parkinson's Disease and Multiple System Atrophy. *Mov. Disord.* **2001**, doi:10.1002/mds.1211.

123. Mukaetova-Ladinska, E.B.; McKeith, I.G. Pathophysiology of Synuclein Aggregation in Lewy Body Disease. In Proceedings of the Mechanisms of Ageing and Development; 2006.

124. McKeith, I.G.; Galasko, D.; Kosaka, K.; Perry, E.K.; Dickson, D.W.; Hansen, L.A.; Salmon, D.P.; Lowe, J.; Mirra, S.S.; Byrne, E.J.; et al. Consensus Guidelines for the Clinical and Pathologic Diagnosis of Dementia with Lewy Bodies (DLB): Report of the Consortium on DLB International Workshop. *Neurology* 1996.

125. Mrak, R.E.; Griffin, W.S.T. Common Inflammatory Mechanisms in Lewy Body Disease and Alzheimer Disease. *J. Neuropathol. Exp. Neurol.* 2007.

126. McKeith, I.G.; Dickson, D.W.; Lowe, J.; Emre, M.; O'Brien, J.T.; Feldman, H.; Cummings, J.; Duda, J.E.; Lippa, C.; Perry, E.K.; et al. Diagnosis and Management of Dementia with Lewy Bodies: Third Report of the DLB Consortium. *Neurology* 2005.

127. McKeith, I.; Mintzer, J.; Aarsland, D.; Burn, D.; Chiu, H.; Cohen-Mansfield, J.; Dickson, D.; Dubois, B.; Duda, J.E.; Feldman, H.; et al. Dementia with Lewy Bodies. *Lancet Neurol.* 2004.

128. AKATSU, H.; KAMINO, K.; YAMAGATA, H.; ISOJIMA, D.; KONDO, I.; YAMAMOTO, T.; KIDA, T.; TAKEDA, M.; MIKI, T.; KOSAKA, K. Increased Incidence of Dementia with

Lewy Bodies in Patients Carrying the E4-Allele of Apolipoprotein E. *Psychogeriatrics* **2004**, doi:10.1111/j.1479-8301.2004.00058.x.

129. Meeus, B.; Theuns, J.; Van Broeckhoven, C. The Genetics of Dementia with Lewy Bodies: What Are We Missing? *Arch. Neurol.* 2012.

130. Clark, L.N.; Kartsaklis, L.A.; Gilbert, R.W.; Dorado, B.; Ross, B.M.; Kisselev, S.; Verbitsky, M.; Mejia-Santana, H.; Cote, L.J.; Andrews, H.; et al. Association of Glucocerebrosidase Mutations with Dementia with Lewy Bodies. *Arch. Neurol.* **2009**, doi:10.1001/archneurol.2009.54.

131. Boeve, B.F. Clinical, Diagnostic, Genetic and Management Issues in Dementia with Lewy Bodies. *Clin. Sci.* 2005.

132. Aarsland, D.; Ballard, C.; McKeith, I.; Perry, R.H.; Larsen, J.P. Comparison of Extrapyramidal Signs in Dementia with Lewy Bodies and Parkinson's Disease. *J. Neuropsychiatry Clin. Neurosci.* **2001**, doi:10.1176/jnp.13.3.374.

133. TJ, F.; GE, S.; BF, B.; RJ, I.; RC, P.; Knopman, D.; Graff-Radford, N.; Parisi, J.; DW, D.; Ferman, T.J.; et al. DLB Fluctuations: Specific Features That Reliably Differentiate DLB from AD and Normal Aging. *Neurology* **2004**.

134. McKeith, I.; O'Brien, J.; Walker, Z.; Tatsch, K.; Booij, J.; Darcourt, J.; Padovani, A.; Giubbini, R.; Bonuccelli, U.; Volterrani, D.; et al. Sensitivity and Specificity of Dopamine Transporter Imaging with 123I-FP-CIT SPECT in Dementia with Lewy Bodies: A Phase III, Multicentre Study. *Lancet Neurol.* **2007**, doi:10.1016/S1474-4422(07)70057-1.

135. Ferman, T.J.; Arvanitakis, Z.; Fujishiro, H.; Duara, R.; Parfitt, F.; Purdy, M.; Waters, C.; Barker, W.; Graff-Radford, N.R.; Dickson, D.W. Pathology and Temporal Onset of Visual Hallucinations, Misperceptions and Family Misidentification Distinguishes Dementia with Lewy Bodies from Alzheimer's Disease. *Park. Relat. Disord.* **2013**, doi:10.1016/j.parkreldis.2012.10.013.

136. McKeith, I.G. Dementia with Lewy Bodies. *Br. J. Psychiatry* 2002.

137. Thaisetthawatkul, P.; Boeve, B.F.; Benarroch, E.E.; Sandroni, P.; Ferman, T.J.; Petersen, R.; Low, P.A. Autonomic Dysfunction in Dementia with Lewy Bodies. *Neurology* **2004**, doi:10.1212/01.WNL.0000125192.69777.6D.

138. Allan, L.M.; Ballard, C.G.; Allen, J.; Murray, A.; Davidson, A.W.; McKeith, I.G.; Kenny, R.A. Autonomic Dysfunction in Dementia. *J. Neurol. Neurosurg. Psychiatry* **2007**, doi:10.1136/jnnp.2006.102343.

139. Idiaquez, J.; Roman, G.C. Autonomic Dysfunction in Neurodegenerative Dementias. *J. Neurol. Sci.* 2011.

140. McKeith, I.G.; Boeve, B.F.; DIckson, D.W.; Halliday, G.; Taylor, J.P.; Weintraub, D.; Aarsland, D.; Galvin, J.; Attems, J.; Ballard, C.G.; et al. Diagnosis and Management of Dementia with Lewy Bodies. *Neurology* 2017.

141. Gilman, S.; Koeppe, R.A.; Little, R.; An, H.; Junck, L.; Giordani, B.; Persad, C.; Heumann, M.; Wernette, K. Differentiation of Alzheimer's Disease from Dementia with Lewy Bodies Utilizing Positron Emission Tomography with [18F]Fluorodeoxyglucose and Neuropsychological Testing. *Exp. Neurol.* **2005**, doi:10.1016/j.expneurol.2004.06.017.

142. Williams, M.M.; Xiong, C.; Morris, J.C.; Galvin, J.E. Survival and Mortality Differences between Dementia with Lewy Bodies vs Alzheimer Disease. *Neurology* **2006**, doi:10.1212/01.wnl.0000247041.63081.98.

143. Mori, E.; Ikeda, M.; Kosaka, K. Donepezil for Dementia with Lewy Bodies: A Randomized, Placebo-Controlled Trial. *Ann. Neurol.* **2012**, doi:10.1002/ana.23557.

144. McKeith, I.; Del Ser, T.; Spano, P.F.; Emre, M.; Wesnes, K.; Anand, R.; Cicin-Sain, A.; Ferrara, R.; Spiegel, R. Efficacy of Rivastigmine in Dementia with Lewy Bodies: A Randomised, Double-Blind, Placebo-Controlled International Study. *Lancet* **2000**, doi:10.1016/S0140-6736(00)03399-7.

145. Aarsland, D.; Hutchinson, M.; Larsen, J.P. Cognitive, Psychiatric and Motor Response to Galantamine in Parkinson's Desease with Dementia. *Int. J. Geriatr. Psychiatry* **2003**, doi:10.1002/gps.949.

146. Vasconcellos, L.F.R.; Pereira, J.S. Parkinson's Disease Dementia: Diagnostic Criteria and Risk Factor Review. *J. Clin. Exp. Neuropsychol.* 2015.

147. Parkkinen, L.; Pirttilä, T.; Tervahauta, M.; Alafuzoff, I. Widespread and Abundant α-Synuclein Pathology in a Neurologically Unimpaired Subject. *Neuropathology* **2005**, doi:10.1111/j.1440-1789.2005.00644.x.

148. Zaccai, J.; Brayne, C.; Matthews, F.E.; Ince, P.G. Alpha-Synucleinopathy and Neuropsychological Symptoms in a Population-Based Cohort of the Elderly. *Alzheimer's Res. Ther.* **2015**, doi:10.1186/s13195-015-0101-x.

149. Elobeid, A.; Libard, S.; Leino, M.; Popova, S.N.; Alafuzoff, I. Altered Proteins in the Aging Brain. *J. Neuropathol. Exp. Neurol.* **2016**, doi:10.1093/jnen/nlw002.

150. Gray, M.T.; Munoz, D.G.; Gray, D.A.; Schlossmacher, M.G.; Woulfe, J.M. Alpha-Synuclein in the Appendiceal Mucosa of Neurologically Intact Subjects. *Mov. Disord.* **2014**, doi:10.1002/mds.25779.

151. Coon, E.A.; Singer, W.; Low, P.A. Pure Autonomic Failure. *Mayo Clin. Proc.* 2019.

152. Orimo, S.; Suzuki, M.; Inaba, A.; Mizusawa, H. 123I-MIBG Myocardial Scintigraphy for Differentiating Parkinson's Disease from Other Neurodegenerative Parkinsonism: A Systematic Review and Meta-Analysis. *Park. Relat. Disord.* **2012**, doi:10.1016/j.parkreldis.2012.01.009.

153. Donadio, V.; Incensi, A.; Rizzo, G.; De Micco, R.; Tessitore, A.; Devigili, G.; Del Sorbo, F.; Bonvegna, S.; Infante, R.; Magnani, M.; et al. Skin Biopsy May Help to Distinguish Multiple System Atrophy–Parkinsonism from Parkinson's Disease With Orthostatic Hypotension. *Mov. Disord.* **2020**, doi:10.1002/mds.28126.

154. Hussl, A.; Mahlknecht, P.; Scherfler, C.; Esterhammer, R.; Schocke, M.; Poewe, W.; Seppi, K. Diagnostic Accuracy of the Magnetic Resonance Parkinsonism Index and the Midbrain-to-Pontine Area Ratio to Differentiate Progressive Supranuclear Palsy from Parkinson's Disease and the Parkinson Variant of Multiple System Atrophy. *Mov. Disord.* **2010**, doi:10.1002/mds.23351.

155. Glass, P.G.; Lees, A.J.; Mathias, C.; Mason, L.; Best, C.; Williams, D.R.; Katzenschlager, R.; Silveira-Moriyama, L. Olfaction in Pathologically Proven Patients with Multiple System

Atrophy. *Mov. Disord.* **2012**, *27*, 327–328, doi:10.1002/mds.23972.

156. Pellecchia, M.T.; Barone, P.B.; Mollica, C.; Salvatore, E.; Ianniciello, M.; Longo, K.; Varrone, A.; Vicidomini, C.; Picillo, M.; De Michele, G.; et al. Diffusion-Weighted Imaging in Multiple System Atrophy: A Comparison between Clinical Subtypes. *Mov. Disord.* **2009**, doi:10.1002/mds.22440.

157. Palma, J.-A.; Norcliffe-Kaufmann, L.; Kaufmann, H. Diagnosis of Multiple System Atrophy. *Auton. Neurosci.* **2018**, *211*, 15–25, doi:10.1016/j.autneu.2017.10.007.

158. Kaufmann, H.; Norcliffe-Kaufmann, L.; Palma, J.A.; Biaggioni, I.; Low, P.A.; Singer, W.; Goldstein, D.S.; Peltier, A.C.; Shibao, C.A.; Gibbons, C.H.; et al. Natural History of Pure Autonomic Failure: A United States Prospective Cohort. *Ann. Neurol.* **2017**, doi:10.1002/ana.24877.

159. Aarsland, D.; Ballard, C.G.; Halliday, G. Are Parkinson's Disease with Dementia and Dementia with Lewy Bodies the Same Entity? *J. Geriatr. Psychiatry Neurol.* 2004.

160. Goldmann Gross, R.; Siderowf, A.; Hurtig, H.I. Cognitive Impairment in Parkinson's Disease and Dementia with Lewy Bodies: A Spectrum of Disease. *NeuroSignals* 2007.

161. Emre, M.; Aarsland, D.; Brown, R.; Burn, D.J.; Duyckaerts, C.; Mizuno, Y.; Broe, G.A.; Cummings, J.; Dickson, D.W.; Gauthier, S.; et al. Clinical Diagnostic Criteria for Dementia Associated with Parkinson's Disease. *Mov. Disord.* 2007.

162. Calderon, J.; Perry, R.J.; Erzinclioglu, S.W.; Berrios, G.E.; Dening, T.R.; Hodges, J.R. Perception, Attention, and Working Memory Are Disproportionately Impaired in Dementia with Lewy Bodies Compared with Alzheimer's Disease. *J. Neurol. Neurosurg. Psychiatry* **2001**, doi:10.1136/jnnp.70.2.157.

163. Watanabe, H.; Ieda, T.; Katayama, T.; Takeda, A.; Aiba, I.; Doyu, M.; Hirayama, M.; Sobue, G. Cardiac 123I-Meta-Iodobenzylguanidine (MIBG) Uptake in Dementia with Lewy Bodies: Comparison with Alzheimer's Disease. *J. Neurol. Neurosurg. Psychiatry* **2001**, doi:10.1136/jnnp.70.6.781.

164. Yoshita, M.; Arai, H.; Arai, H.; Arai, T.; Asada, T.; Fujishiro, H.; Hanyu, H.; Iizuka, O.; Iseki, E.; Kashihara, K.; et al. Diagnostic Accuracy Of123I-Meta-Iodobenzylguanidine Myocardial Scintigraphy in Dementia with Lewy Bodies: A Multicenter Study. *PLoS One* **2015**, doi:10.1371/journal.pone.0120540.

165. Kovacs, G.G. Molecular Pathological Classification of Neurodegenerative Diseases: Turning towards Precision Medicine. *Int. J. Mol. Sci.* 2016.

166. Beyreuther, K.; Jäkälä, P.; Gai, W.P.; Culvenor, J.G.; McLean, C.A.; Masters, C.L.; Campbell, B.C. V.; Li, Q.-X.; Blumbergs, P.C. The Solubility of Alpha-Synuclein in Multiple System Atrophy Differs from That of Dementia with Lewy Bodies and Parkinson's Disease. *J. Neurochem.* **2001**.

167. Rascovsky, K.; Hodges, J.R.; Knopman, D.; Mendez, M.F.; Kramer, J.H.; Neuhaus, J.; Van Swieten, J.C.; Seelaar, H.; Dopper, E.G.P.; Onyike, C.U.; et al. Sensitivity of Revised Diagnostic Criteria for the Behavioural Variant of Frontotemporal Dementia. *Brain* **2011**, doi:10.1093/brain/awr179.

168. McKhann, G.M.; Knopman, D.S.; Chertkow, H.; Hyman, B.T.; Jack, C.R.; Kawas, C.H.;

Klunk, W.E.; Koroshetz, W.J.; Manly, J.J.; Mayeux, R.; et al. The Diagnosis of Dementia Due to Alzheimer's Disease: Recommendations from the National Institute on Aging-Alzheimer's Association Workgroups on Diagnostic Guidelines for Alzheimer's Disease. *Alzheimer's Dement.* **2011**, *7*, doi:10.1016/j.jalz.2011.03.005.

169. Adler, C.H.; Beach, T.G.; Hentz, J.G.; Shill, H.A.; Caviness, J.N.; Driver-Dunckley, E.; Sabbagh, M.N.; Sue, L.I.; Jacobson, S.A.; Belden, C.M.; et al. Low Clinical Diagnostic Accuracy of Early vs Advanced Parkinson Disease: Clinicopathologic Study. *Neurology* **2014**, doi:10.1212/WNL.0000000000000641.

170. McKeith, I.G.; Ballard, C.G.; Perry, R.H.; Ince, P.G.; O'Brien, J.T.; Neill, D.; Lowery, K.; Jaros, E.; Barber, R.; Thompson, P.; et al. Prospective Validation of Consensus Criteria for the Diagnosis of Dementia with Lewy Bodies. *Neurology* **2000**, doi:10.1212/WNL.54.5.1050.

171. Merdes, A.R.; Hansen, L.A.; Jeste, D. V.; Galasko, D.; Hofstetter, C.R.; Ho, G.J.; Thal, L.J.; Corey-Bloom, J. Influence of Alzheimer Pathology on Clinical Diagnostic Accuracy in Dementia with Lewy Bodies. *Neurology* **2003**, doi:10.1212/01.WNL.0000065889.42856.F2.

172. Postuma, R.B.; Berg, D.; Stern, M.; Poewe, W.; Olanow, C.W.; Oertel, W.; Obeso, J.; Marek, K.; Litvan, I.; Lang, A.E.; et al. MDS Clinical Diagnostic Criteria for Parkinson's Disease. *Mov. Disord.* **2015**, *30*, 1591–1601, doi:10.1002/mds.26424.

173. Rizzo, G.; Arcuti, S.; Copetti, M.; Alessandria, M.; Savica, R.; Fontana, A.; Liguori, R.; Logroscino, G. Accuracy of Clinical Diagnosis of Dementia with Lewy Bodies: A Systematic Review and Meta-Analysis. *J. Neurol. Neurosurg. Psychiatry* 2018.

174. Simon, R. Sensitivity, Specificity, PPV, and NPV for Predictive Biomarkers. *J. Natl. Cancer Inst.* **2015**, doi:10.1093/jnci/djv153.

175. Brower, V. Biomarkers: Portents of Malignancy. *Nature* **2011**, doi:10.1038/471S19a.

176. Agrawal, M.; Biswas, A. Molecular Diagnostics of Neurodegenerative Disorders. *Front. Mol. Biosci.* 2015.

177. Singer, W.; Schmeichel, A.M.; Shahnawaz, M.; Schmelzer, J.D.; Sletten, D.M.; Gehrking, T.L.; Gehrking, J.A.; Olson, A.D.; Suarez, M.D.; Misra, P.P.; et al. Alpha-Synuclein Oligomers and Neurofilament Light Chain Predict Phenoconversion of Pure Autonomic Failure. *Ann. Neurol.* **2021**, doi:10.1002/ana.26089.

178. Xue, C.; Lin, T.Y.; Chang, D.; Guo, Z. Thioflavin T as an Amyloid Dye: Fibril Quantification, Optimal Concentration and Effect on Aggregation. *R. Soc. Open Sci.* **2017**, doi:10.1098/rsos.160696.

179. Atarashi, R.; Satoh, K.; Sano, K.; Fuse, T.; Yamaguchi, N.; Ishibashi, D.; Matsubara, T.; Nakagaki, T.; Yamanaka, H.; Shirabe, S.; et al. Ultrasensitive Human Prion Detection in Cerebrospinal Fluid by Real-Time Quaking-Induced Conversion. *Nat. Med.* **2011**, doi:10.1038/nm.2294.

180. Groveman, B.R.; Orrù, C.D.; Hughson, A.G.; Raymond, L.D.; Zanusso, G.; Ghetti, B.; Campbell, K.J.; Safar, J.; Galasko, D.; Caughey, B. Rapid and Ultra-Sensitive Quantitation of Disease-Associated α-Synuclein Seeds in Brain and Cerebrospinal Fluid by ASyn RT-QuIC. *Acta Neuropathol. Commun.* **2018**, *6*, 7, doi:10.1186/s40478-018-0508-2.

181. Zanusso, G.; Monaco, S.; Pocchiari, M.; Caughey, B. Advanced Tests for Early and Accurate Diagnosis of Creutzfeldt-Jakob Disease. *Nat. Rev. Neurol.* 2016.

182. Franceschini, A.; Baiardi, S.; Hughson, A.G.; McKenzie, N.; Moda, F.; Rossi, M.; Capellari, S.; Green, A.; Giaccone, G.; Caughey, B.; et al. High Diagnostic Value of Second Generation CSF RT-QuIC across the Wide Spectrum of CJD Prions. *Sci. Rep.* **2017**, doi:10.1038/s41598-017-10922-w.

183. Orrú, C.D.; Groveman, B.R.; Hughson, A.G.; Zanusso, G.; Coulthart, M.B.; Caughey, B. Rapid and Sensitive RT-QuIC Detection of Human Creutzfeldt-Jakob Disease Using Cerebrospinal Fluid. *MBio* **2015**, doi:10.1128/mBio.02451-14.

184. Redaelli, V.; Bistaffa, E.; Zanusso, G.; Salzano, G.; Sacchetto, L.; Rossi, M.; De Luca, C.M.G.; Di Bari, M.; Portaleone, S.M.; Agrimi, U.; et al. Detection of Prion Seeding Activity in the Olfactory Mucosa of Patients with Fatal Familial Insomnia. *Sci. Rep.* **2017**, *7*, 46269, doi:10.1038/srep46269.

185. Orrú, C.D.; Yuan, J.; Appleby, B.S.; Li, B.; Li, Y.; Winner, D.; Wang, Z.; Zhan, Y.-A.; Rodgers, M.; Rarick, J.; et al. Prion Seeding Activity and Infectivity in Skin Samples from Patients with Sporadic Creutzfeldt-Jakob Disease. *Sci. Transl. Med.* **2017**, *9*, eaam7785, doi:10.1126/scitranslmed.aam7785.

186. Satoh, K.; Fuse, T.; Nonaka, T.; Dong, T.; Takao, M.; Nakagaki, T.; Ishibashi, D.; Taguchi, Y.; Mihara, B.; Iwasaki, Y.; et al. Postmortem Quantitative Analysis of Prion Seeding Activity in the Digestive System. *Molecules* **2019**, *24*, 4601, doi:10.3390/molecules24244601.

187. Bistaffa, E.; Vuong, T.T.; Cazzaniga, F.A.; Tran, L.; Salzano, G.; Legname, G.; Giaccone, G.; Benestad, S.L.; Moda, F. Use of Different RT-QuIC Substrates for Detecting CWD Prions in the Brain of Norwegian Cervids. *Sci. Rep.* **2019**, doi:10.1038/s41598-019-55078-x.

188. Kang, H.E.; Mo, Y.; Abd Rahim, R.; Lee, H.M.; Ryou, C. Prion Diagnosis: Application of Real-Time Quaking-Induced Conversion. *Biomed Res. Int.* 2017.

189. Shahnawaz, M.; Tokuda, T.; Waraga, M.; Mendez, N.; Ishii, R.; Trenkwalder, C.; Mollenhauer, B.; Soto, C. Development of a Biochemical Diagnosis of Parkinson Disease by Detection of α-Synuclein Misfolded Aggregates in Cerebrospinal Fluid. *JAMA Neurol.* **2017**, doi:10.1001/jamaneurol.2016.4547.

190. Fairfoul, G.; McGuire, L.I.; Pal, S.; Ironside, J.W.; Neumann, J.; Christie, S.; Joachim, C.; Esiri, M.; Evetts, S.G.; Rolinski, M.; et al. Alpha-Synuclein RT-QuIC in the CSF of Patients with Alpha-Synucleinopathies. *Ann. Clin. Transl. Neurol.* **2016**, doi:10.1002/acn3.338.

191. Groveman, B.R.; Orrù, C.D.; Hughson, A.G.; Raymond, L.D.; Zanusso, G.; Ghetti, B.; Campbell, K.J.; Safar, J.; Galasko, D.; Caughey, B. Rapid and Ultra-Sensitive Quantitation of Disease-Associated α-Synuclein Seeds in Brain and Cerebrospinal Fluid by ASyn RT-QuIC. *Acta Neuropathol. Commun.* **2018**, *6*, 7, doi:10.1186/s40478-018-0508-2.

192. Shahnawaz, M.; Mukherjee, A.; Pritzkow, S.; Mendez, N.; Rabadia, P.; Liu, X.; Hu, B.; Schmeichel, A.; Singer, W.; Wu, G.; et al. Discriminating α-Synuclein Strains in Parkinson's Disease and Multiple System Atrophy. *Nature* **2020**, *578*, 273–277, doi:10.1038/s41586-020-1984-7.

193. Rossi, M.; Candelise, N.; Baiardi, S.; Capellari, S.; Giannini, G.; Orrù, C.D.; Antelmi, E.;

Mammana, A.; Hughson, A.G.; Calandra-Buonaura, G.; et al. Ultrasensitive RT-QuIC Assay with High Sensitivity and Specificity for Lewy Body-Associated Synucleinopathies. *Acta Neuropathol.* **2020**, *140*, 49–62, doi:10.1007/s00401-020-02160-8.

194. van Rumund, A.; Green, A.J.E.; Fairfoul, G.; Esselink, R.A.J.; Bloem, B.R.; Verbeek, M.M. A-Synuclein Real-time Quaking-induced Conversion in the Cerebrospinal Fluid of Uncertain Cases of Parkinsonism. *Ann. Neurol.* **2019**, *85*, 777–781, doi:10.1002/ana.25447.

195. Poggiolini, I.; Vandana, G.; Lawton, M.; Lee, S.; El-turabi, A.; Querejeta-Coma, A.; Trenkwalder, C.; Sixel-Döring, F.; Montplaisir, J.Y.; Gagnon, J.F.; et al. Diagnostic Value of Cerebrospinal Fluid Alpha-Synuclein Seed Quantification in Synucleinopathies. *Brain* **2022**, *145*, 584–595.

196. Visanji, N.P.; Mollenhauer, B.; Beach, T.G.; Adler, C.H.; Coffey, C.S.; Kopil, C.M.; Dave, K.D.; Foroud, T.; Chahine, L.; Jennings, D. The Systemic Synuclein Sampling Study: Toward a Biomarker for Parkinson's Disease. *Biomark. Med.* **2017**, doi:10.2217/bmm-2016-0366.

197. Manne, S.; Kondru, N.; Jin, H.; Serrano, G.E.; Anantharam, V.; Kanthasamy, A.; Adler, C.H.; Beach, T.G.; Kanthasamy, A.G. Blinded <scp>RT-QuIC</Scp> Analysis of <scp>α-Synuclein</Scp> Biomarker in Skin Tissue From Parkinson's Disease Patients. *Mov. Disord.* **2020**, *35*, 2230–2239, doi:10.1002/mds.28242.

198. Brozzetti, L.; Sacchetto, L.; Cecchini, M.P.; Avesani, A.; Perra, D.; Bongianni, M.; Portioli, C.; Scupoli, M.; Ghetti, B.; Monaco, S.; et al. Neurodegeneration-Associated Proteins in Human Olfactory Neurons Collected by Nasal Brushing. *Front. Neurosci.* **2020**, doi:10.3389/fnins.2020.00145.

199. Rey, N.L.; George, S.; Steiner, J.A.; Madaj, Z.; Luk, K.C.; Trojanowski, J.Q.; Lee, V.M.Y.; Brundin, P. Spread of Aggregates after Olfactory Bulb Injection of α-Synuclein Fibrils Is Associated with Early Neuronal Loss and Is Reduced Long Term. *Acta Neuropathol.* **2018**, doi:10.1007/s00401-017-1792-9.

200. Orrú, C.D.; Bongianni, M.; Tonoli, G.; Ferrari, S.; Hughson, A.G.; Groveman, B.R.; Fiorini, M.; Pocchiari, M.; Monaco, S.; Caughey, B.; et al. A Test for Creutzfeldt–Jakob Disease Using Nasal Brushings. *N. Engl. J. Med.* **2014**, doi:10.1056/nejmoa1315200.

201. Donadio, V.; Wang, Z.; Incensi, A.; Rizzo, G.; Fileccia, E.; Vacchiano, V.; Capellari, S.; Magnani, M.; Scaglione, C.; Stanzani Maserati, M.; et al. In Vivo Diagnosis of Synucleinopathies: A Comparative Study of Skin Biopsy and RT-QuIC. *Neurology* **2021**, doi:10.1212/WNL.0000000000011935.

202. Mammana, A.; Baiardi, S.; Quadalti, C.; Rossi, M.; Donadio, V.; Capellari, S.; Liguori, R.; Parchi, P. <scp>RT-QuIC</Scp> Detection of Pathological A-Synuclein in Skin Punches of Patients with Lewy Body Disease. *Mov. Disord.* **2021**, *36*, 2173–2177, doi:10.1002/mds.28651.

203. Wang, Z.; Becker, K.; Donadio, V.; Siedlak, S.; Yuan, J.; Rezaee, M.; Incensi, A.; Kuzkina, A.; Orrú, C.D.; Tatsuoka, C.; et al. Skin α-Synuclein Aggregation Seeding Activity as a Novel Biomarker for Parkinson Disease. *JAMA Neurol.* **2021**, *78*, 30, doi:10.1001/jamaneurol.2020.3311.

204. Kuzkina, A.; Bargar, C.; Schmitt, D.; Rößle, J.; Wang, W.; Schubert, A.L.; Tatsuoka, C.;

Gunzler, S.A.; Zou, W.Q.; Volkmann, J.; et al. Diagnostic Value of Skin RT-QuIC in Parkinson's Disease: A Two-Laboratory Study. *npj Park. Dis.* **2021**, doi:10.1038/s41531-021-00242-2.

205. Manne, S.; Kondru, N.; Jin, H.; Anantharam, V.; Huang, X.; Kanthasamy, A.; Kanthasamy, A.G. α-Synuclein Real-Time Quaking-Induced Conversion in the Submandibular Glands of Parkinson's Disease Patients. *Mov. Disord.* **2020**, doi:10.1002/mds.27907.

206. Luan, M.; Sun, Y.; Chen, J.; Jiang, Y.; Li, F.; Wei, L.; Sun, W.; Ma, J.; Song, L.; Liu, J.; et al. Diagnostic Value of Salivary Real-Time Quaking-Induced Conversion in Parkinson's Disease and Multiple System Atrophy. *Mov. Disord.* **2022**, doi:10.1002/mds.28976.

207. Iranzo, A.; Molinuevo, J.L.; Santamaría, J.; Serradell, M.; Martí, M.J.; Valldeoriola, F.; Tolosa, E. Rapid-Eye-Movement Sleep Behaviour Disorder as an Early Marker for a Neurodegenerative Disorder: A Descriptive Study. *Lancet Neurol.* **2006**, doi:10.1016/S1474-4422(06)70476-8.

208. Postuma, R.B.; Gagnon, J.F.; Bertrand, J.A.; Génier Marchand, D.; Montplaisir, J.Y. Parkinson Risk in Idiopathic REM Sleep Behavior Disorder: Preparing for Neuroprotective Trials. *Neurology* **2015**, doi:10.1212/WNL.0000000000001364.

209. Iranzo, A.; Fernández-Arcos, A.; Tolosa, E.; Serradell, M.; Molinuevo, J.L.; Valldeoriola, F.; Gelpi, E.; Vilaseca, I.; Sánchez-Valle, R.; Lladó, A.; et al. Neurodegenerative Disorder Risk in Idiopathic REM Sleep Behavior Disorder: Study in 174 Patients. *PLoS One* **2014**, doi:10.1371/journal.pone.0089741.

210. Iranzo, A.; Fairfoul, G.; Ayudhaya, A.C.N.; Serradell, M.; Gelpi, E.; Vilaseca, I.; Sanchez-Valle, R.; Gaig, C.; Santamaria, J.; Tolosa, E.; et al. Detection of α-Synuclein in CSF by RT-QuIC in Patients with Isolated Rapid-Eye-Movement Sleep Behaviour Disorder: A Longitudinal Observational Study. *Lancet Neurol.* **2021**, *20*, 203–212, doi:10.1016/S1474-4422(20)30449-X.

211. Quadalti, C.; Calandra-Buonaura, G.; Baiardi, S.; Mastrangelo, A.; Rossi, M.; Zenesini, C.; Giannini, G.; Candelise, N.; Sambati, L.; Polischi, B.; et al. Neurofilament Light Chain and α-Synuclein RT-QuIC as Differential Diagnostic Biomarkers in Parkinsonisms and Related Syndromes. *npj Park. Dis.* **2021**, doi:10.1038/s41531-021-00232-4.

212. Strohäker, T.; Jung, B.C.; Liou, S.-H.; Fernandez, C.O.; Riedel, D.; Becker, S.; Halliday, G.M.; Bennati, M.; Kim, W.S.; Lee, S.-J.; et al. Structural Heterogeneity of α-Synuclein Fibrils Amplified from Patient Brain Extracts. *Nat. Commun.* **2019**, *10*, 5535, doi:10.1038/s41467-019-13564-w.

213. Schweighauser, M.; Shi, Y.; Tarutani, A.; Kametani, F.; Murzin, A.G.; Ghetti, B.; Matsubara, T.; Tomita, T.; Ando, T.; Hasegawa, K.; et al. Structures of α-Synuclein Filaments from Multiple System Atrophy. *Nature* **2020**, *585*, 464–469, doi:10.1038/s41586-020-2317-6.

214. Van der Perren, A.; Gelders, G.; Fenyi, A.; Bousset, L.; Brito, F.; Peelaerts, W.; Van den Haute, C.; Gentleman, S.; Melki, R.; Baekelandt, V. The Structural Differences between Patient-Derived α-Synuclein Strains Dictate Characteristics of Parkinson's Disease, Multiple System Atrophy and Dementia with Lewy Bodies. *Acta Neuropathol.* **2020**, doi:10.1007/s00401-020-02157-3.

215. Schmitz, M.; Cramm, M.; Llorens, F.; Candelise, N.; Müller-Cramm, D.; Varges, D.; Schulz-Schaeffer, W.J.; Zafar, S.; Zerr, I. Application of an in Vitro-Amplification Assay as a

Novel Pre-Screening Test for Compounds Inhibiting the Aggregation of Prion Protein Scrapie. *Sci. Rep.* **2016**, doi:10.1038/srep28711.

216. Dominguez-Meijide, A.; Parrales, V.; Vasili, E.; González-Lizárraga, F.; König, A.; Lázaro, D.F.; Lannuzel, A.; Haik, S.; Del Bel, E.; Chehín, R.; et al. Doxycycline Inhibits α-Synuclein-Associated Pathologies in Vitro and in Vivo. *Neurobiol. Dis.* **2021**, doi:10.1016/j.nbd.2021.105256.

217. Pandey, N.; Strider, J.; Nolan, W.C.; Yan, S.X.; Galvin, J.E. Curcumin Inhibits Aggregation of α-Synuclein. *Acta Neuropathol.* **2008**, doi:10.1007/s00401-007-0332-4.

218. Dominguez-Meijide, A.; Vasili, E.; König, A.; Cima-Omori, M.S.; Ibáñez de Opakua, A.; Leonov, A.; Ryazanov, S.; Zweckstetter, M.; Griesinger, C.; Outeiro, T.F. Effects of Pharmacological Modulators of α-Synuclein and Tau Aggregation and Internalization. *Sci. Rep.* **2020**, doi:10.1038/s41598-020-69744-y.

219. Bieschke, J.; Russ, J.; Friedrich, R.P.; Ehrnhoefer, D.E.; Wobst, H.; Neugebauer, K.; Wanker, E.E. EGCG Remodels Mature α-Synuclein and Amyloid-β Fibrils and Reduces Cellular Toxicity. *Proc. Natl. Acad. Sci. U. S. A.* **2010**, doi:10.1073/pnas.0910723107.

220. Prabhudesai, S.; Sinha, S.; Attar, A.; Kotagiri, A.; Fitzmaurice, A.G.; Lakshmanan, R.; Ivanova, M.I.; Loo, J.A.; Klärner, F.G.; Schrader, T.; et al. A Novel "Molecular Tweezer" Inhibitor of α-Synuclein Neurotoxicity in Vitro and in Vivo. *Neurotherapeutics* **2012**, doi:10.1007/s13311-012-0105-1.

221. Hughes, A.J.; Daniel, S.E.; Kilford, L.; Lees, A.J. Accuracy of Clinical Diagnosis of Idiopathic Parkinson's Disease: A Clinico-Pathological Study of 100 Cases. *J. Neurol. Neurosurg. Psychiatry* **1992**, doi:10.1136/jnnp.55.3.181.

222. Höglinger, G.U.; Respondek, G.; Stamelou, M.; Kurz, C.; Josephs, K.A.; Lang, A.E.; Mollenhauer, B.; Müller, U.; Nilsson, C.; Whitwell, J.L.; et al. Clinical Diagnosis of Progressive Supranuclear Palsy: The Movement Disorder Society Criteria. *Mov. Disord.* **2017**, *32*, doi:10.1002/mds.26987.

223. Armstrong, M.J.; Litvan, I.; Lang, A.E.; Bak, T.H.; Bhatia, K.P.; Borroni, B.; Boxer, A.L.; Dickson, D.W.; Grossman, M.; Hallett, M.; et al. Criteria for the Diagnosis of Corticobasal Degeneration. *Neurology* **2013**, doi:10.1212/WNL.0b013e31827f0fd1.

224. Nonaka, T.; Watanabe, S.T.; Iwatsubo, T.; Hasegawa, M. Seeded Aggregation and Toxicity of α-Synuclein and Tau. *J. Biol. Chem.* **2010**, *285*, 34885–34898, doi:10.1074/jbc.M110.148460.

225. de Waal, G.M.; de Villiers, W.J.S.; Forgan, T.; Roberts, T.; Pretorius, E. Colorectal Cancer Is Associated with Increased Circulating Lipopolysaccharide, Inflammation and Hypercoagulability. *Sci. Rep.* **2020**, doi:10.1038/s41598-020-65324-2.

226. Hughes, A.J.; Daniel, S.E.; Ben-Shlomo, Y.; Lees, A.J. The Accuracy of Diagnosis of Parkinsonian Syndromes in a Specialist Movement Disorder Service. *Brain* **2002**, *125*, 861–870, doi:10.1093/brain/awf080.

227. Nagaishi, M.; Yokoo, H.; Nakazato, Y. Tau-Positive Glial Cytoplasmic Granules in Multiple System Atrophy. *Neuropathology* **2011**, doi:10.1111/j.1440-1789.2010.01159.x.

228. Uversky, V.; Eliezer, D. Biophysics of Parkinsons Disease: Structure and Aggregation of

α- Synuclein. *Curr. Protein Pept. Sci.* **2009**, doi:10.2174/138920309789351921.

229. Lawton, M.; Baig, F.; Rolinski, M.; Ruffman, C.; Nithi, K.; May, M.T.; Ben-Shlomo, Y.; Hu, M.T.M. Parkinson's Disease Subtypes in the Oxford Parkinson Disease Centre (OPDC) Discovery Cohort. *J. Parkinsons. Dis.* **2015**, doi:10.3233/JPD-140523.

230. De Luca, C.M.G.; Elia, A.E.; Portaleone, S.M.; Cazzaniga, F.A.; Rossi, M.; Bistaffa, E.; De Cecco, E.; Narkiewicz, J.; Salzano, G.; Carletta, O.; et al. Efficient RT-QuIC Seeding Activity for α-Synuclein in Olfactory Mucosa Samples of Patients with Parkinson's Disease and Multiple System Atrophy. *Transl. Neurodegener.* **2019**, *8*, doi:10.1186/s40035-019-0164-x.

231. Kasanuki, K.; Josephs, K.A.; Ferman, T.J.; Murray, M.E.; Koga, S.; Konno, T.; Sakae, N.; Parks, A.; Uitti, R.J.; Van Gerpen, J.A.; et al. Diffuse Lewy Body Disease Manifesting as Corticobasal Syndrome A Rare Form of Lewy Body Disease. *Neurology* **2018**, doi:10.1212/WNL.0000000000005828.

232. Mandal, P.K.; Pettegrew, J.W.; Masliah, E.; Hamilton, R.L.; Mandal, R. Interaction between Aβ Peptide and α Synuclein: Molecular Mechanisms in Overlapping Pathology of Alzheimer's and Parkinson's in Dementia with Lewy Body Disease. *Neurochem. Res.* **2006**, doi:10.1007/s11064-006-9140-9.

233. Tsigelny, I.F.; Crews, L.; Desplats, P.; Shaked, G.M.; Sharikov, Y.; Mizuno, H.; Spencer, B.; Rockenstein, E.; Trejo, M.; Platoshyn, O.; et al. Mechanisms of Hybrid Oligomer Formation in the Pathogenesis of Combined Alzheimer's and Parkinson's Diseases. *PLoS One* **2008**, doi:10.1371/journal.pone.0003135.

234. Clinton, L.K.; Blurton-Jones, M.; Myczek, K.; Trojanowski, J.Q.; LaFerla, F.M. Synergistic Interactions between Aβ, Tau, and α-Synuclein: Acceleration of Neuropathology and Cognitive Decline. *J. Neurosci.* **2010**, doi:10.1523/JNEUROSCI.0490-10.2010.

235. Ono, K.; Takahashi, R.; Ikeda, T.; Yamada, M. Cross-Seeding Effects of Amyloid β-Protein and α-Synuclein. *J. Neurochem.* **2012**, doi:10.1111/j.1471-4159.2012.07847.x.

236. Ma, Q.; Ineichen, B. V.; Detmar, M.; Proulx, S.T. Outflow of Cerebrospinal Fluid Is Predominantly through Lymphatic Vessels and Is Reduced in Aged Mice. *Nat. Commun.* **2017**, doi:10.1038/s41467-017-01484-6.

237. Candelise, N.; Schmitz, M.; Llorens, F.; Villar-Piqué, A.; Cramm, M.; Thom, T.; da Silva Correia, S.M.; da Cunha, J.E.G.; Möbius, W.; Outeiro, T.F.; et al. Seeding Variability of Different Alpha Synuclein Strains in Synucleinopathies. *Ann. Neurol.* **2019**, doi:10.1002/ana.25446.

238. Zijlmans, J.C.M.; Daniel, S.E.; Hughes, A.J.; Révész, T.; Lees, A.J. Clinicopathological Investigation of Vascular Parkinsonism, Including Clinical Criteria for Diagnosis. *Mov. Disord.* **2004**, doi:10.1002/mds.20083.

239. Katzenschlager, R.; Zijlmans, J.; Evans, A.; Watt, H.; Lees, A.J. Olfactory Function Distinguishes Vascular Parkinsonism from Parkinson's Disease. *J. Neurol. Neurosurg. Psychiatry* **2004**, doi:10.1136/jnnp.2003.035287.

240. Shahnawaz, M.; Tokuda, T.; Waragai, M.; Mendez, N.; Ishii, R.; Trenkwalder, C.; Mollenhauer, B.; Soto, C. Development of a Biochemical Diagnosis of Parkinson Disease by Detection of α-Synuclein Misfolded Aggregates in Cerebrospinal Fluid. *JAMA Neurol.*

2017, *74*, 163, doi:10.1001/jamaneurol.2016.4547.

241. Shahnawaz, M.; Mukherjee, A.; Pritzkow, S.; Mendez, N.; Rabadia, P.; Liu, X.; Hu, B.; Schmeichel, A.; Singer, W.; Wu, G.; et al. Discriminating α-Synuclein Strains in Parkinson's Disease and Multiple System Atrophy. *Nature* 2020, *578*, 273–277, doi:10.1038/s41586-020-1984-7.

242. Stefani, A.; Iranzo, A.; Holzknecht, E.; Perra, D.; Bongianni, M.; Gaig, C.; Heim, B.; Serradell, M.; Sacchetto, L.; Garrido, A.; et al. Alpha-Synuclein Seeds in Olfactory Mucosa of Patients with Isolated REM Sleep Behaviour Disorder. *Brain* 2021, doi:10.1093/brain/awab005.

243. De Luca, C.M.G.; Consonni, A.; Cazzaniga, F.A.; Bistaffa, E.; Bufano, G.; Quitarrini, G.; Celauro, L.; Legname, G.; Eleopra, R.; Baggi, F.; et al. The Alpha-Synuclein RT-QuIC Products Generated by the Olfactory Mucosa of Patients with Parkinson's Disease and Multiple System Atrophy Induce Inflammatory Responses in SH-SY5Y Cells. *Cells* 2022, doi:10.3390/cells11010087.

244. Bargar, C.; De Luca, C.M.G.; Devigili, G.; Elia, A.E.; Cilia, R.; Portaleone, S.M.; Wang, W.; Tramacere, I.; Bistaffa, E.; Cazzaniga, F.A.; et al. Discrimination of MSA-P and MSA-C by RT-QuIC Analysis of Olfactory Mucosa: The First Assessment of Assay Reproducibility between Two Specialized Laboratories. *Mol. Neurodegener.* 2021, doi:10.1186/s13024-021-00491-y.

245. Ding, X.; Zhou, L.; Jiang, X.; Liu, H.; Yao, J.; Zhang, R.; Liang, D.; Wang, F.; Ma, M.; Tang, B.; et al. Propagation of Pathological α-Synuclein from the Urogenital Tract to the Brain Initiates MSA-like Syndrome. *iScience* 2020, doi:10.1016/j.isci.2020.101166.

246. Bongianni, M.; Ladogana, A.; Capaldi, S.; Klotz, S.; Baiardi, S.; Cagnin, A.; Perra, D.; Fiorini, M.; Poleggi, A.; Legname, G.; et al. A-Synuclein RT-QuIC Assay in Cerebrospinal Fluid of Patients with Dementia with Lewy Bodies. *Ann. Clin. Transl. Neurol.* 2019, *6*, 2120–2126, doi:10.1002/acn3.50897.

247. Peng, C.; Gathagan, R.J.; Covell, D.J.; Medellin, C.; Stieber, A.; Robinson, J.L.; Zhang, B.; Pitkin, R.M.; Olufemi, M.F.; Luk, K.C.; et al. Cellular Milieu Imparts Distinct Pathological α-Synuclein Strains in α-Synucleinopathies. *Nature* 2018, doi:10.1038/s41586-018-0104-4.

248. Pavel, A.; Murray, D.K.; Stoessl, A.J. COVID-19 and Selective Vulnerability to Parkinson's Disease. *Lancet Neurol.* 2020, *19*, 719, doi:10.1016/S1474-4422(20)30269-6.